REPORT ON THE ANALYSIS OF THE SHORELINE FAULT ZONE, CENTRAL COASTAL CALIFORNIA

Report to the U.S. Nuclear Regulatory Commission
January 2011

Pacific Gas and Electric Company

Diablo Canyon Power Plant

TABLE OF CONTENTS

TABLES

FIGURES

PLATE

APPENDICES

GLOSSARY OF ACRONYMS AND TECHNICAL TERMS

ACRONYMS

ASW	auxiliary salt water
CCSN	Central Coast Seismic Network
CDF	core damage frequency
CRADA	Cooperative Research and Development Agreement
DCPP	Diablo Canyon Power Plant
DSHA	deterministic seismic hazard analysis
FSAR	final safety analysis report
GMPE	ground motion prediction equation
GPS	global positioning system
ISFSI	independent spent fuel storage installation
LGM	Last Glacial Maximum
LiDAR	light detection and ranging
LOSM	Los Osos–Santa Maria
LTSP	Long Term Seismic Program
MBES	multibeam echo sounding
MIS	marine oxygen isotope stage
MLLW	mean lower low water
NEHRP	National Earthquake Hazards Reduction Program
NGA	Next Generation Attenuation
NRC	U. S. Nuclear Regulatory Commission
OBS	ocean bottom seismometer
PG&E	Pacific Gas and Electric Company
PSHA	probabilistic seismic hazard analysis
RMS	root mean square
USGS	U. S. Geological Survey

TECHNICAL TERMS

Coastline – A broad region in the vicinity of a shoreline that includes coastal landforms, such as beaches, wave-cut platforms, sea cliffs, marine terraces, and seaward-facing hill slopes.

DCPP – Diablo Canyon Power Plant The area includes the power block where the reactors and generators are located, and the adjacent support facilities.

High Stand – a still stand of sea level caused when glaciers reach temporary equilibrium between accumulating snow/ice and melting snow/ice causing rising sea level to stop before falling.

Islay shelf – The rocky portion of the inner continental shelf that lies offshore of Point Buchon. It extends from the coastline to the continental slope on the west and from Estero Bay on the north to the general latitude of the DCPP on the south. It is generally characterized by wide, gently sloping subsea exposures of rock, but also includes limited areas of thin late Quaternary marine deposits and mobile sand sheet deposits.

Low Stand – a still stand of sea level caused when glaciers reach temporary equilibrium between melting snow/ice and accumulating snow/ice causing falling sea level to stop before rising.

Mean sea level (MSL) – Sea level measured at the mean of all tides in the region. This is approximately coincident with NAVD 88, the reference datum for project topographic surveys. In this study we reference all maps to NAD 83_1983_UTM Zone _10N.

Mean lower-low water (MLLW) – Sea level measured at the mean of the low tides, 2.6 feet (0.8 m) below MSL in the DCPP area.

Mean higher-high water (MHHW) – Sea level measured at the mean of the high tides, 2.5 feet (0.77 m) above MSL in the DCPP area.

Paleoshoreline – A preserved remnant of an ancient shoreline. In the DCPP area, these are discontinuous features related to sea-level highstands onshore and high- and lowstands offshore. Paleoshorelines are typically associated with wave-cut platforms and paleosea cliffs and/or paleobeaches. In the DCPP area, about 10 paleoshorelines of different ages are preserved onshore and at least 10 offshore; locally, multiple closely spaced strandlines are grouped with a single paleoshoreline.

San Luis Bay fault zone – The northern group of faults in the Southwest Boundary fault zone. These consist of the San Luis Bay, Rattlesnake, and Olson faults.

Santa Rosa Reef shelf – The rocky portion of the inner continental shelf that lies offshore of Point San Luis. It extends from the coastline to the continental slope on the west and from the general latitude of the DCPP on the north to the limit of bedrock outcrops south and southeast of Point San Luis. It is generally characterized by the wide, gently sloping and flat subsea exposures of rock, but also includes limited areas of thin late Quaternary marine deposits and mobile sand sheet deposits.

Shoreline – The location where the sea surface meets the land. It includes the entire tidal range.

Shoreline angle – The point (typically in profile) where a wave-cut platform meets a sea cliff. Because of natural variation in wave-cut platform surfaces, shoreline angles can be formed at a variety of elevations with respect to the tidal range, ranging from as low as MSL (approximately elevation 0 relative to NAVD 88) to a few meters above MSL. In the DCPP area, the most common elevation of shoreline angles on the modern coastline is 2 m, approximately coincident with MHHW. An ancient shoreline angle provides an approximate record of the relative sea level at the time the paleoshoreline formed.

Shoreline fault zone – The geologic structure interpreted to have produced the seismicity lineament as recognized by Hardebeck (2010).

Still Stand – Sea level remains at remains at a constant elevation (level) for a period of a few thousand or more years during the Quaternary Period. This occurs when glacier melt and snow accumulation maintain equilibrium.

Strandline – The two-dimensional geomorphic record of sea level. On an erosional coastline (such as the Irish Hills coastline), it is marked by the intersection of a sea cliff and wave-cut platform. On a depositional coastline, it is marked (less precisely) by a beach berm. As with shoreline angles, modern strandlines in the DCPP area typically occur about 2 m above MSL, but may range from MSL to a few meters above MSL. An ancient strandline provides an approximate record of the relative sea level at the time the paleoshoreline formed.

Wave-cut platform – A broad bedrock platform that slopes gently seaward from a sea cliff. Wave-cut platforms are carved predominantly by wave erosion; however, other processes may contribute to their genesis, such as chemical and salt weathering, bio-erosion, and expansion-contraction of clays and ice.

EXECUTIVE SUMMARY

In November 2008, Pacific Gas and Electric (PG&E) informed the US Nuclear Regulatory Commission (NRC) that preliminary results from the Diablo Canyon Power Plant (DCPP) Long Term Seismic Program (LTSP) Update showed that there was an alignment of microseismicity subparallel to the coastline indicating the possible presence of a previously unidentified fault located about 1 km offshore of DCPP. This previously unidentified fault was named the Shoreline fault zone.

As part of the notification to the NRC in 2008, PG&E conducted an initial sensitivity study to evaluate the potential impact of the Shoreline fault zone on the seismic safety of DCPP using a seismic margin approach (PG&E, 2008). Using conservative assumptions about the total length of the fault zone, a magnitude 6.5 strike-slip earthquake at a distance of 1 km was considered. The results of this sensitivity study demonstrated that the 84th percentile ground motion from the Shoreline fault zone was lower than the 1991 LTSP/SSER34 84th percentile ground motion for which the plant had been evaluated and shown to have adequate margin (NRC, 1991). Therefore, PG&E concluded that the plant had adequate seismic margin to withstand the ground motions from the Shoreline fault zone. In early 2009, the NRC conducted an independent study of the potential impacts of the Shoreline fault zone on DCPP and also concluded that there was adequate seismic margin (NRC, 2009).

Although the initial seismic sensitivity studies showed that the plant has adequate margin to withstand ground motion from the potential Shoreline fault zone, both the NRC and PG&E recognized the need to better constrain the four main parameters of the Shoreline fault zone needed for a seismic hazard assessment: geometry (fault length, fault dip, down-dip width), segmentation, distance offshore from DCPP, and slip-rate. To address this need, PG&E conducted an extensive program in 2009 and 2010 to acquire, analyze, and interpret new geological, geophysical, seismological, and bathymetric data as part of the ongoing PG&E LTSP Update. These investigations have led to an improved understanding of the Shoreline fault zone, and its relationship to other seismic sources including the Hosgri and Southwestern Boundary fault zones. These findings are summarized in Table 1.

DETERMINISTIC GROUND MOTIONS

In addition to the updated information on the faulting in the DCPP region, updated ground motion models and methods are also available. The Next Generation Attenuation (NGA) models are used for the ground motion models with site-specific modifications calibrated from observed ground motions at the DCPP site. Using updated ground motion models, the ground motions from strike-slip earthquakes along the Hosgri fault zone have decreased and the ground motions from the reverse-slip earthquakes on the Los Osos and San Luis Bay fault zones have remained about the same relative to ground motions computed using the 1988 LTSP ground motion models. As a result, the relative importance of the faults to the hazard at DCPP has changed from the 1988 LTSP report,

and the 84th percentile ground motions from these faults computed using the updated ground motion models remains bounded by the 1988 LTSP spectrum.

The magnitude of deterministic earthquakes for the Shoreline fault (M6.5) is less than the magnitudes for the Hosgri (M7.1), but due to the shorter distance, the ground motions from the 84th percentile ground motions for Shoreline fault are greater than the updated ground motions from the Hosgri fault source. Nonetheless, the ground motions from the Shoreline fault source are still bounded by the 1991 LTSP/SSER34 spectrum.

Deterministic analyses for the Hosgri, Shoreline, San Luis Bay and Los Osos fault zones, using conservative estimates of the fault dips for each fault, indicate that the 84th percentile ground motions fall below the 1977 Hosgri Earthquake (HE) Design Spectrum and the 1991 LTSP/SSER34 spectrum (Figures ES-1).

PROBABILISTIC HAZARD ANALYSIS

Probabilistic hazard calculations show that the primary contribution to the 3-8.5 Hz hazard at DCPP is from the Hosgri fault zone with the Los Osos, Shoreline, and San Luis Bay faults providing smaller contributions (Figure ES-2). The inclusion of new Ground Motion Prediction Equations and the use of the updated source characterization in the DCPP hazard model has resulted in a reduced level of the hazard as compared to the 1988 LTSP hazard at most ground motion levels, but the slope of the updated hazard is reduced so that the updated hazard crosses the 1988 LTSP hazard curve at about 3 g. These changes in the hazard curve are primarily due to the changes in the ground motion models: the NGA models with site-specific effects result in lower median ground motions for sites close to large strike-slip earthquakes, but with an increased standard deviation. Because the updated hazard curve is not enveloped by the 1988 LTSP hazard curve, the seismic core damage frequency (CDF) was reevaluated: the seismic CDF decreases from 3.8E-5 for the1988 LTSP to 2.1 E-5 for the updated models. The reduction in the seismic CDF is mainly due to the use of the NGA ground motion models with the single-station sigma approach incorporating the site-specific amplification.

SECONDARY FAULT DEFORMATION

The potential for secondary fault deformation associated with rupture of the Shoreline fault zone was evaluated using a deterministic approach. The Central segment of the Shoreline fault zone is located 300 meters southwest of the Intake structure and 600 meters southwest of the Power Block. The deterministic assessment of the geology at the DCPP site and vicinity documented the absence of late Quaternary primary or secondary surface faulting or other forms of late Quaternary tectonic deformation (e.g., tilting, folding, and subsidence) within the DCPP site that may be associated with a maximum earthquake on the nearby Shoreline fault zone. Therefore, PG&E concludes that secondary fault deformation does not affect the safety of the DCPP.

CONCLUSIONS

New seismic and ground motion data, including site-specific site amplification based on earthquake recordings at the DCPP site, have resulted in a reduction of the uncertainty in the seismic hazard at the DCPP site. Deterministic analyses for the Hosgri, Shoreline, San Luis Bay and Los Osos fault zones, using conservative estimates of the fault dips for each fault, indicate that the 84th percentile ground motions fall below the 1977 Hosgri Earthquake (HE) Design Spectrum and the 1991 LTSP/SSER34 84th percentile deterministic spectrum. Probabilistic analyses shows that the inclusion of the Shoreline fault zone contributes about 20 percent to the seismic CDF seismic, but the seismic CDF is reduced from the 1988 LTSP estimates.

The original completion date of 2011 for the LTSP Update, as stated in the Action Plan and Revised Action Plan (Appendix A-1 and A-3), has been extended to allow completion of additional studies to further refine the models presented in this report. These studies include three-dimensional (3-D) marine and two-dimensional (2-D) onshore seismic reflection profiling, additional potential field mapping, GPS monitoring, and the feasibility of installing an ocean bottom seismograph network. These activities will further refine the characterization of those seismic sources and ground motions most important to the DCPP: the Hosgri, Shoreline, Los Osos, and San Luis Bay fault zones and other faults within the Southwestern Boundary zone.

TABLE 1 Summary of Shoreline Fault Zone Parameters

PARAMETER	DESCRIPTION
FAULT LENGTH	Total Length: up to 23 km Overall Strike: N60°W to N70°W
SEGMENTATION	Three segments: North segment, ~8 km long; Central segment, ~8 km long; South segment, ~7 km long
FAULT DIP	90° based on seismicity and magnetic potential field data
DOWN DIP WIDTH	10 to 15 km from the surface
FAULTING STYLE	Right-lateral strike slip based on linear surface expression of bathymetric lineaments and focal mechanisms.
RELATIONSHIP TO OTHER STRUCTURES	Hosgri fault zone (HFZ) Rupture is inhibited from branching from the HFZ to the Shoreline fault zone North Segment dies out before, or terminates at, the HFZ. San Luis Bay fault zone (SLBFZ) Relationship to late Quaternary deformation on the SLBFZ is uncertain
SLIP RATE	Preferred slip rate: 0.2 to 0.3 mm/yr
DISTANCE FROM DCPP	Central Segment: 600 m southwest of Power Block 300 m southwest of Intake Structure
SECONDARY FAULT DEFORMATION AT DCPP SITE	A deterministic evaluation documented the absence of late Quaternary primary or secondary surface faulting or other forms of late Quaternary tectonic deformation (e.g., tilting, folding, and subsidence) within the DCPP site that might have been associated with a maximum earthquake on the nearby Shoreline fault zone.

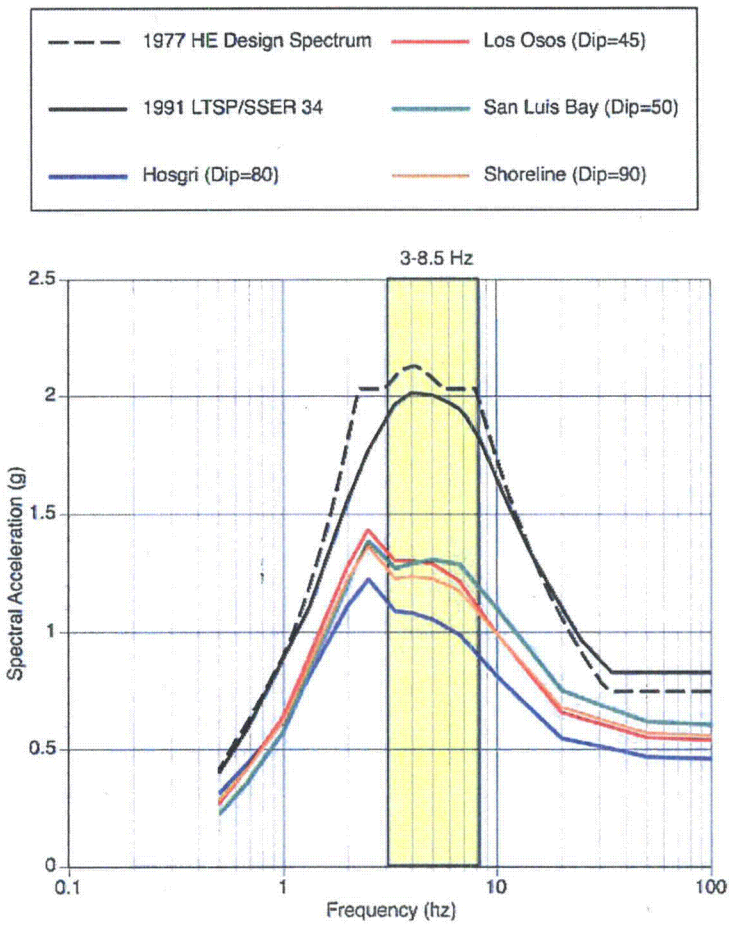

Figure ES-1. Comparison of deterministic spectra using conservative values for the dip angles on the Hosgri, Shoreline, Los Osos, and San Luis Bay faults. The peak in the spectra at 2.5 Hz reflects the site-specific amplification of the rock at DCPP based on ground motions recorded at the DCPP site. The Shoreline fault, with M6.5 at 0.6 km, leads to a higher deterministic ground motion than new estimates for the Hosgri fault, but the ground motions are bounded by the 1991 LTSP/SSER34 spectrum and by the 1977 Hosgri Earthquake (HE) design spectrum. Ground motions from the San Luis and Los Osos faults also remain bounded by the LTSP/SSER34 spectrum, but they are now larger than the updated Hosgri ground motion. Although San Luis Bay fault is from a smaller magnitude (M6.3) at a larger distance (1.9 km) than the Shoreline fault, the spectrum for the San Luis Bay is slightly above the spectrum for the Shoreline fault due to hanging wall effects. The spectrum from the Los Osos fault (M6.8, distance=7.6 km, HW) is also similar to the spectrum from the Shoreline and San Luis Bay faults.

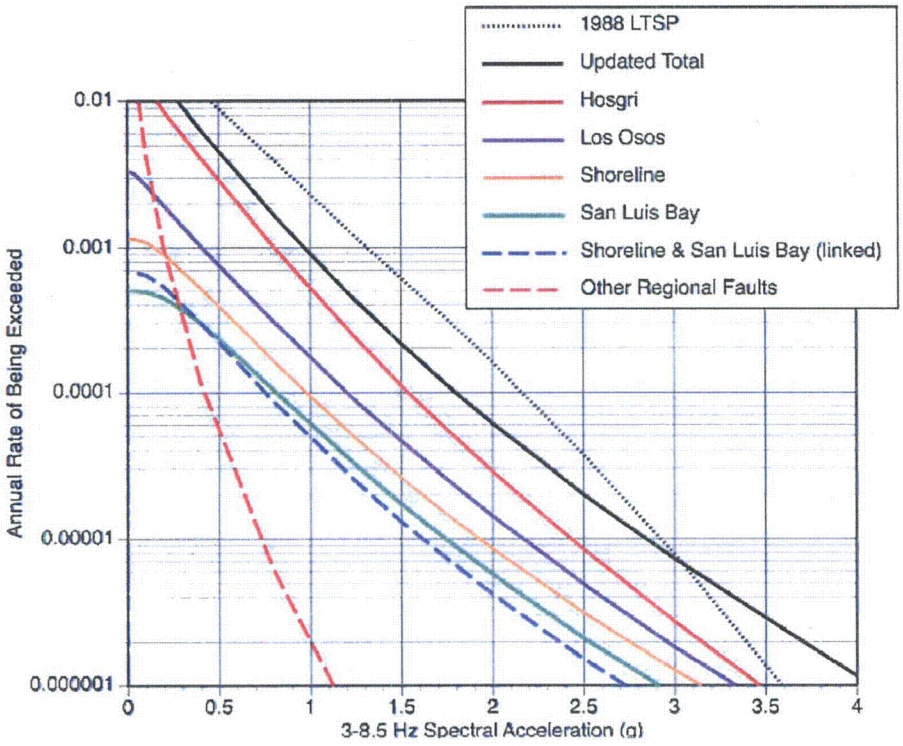

Figure ES-2. Probabilistic hazard curves for the Hosgri, Los Osos, San Luis Bay, and Shoreline fault zones.
Probabilistic seismic hazard is dominated by the Hosgri fault due to the higher rate of slip of the Hosgri compared to the other nearby faults. Hazard curves for the Los Osos, Shoreline, and San Luis Bay faults are less than the Hosgri and similar to each other.

1.0 INTRODUCTION

This report presents the results of a two-year Pacific Gas and Electric (PG&E) study of the Shoreline fault zone, which is located offshore of the Diablo Canyon Power Plant (DCPP). In November 2008, PG&E informed the U.S. Nuclear Regulatory Commission (NRC) that preliminary results from the DCPP Long Term Seismic Program (LTSP) seismic hazard update showed an alignment of seismicity that suggested the presence of a previously unidentified fault approximately 1 kilometer (km) offshore of DCPP. This previously unidentified fault was subsequently named the Shoreline fault zone by PG&E.

Using a seismic margin approach, PG&E conducted an initial sensitivity study to evaluate the potential impact of the Shoreline fault zone on the seismic safety of DCPP (PG&E, 2008). PG&E used conservative assumptions about the total length of the fault zone to consider a magnitude 6.5 strike-slip earthquake at a distance of 1 km from DCPP. The results of this sensitivity study demonstrated that the 84th percentile ground motion from the Shoreline fault zone was lower than the 1991 LTSP ground motion for which the plant had been evaluated and shown to have adequate margin (NRC, 1991). Therefore, PG&E concluded that the plant had adequate seismic margin to withstand the ground motions from the Shoreline fault zone. In early 2009, the NRC conducted an independent study of the potential impacts of the Shoreline fault zone on DCPP and also concluded that there was adequate seismic margin (NRC, 2009).

Although these initial sensitivity studies show that the plant has adequate margin to withstand ground motion from the potential Shoreline fault zone, four main parameters of the Shoreline fault zone were not well constrained: geometry (length, width, dip); segmentation; location offshore of DCPP; and slip rate. To address the uncertainties in these source parameters and analyze the earthquake relocations, PG&E prepared a two-year Action Plan in 2009 (Appendix A1) to collect additional data to better characterize the Shoreline fault zone. Figure 1-1 shows the location of the Shoreline fault zone study area. A Progress Report was issued in January of 2010 that summarized the first-year activities (see PG&E, 2010a, Appendix A).

1.1 Organization of This Report

This report presents the results of the two-year study and comprises the following:

- A more complete evaluation of the geologic and seismologic characteristics of the Shoreline fault zone (geometry, location, segmentation, and slip rate).
- An assessment of the ground motion hazard at the DCPP that includes the Shoreline fault zone.
- An assessment of the potential for secondary fault deformation on the DCPP site.

Section 1 provides background on prior coastal investigations and the LTSP. Section 2 summarizes the geologic; geophysical (gravity and magnetic surveys, multibeam echo sounding [MBES], and seismic reflection profiling); and seismicity data that were collected from 2008 to 2010 for this report. More detailed descriptions of specific data sets are presented in Appendices B through I. Independent reviews of the Hardebeck

earthquake relocations are in Appendices C1 and C2. Section 3 discusses the tectonic, geologic, and seismologic setting of the Shoreline fault zone study area. Section 4 describes the geological, seismological, and geophysical characteristics of the Shoreline fault zone. Section 5 presents the source characterization of the Shoreline fault zone, and Section 6 describes the ground-motion impacts to DCPP. Further details are provided in Appendices J and K. Section 7 describes the potential for secondary fault deformation at the DCPP site. Section 8 summarizes the findings of this report and presents PG&E's conclusions. Finally, Section 9 contains the references cited in this report.

1.2 Background

The existence of an offshore fault zone between Point Buchon and Point San Luis was discussed by NRC staff in 1989 and was based on the linear nature of the coastline in this area and the presence of lineaments and escarpments parallel to the coast, as well as a postulated slip deficit across the San Luis–Pismo structural block. Nitchman (1988) described the San Luis Range as being bounded by the Los Osos fault to the north, the Hosgri fault to the west, and several reverse faults to the south. The southern boundary included the Wilmar Avenue fault, the San Luis Bay fault, and an inferred northeast-dipping reverse fault that Nitchman (1988) called the Inferred Offshore fault. The basis for Nitchman's (1988) interpretation was the observation that the shoreline was parallel to the N60°W trending San Luis Range, and the lack of tilting of marine terraces (Killeen, 1988). This suggested that the range is uplifting as a block and, he thought, is probably bounded to the southwest by a matching reverse fault that is a mirror image of the Los Osos fault.

PG&E presented evidence supporting its conclusion that there was no significant undetected fault paralleling the coast in the zone from the shore out to a distance of 1–2 km, within which shallow water precluded obtaining seismic reflection profiles (PG&E, 1989a, Response to Question 43e; 1990). This evidence consisted of seismic reflection data that covered the area offshore of the shallow water zone, and seismic reflection lines that would have crossed any significant coast-parallel faulting extending into Estero Bay. PG&E recognized the difficulties of identifying faults in shallow water with an acoustic basement characterized by steeply dipping structures, and examined other lines of evidence, mainly bathymetric data in the near shore from Morro Bay to Point San Luis. Prominent bathymetric escarpments that could be traced from Point Buchon to Point San Luis were identified and interpreted to be a series of closely spaced shoreline features that formed during previous low sea-level conditions (PG&E, 1990). Although the general trend of these escarpments appeared to cut obliquely across bathymetric contours, each individual slope break was subparallel to the bathymetric contours, sinuous and irregular, indicating that the breaks in slope were not tectonically controlled. NRC staff concluded that while the evidence presented by PG&E supported the absence of a coast-parallel fault, the presence of such a fault could not be completely ruled out (NRC, 1991, pp. 2-29 to 2-30).

PG&E established the LTSP in 1984, and assembled a robust geosciences and engineering program to support licensing and operation of DCPP. Following the success of the LTSP in satisfying the NRC's licensing requirements for DCPP, this program has

grown to include partnerships with the U.S. Geological Survey (USGS) as well as state, local, and academic institutions such as the Seafloor Mapping Lab at the California State University Monterey Bay and the Pacific Earthquake Engineering Research Center at the University of California, Berkeley.

Long Term Seismic Program

Following the successful completion of the LTSP in 1991, PG&E maintained the LTSP staff of geoscience and engineering experts to keep abreast of new geological, geophysical, seismological, and seismic engineering information that might apply to Diablo Canyon. PG&E recognized that some issues (e.g., the type of fault motion on the Hosgri fault, the characterization of the Southwestern Boundary zone, and ground motion estimates for oblique-slip earthquakes) were controversial due to lack of definitive evidence, and assumed that future geoscience discoveries would bring these issues to a firm conclusion. As a result, PG&E made a commitment to continue LTSP activities for the life of the plant (PG&E, 1991b; NRC, 1991, p. 1-7).

PG&E–USGS Cooperative Research and Development Agreement

Both the 2003 San Simeon and 2004 Parkfield earthquakes provided extensive data and new opportunities to better understand and more accurately characterize details of the tectonic environment in the central coastal California region and to compare this new information with existing knowledge. PG&E and USGS have collaborated on studies of the San Simeon and Parkfield earthquakes as part of a Cooperative Research and Development Agreement (CRADA) that was established in 1992 to improve rapid earthquake notifications and develop new geoscience data and advanced analysis methods leading to reducing earthquake risks in PG&E's service territory in northern and central California. The PG&E–USGS CRADA has provided a unique and productive opportunity to conduct collaborative research that is of mutual interest to both PG&E and the USGS.

Examples of CRADA-supported mutual-interest research include fixed-wing and marine geomagnetic surveys that were conducted in 2008 and 2009, as well as high-resolution marine seismic reflection profiles that were collected as part of the California Seafloor Mapping Program (http://walrus.wr.usgs.gov/mapping/csmp/). The advent of differential GPS navigation and improvements in offshore geophysical mapping technology have enabled higher-resolution imaging of the shallow water areas along the California coast. These modern geologic and geophysical data have helped to improve the regional tectonic characterization in south-central coastal California.

LTSP Update

Beginning in 2006, PG&E embarked on an effort, called the LTSP Update, to update its geological geophysical, and seismological databases and to incorporate new scientific information and emerging tectonic concepts to advance the understanding of earthquake hazards in the south-central coastal region. One of the initial tasks in this plan was to combine the occurrence of additional seismicity since the original LTSP with the development and application of recently-developed advanced earthquake location techniques (tomoDD [Zhang and Thurber, 2003] and hypoDD [Waldhauser, 2001]). This

work led to identifying a seismicity lineament that parallels the coast between Point Buchon and Point San Luis (Hardebeck, 2010). This lineament was not apparent at the time of completion of the original LTSP in 1991. While these newer data appear to confirm the location, orientation, and approximate length of Nitchman's reverse-slip Inferred Offshore fault, the focal mechanisms of earthquakes that have occurred along the Shoreline fault zone from 1988 to 2008 are more consistent with right-lateral strike-slip motion than reverse motion. The new geologic and geophysical data that have been collected as part of the LTSP Update are being used in conjunction with the earthquake locations to constrain the geometry, segmentation, location, and slip rate of the Shoreline fault zone for this report.

The original completion date of 2011 for the LTSP Update, as stated in the Action Plan and Revised Action Plan (Appendix A-1 and A-3), has been extended to allow completion of additional studies to further refine the models presented in this report. These studies include three-dimensional (3-D) marine and two-dimensional (2-D) onshore seismic reflection profiling, additional potential field mapping, GPS monitoring, and the feasibility of installing an ocean bottom seismograph network.

1.3 Acknowledgments

This study originated as part of the Diablo Canyon LTSP Update conducted by PG&E under the direction of Mr. Lloyd S. Cluff. The PG&E Staff who contributed to this study include Dr. Norman Abrahamson, Mr. Kent Ferré, Mr. William Horstman, Ms. Debbie Kwok, Ms. Marcia McLaren, Dr. Stuart Nishenko, Dr. William Page, Ms. Megan Stanton, Mr. Richard Van der Linden, and Ms. Katie Wooddell.

A study of this scope and complexity would not have been possible without the cooperation of numerous individuals and organizations outside of PG&E. In particular, the excellent efforts of PG&E's CRADA partners at the USGS are acknowledged. Much of the new geophysical data used in this report were collected under the PG&E–USGS CRADA as part of the LTSP Update. PG&E thanks Dr. Thomas Brocher, Dr. William Ellsworth, Dr. Jeanne Hardebeck, Ms. Vickie Langenheim, Dr. Robert Jachens, Dr. William Savage, Dr. Carl Wentworth, Dr. Samuel Johnson, Ms. Janet Watt, and the crew of the *R/V Parke Snavely.*

PG&E also gratefully acknowledges the assistance of Prof. Rikk Kvitek and the crew of the *R/V Ven Tresca* from the Seafloor Mapping Lab at the California State University of Monterey Bay with collecting and processing the MBES bathymetry data offshore of DCPP.

PG&E's Interpretation Team reviewed and interpreted the newly collected multibeam bathymetry and high-resolution seismic reflection data, as well as older geophysical and geological data sets, to develop the geologic maps in this report. The Interpretation Team includes Dr. Gary Greene (consultant); Mr. Serkan Bozkurt, Ms. Kathryn Hanson, Mr. Hans AbramsonWard, Ms. Alexis Lavine (AMEC Geomatrix); Dr. William Lettis, Mr. Michael Angell, Dr. Daniel O'Connell, Dr. Stephen Thompson, Mr. Andrew Lutz

(FUGRO-William Lettis & Associates); and Dr. Jan Rietman and Dr. Phillip Hogan (Fugro West, Inc.).

PG&E also established an Advisory Board to provide an independent review of the data and conclusions developed in the LTSP Update, including the Shoreline fault zone study. Members of the Advisory Board are Prof. Julian Bommer (Imperial College); Dr. Kevin Coppersmith (Coppersmith Consulting, Inc.); Prof. Steven Day (San Diego State University); Dr. Robert Kennedy (RPK Structural Mechanics Consulting, Inc.); and Prof. Raymond Weldon (University of Oregon).

Additional consultants who assisted in addressing specific issues for this report include Dr. Gary Carver (Carver Geologic Inc.); Mr. Lew Rosenberg (Consulting Geologist to San Luis Obispo County); Prof. Clifford Thurber (University of Wisconsin–Madison); and Dr. Felix Waldhauser (Lamont-Doherty Earth Observatory).

LEGEND

Study area

Shoreline, Hosgri, San Luis Bay, and Wilmar Avenue faults, dashed where approximate, dotted where concealed

N
W E
S

0 1 2 Miles
0 2 4 Kilometers

Map projection and scale: NAD 1983, UTM Zone 10N, 1:200,000

Map of Shoreline fault zone study area

SHORELINE FAULT ZONE STUDY

Pacific Gas and Electric Company

Figure **1-1**

File path: S:\13800\13838\13838.002\Figures\20101112_Report\Figure_1-1.mxd; Date: [12/21/2010]; User: Serkan Bozkurt, AMEC Geomatrix, Inc.

2.0 DATA COLLECTION

Continued seismic monitoring and the acquisition of high-resolution potential field (magnetics and gravity), seismic reflection, bathymetric, and topographic data have significantly improved the ability to resolve geologic and tectonic structures in the vicinity of DCPP since the original LTSP Final Report and Addendum (PG&E, 1988, 1991a).

Many of the regional geophysical data sets discussed in this report were collected as part of the PG&E–USGS CRADA. These new data were combined with onshore and offshore geologic data to update earlier models for the area and were integrated with more site-specific studies of the Shoreline fault zone carried out by PG&E. The following sections summarize the data collection activities from 2008 to 2010. More detailed descriptions of these data sets can be found in the Appendices. Section 2.8 contains definitions for terms used in this report.

2.1 Geology

Onshore and offshore geologic mapping was performed in 2009 and 2010 to prepare a "seamless" onshore/offshore geologic map of the Shoreline fault zone study area (Plate 1). The mapping included (1) detailed mapping of the extensive rock exposures in the sea cliffs and on the wave-cut platform at low tide from Lion Rock (north of Diablo Cove) to south of Rattlesnake Creek, and (2) collection of rock samples offshore.

2.1.1 Onshore Geologic Mapping

The local lithology of the various formations was described, and structures cutting the formations, shear zones, faults, and folds were characterized (Appendix B). Coastline mapping utilized both Light Detection and Ranging (LiDAR) surveys and orthophoto maps (Appendix G). This mapping is more detailed and more accurately located than earlier mapping onshore by Hall (1973) and Hall et al. (1979) and for the LTSP (PG&E, 1988, 1991a). This allowed projecting the onshore geology to the offshore interpretation of the geology based on the multibeam echo sounding (MBES) bathymetry data (Appendix F), magnetic field data (Appendix D), and seismic reflection data (Appendix H).

2.1.2 Offshore Geologic Mapping

Interpretation of the MBES bathymetry image used texture and structures to differentiate various rock units and to identify folds and faults. The magnetic field data helped with differentiation of rock units that have high magnetic signatures, and seismic reflection profiles helped in places with interpretation of folds, faults, and paleoshorelines where the rocks are covered by Quaternary sediments. Fifty new diver samples were collected offshore in July 2010 (see Figure 2-1 for locations and Appendix B) to supplement the diver and drop core samples obtained earlier for the LTSP (PG&E, 1991a). The sampling targeted areas of distinct bathymetric texture as identified from the MBES bathymetry data (Appendix F) and specific locations where preliminary geologic interpretations suggested a conflict between the original LTSP and the current mapping. Diver samples are analyzed to determine bulk physical properties (e.g., density and magnetic

susceptibility). Sample locations are assumed to be accurate to within 10–20 m. The last steps were to complete the offshore geologic interpretations by projecting offshore the formation contacts and structures from the onshore mapping, and to finalize the map shown on Plate 1.

2.2 Seismographic Station Coverage

McLaren and Savage (2001) summarized the seismographic station coverage in the Central Coast region. Aside from early instrumentation installed in 1927 in Santa Barbara and in 1961 at Parkfield, there were very few instruments in this region until about 1981, when the USGS began installing short-period vertical-component instruments with analog telemetry as part of the National Earthquake Hazards Reduction Program (NEHRP) (Lindh et al., 1981) (Figure 2-2). In 1987, PG&E installed the Central Coast Seismic Network (CCSN), consisting of 20 seismographic stations along the coast from Ragged Point to Point Sal. Fifteen of those stations were installed with short-period vertical-component sensors, and five had dual-gain three-component sensors. The minimum magnitude detection threshold value is approximately M 1.0 for onshore earthquakes and M 1.5 for near-offshore events. The network was designed to supplement the USGS network and improve the location accuracy of offshore microearthquakes. The recorded earthquakes were typically located using computer programs that inverted the arrival times from stations to travel times using a one-dimensional (1-D) velocity model. Despite the use of dual gain at the 5 three-component stations, events greater than about M 2.4 at 5–10 km distance from a station were off scale, or clipped, making S-wave arrival picks impossible.

Data processing has consisted of timing P- and S-wave arrivals and locating the earthquakes using the 1-D velocity model of McLaren and Savage (2001) and the location program Hypoinverse (Klein, 1985). Final locations were computed by integrating USGS data. Since about 2003, the PG&E data have been streaming to the USGS for automatic integration with the USGS data for computing locations and for focal mechanisms using the program FPFIT (Reasenberg and Oppenheimer, 1985).

Starting in 2006, PG&E began a five-year program to update approximately 17 of the original 20 stations with digital telemetry and digital recorders for velocity and acceleration (six components). By the end of 2011, PG&E expects to have 16 stations updated (Figure 2-2). The recorded data are markedly improved and should result in more accurate earthquake locations, particularly in the offshore region (Figure 2-2). PG&E is planning to install ocean-bottom seismometers starting in 2011 to further improve offshore locations.

Since 1987, the CCSN has recorded approximately 23,500 earthquakes in the Central Coast region bounded by the area shown on Figure 2-3a. The histogram (Figure 2-3b) shows that most these earthquakes are aftershocks from the moment magnitude (M_w) 6.5 San Simeon earthquake of 2003. The Hardebeck (2010) relocations and focal mechanisms were computed using a subset of the PG&E/USGS seismicity data.

2.3 Potential Field—Magnetic Surveys

Three magnetic surveys were conducted in the DCPP area in 2008 and 2009. These included a regional fixed-wing aeromagnetic survey from San Simeon to Point Concepcion (Langenheim et al., 2009a), a marine magnetic survey from Estero Bay to San Luis Obispo Bay (Sliter et al., 2009), and a helicopter magnetic survey from Point Buchon to Point San Luis (New Sense Geophysics, 2010). All three data sets are described in more detail in Appendix D. Figure 2-4 compares the magnetic data that were available at the time of the original LTSP (PG&E, 1988) with the helicopter magnetic data that were collected in 2009. This comparison illustrates how modern high-resolution data collection techniques have significantly improved imaging the potential field in this area.

2.4 Potential Field—Gravity Surveys

The USGS has compiled, edited, and reprocessed nearly 30,000 gravity measurements to produce an isostatic residual gravity map for the region, from Monterey Bay on the north to the Santa Barbara channel on the south (Langenheim et al., 2008). These data are further discussed in Appendix E. Figure 2-5 compares the gravity data available during the original LTSP (PG&E, 1988) with these newer data. While new gravity data have been collected onshore, little, if any, new data have been collected offshore.

2.5 Multibeam Echo Sounding Surveys

MBES bathymetry data for the Estero Bay to San Luis Obispo Bay near-shore region were acquired by the Seafloor Mapping Lab at the California State University Monterey Bay during 2007, 2009, and 2010. Appendix F contains further details of the data collection and reduction. Figures 2-6 and 2-7 compare seafloor bathymetry offshore of DCPP and Olson Hill using data that were available during the original LTSP (PG&E, 1988) and the newer MBES bathymetry data. Part of the improvement in resolution reflects the use of modern swath mapping techniques, and part is due to the fact that mapping could be done closer to shore than in previous surveys.

These data are used, in conjunction with high-resolution seismic reflection profile data discussed in Section 2.7, to (1) compile a geologic map of the area offshore of DCPP and map the surface expression of the Shoreline, Hosgri, and other faults in the area (see Plate 1 and Appendix B), and (2) map the depth and distribution of paleowave-cut platforms and strandlines (Appendix I).

2.6 LiDAR Survey

As noted in the Introduction (Section 1.2.1), the difficulties of surveying in shallow water have limited the ability to image the seafloor. Therefore, to provide seamless coverage of bathymetry and topography in the intertidal zone, PG&E contracted TetraTech to conduct a LiDAR survey from fixed-wing aircraft during one of the lowest tides of the year (–1.5 feet relative to mean lower low water [MLLW] at 3:02 p.m. on 28 January 2010). Figure 2-1 shows the area of the LiDAR survey. This data set is described in more detail in Appendix G.

2.7 High-Resolution Seismic Reflection Profiling

High-resolution single-channel seismic reflection data were acquired by the USGS in 2008 and 2009 between Piedras Blancas and Pismo Beach, along shore-perpendicular transects spaced 800 meters (m) apart extending from close to shore to beyond the 3-mile limit of California State waters. These data were collected, along with the marine magnetic data described in Section 2.3, as part of the PG&E–USGS CRADA, the California State Waters Mapping Program, the USGS Coastal and Marine Geology Program, and the USGS Earth Surface Processes Program and have been published as USGS Open File Report 2009-1100 (Sliter et al., 2009). Appendix H contains further details. High-resolution seismic reflection profiling provides greater definition of the top few hundred meters beneath the seafloor and is valuable for the identification of recent fault offsets (Appendix B) and for interpretation of paleowave-cut platforms and strandlines (Appendix I).

File path: S:\13800\13838\13838.002\Figures\20101112_Report\Figure_2-1.mxd; Date: [12/22/2010]; User: Serkan Bozkurt, AMEC Geomatrix, Inc.

LEGEND

- Study area
- LIDAR survey extent (This study, Appendix G)
- Diver Samples (This Study, Appendix B: Table B-4 and Attachment 1)
- Diver Samples (PG&E, 1988; Appendix B: Table B-3)
- Dropcore Samples (PG&E, 1988; Appendix B: Table B-2)

N, W, E, S

0 1 2 Miles

0 2 4 Kilometers

Map projection and scale: NAD 1983, UTM Zone 10N, 1:200,000

Offshore samples obtained during the LTSP and in 2010 for this study overlain with the extent of 2010 LiDAR survey

SHORELINE FAULT ZONE STUDY

Pacific Gas and Electric Company | Figure **2-1**

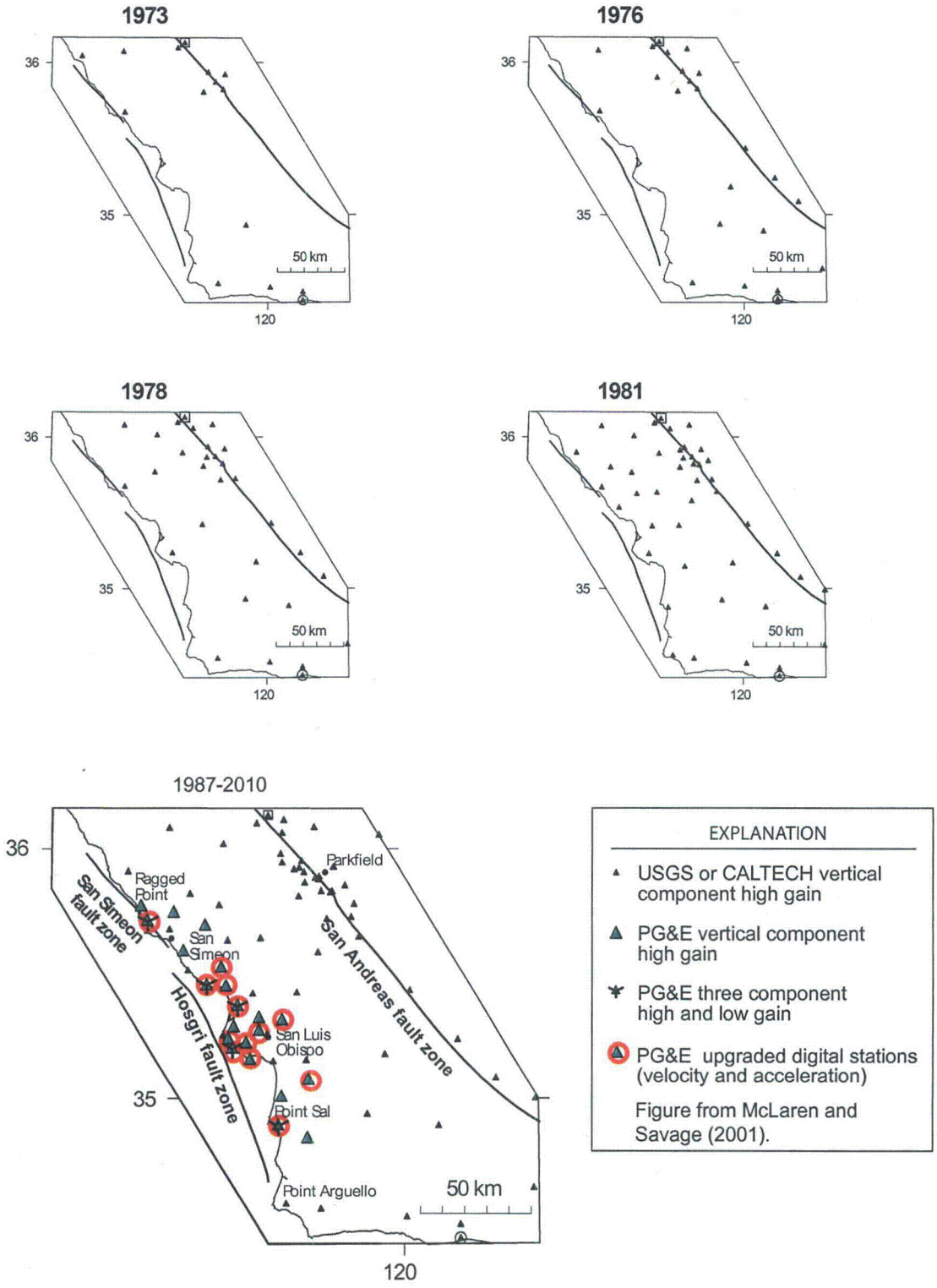

Maps of seismographic station coverage of the California Central Coast region for selected years

SHORELINE FAULT STUDY

Pacific Gas and Electric Company | Figure **2-2**

a)

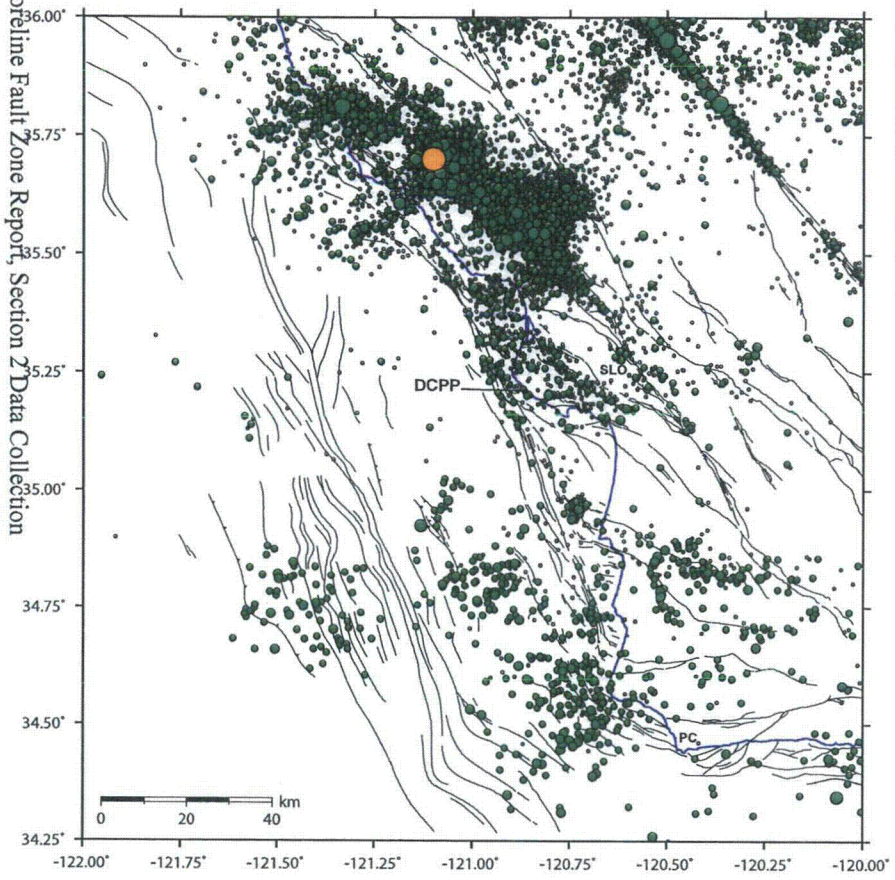

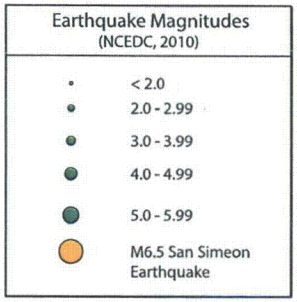

SLO = San Luis Obispo
PC = Point Conception

b)

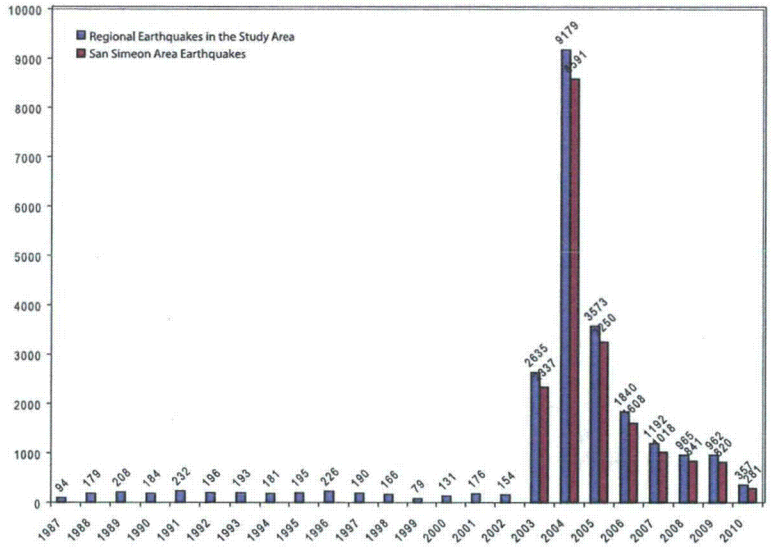

Seismicity recorded by PG&E and the USGS 1987 through August 2010

SHORELINE FAULT STUDY

Pacific Gas and Electric Company

Figure **2-3**

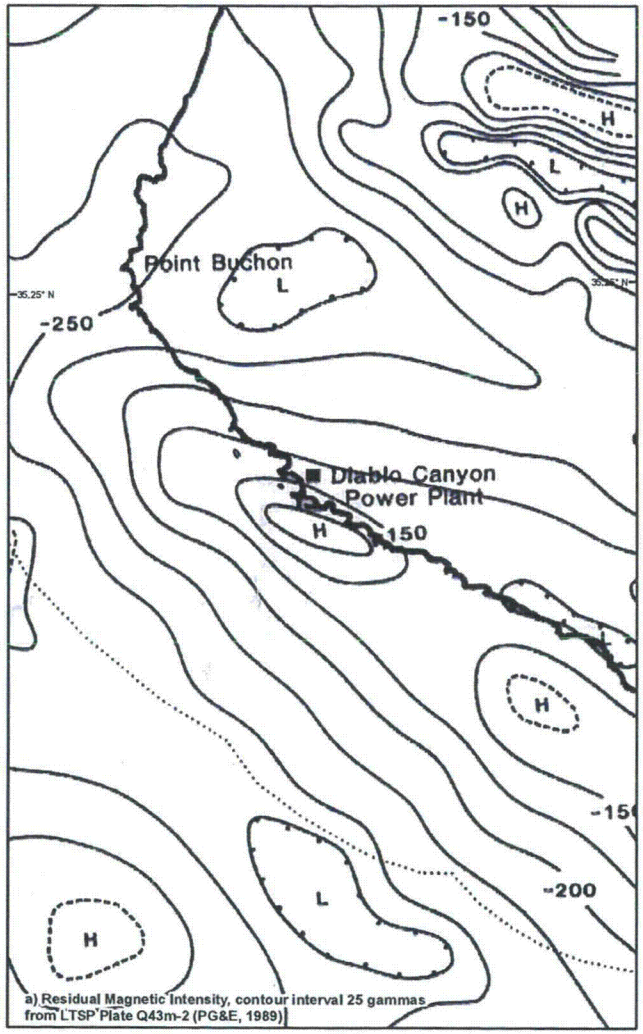

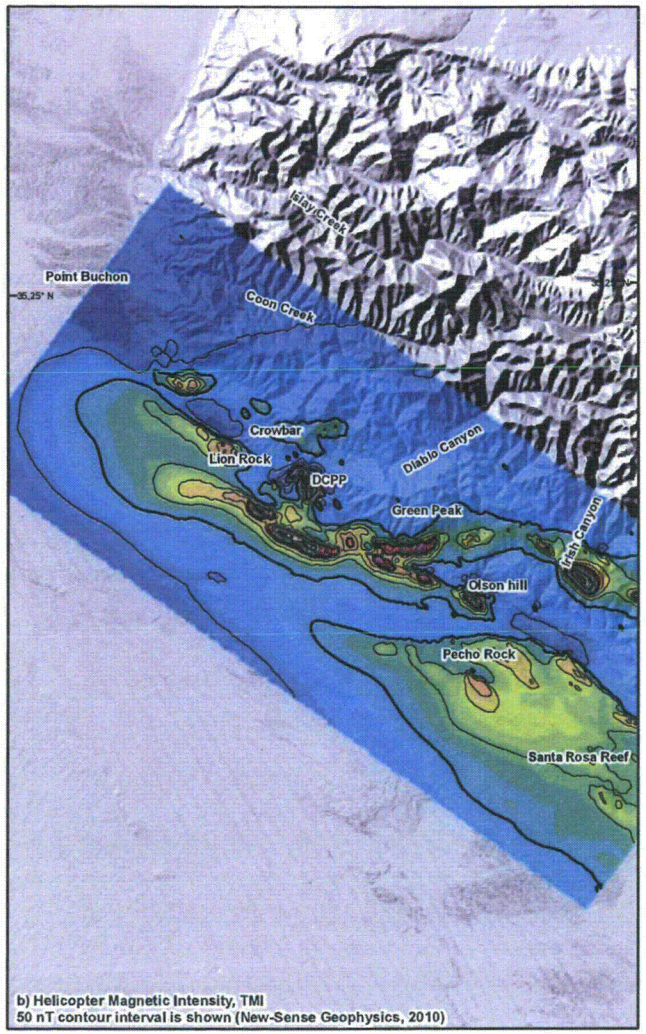

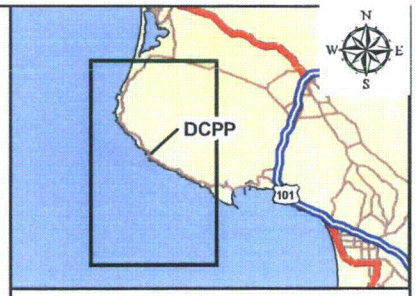

LEGEND

Helicopter Magnetics
(TMI, in nT)

Map scale: 1:100,000
Map projection: NAD 1983, UTM Zone 10 North

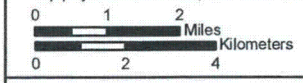

Comparison of 1989 LTSP Residual Magnetic Intensity with 2009 Helicopter Total Magnetic Intensity anomaly map

SHORELINE FAULT ZONE STUDY

Pacific Gas and Electric Company | Figure **2-4**

File path: S:\13800\138381138381138.002\Figures\20101112_Report\Appendix_D\Figure_D-1.mxd; Date: [12/21/2010]; User: Serkan Bozkurt, AMEC Geomatrix, Inc.

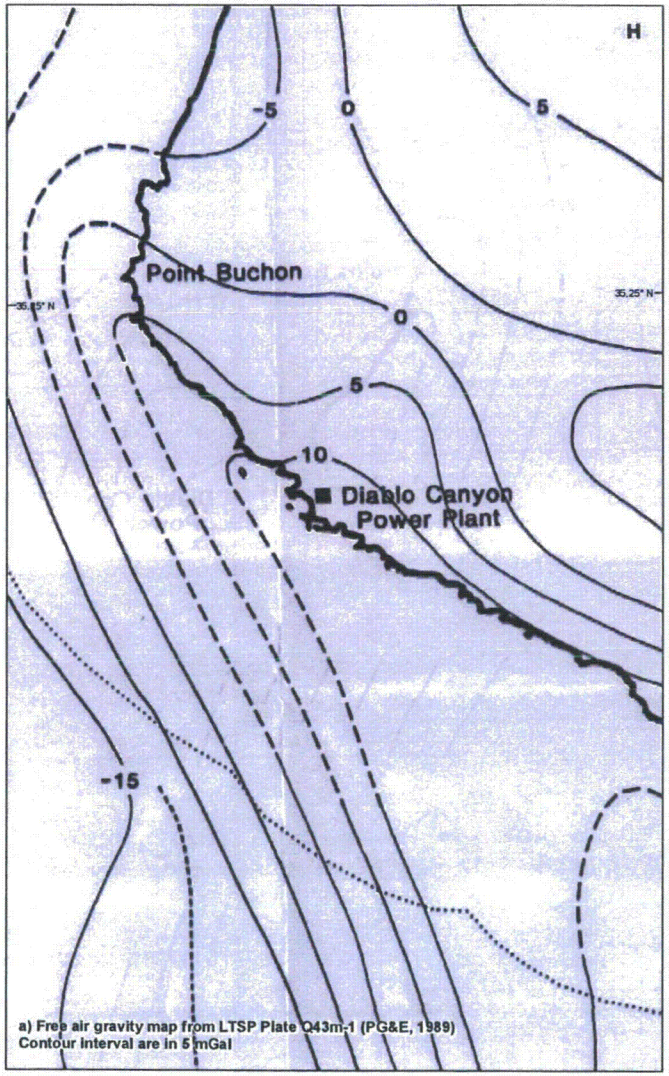

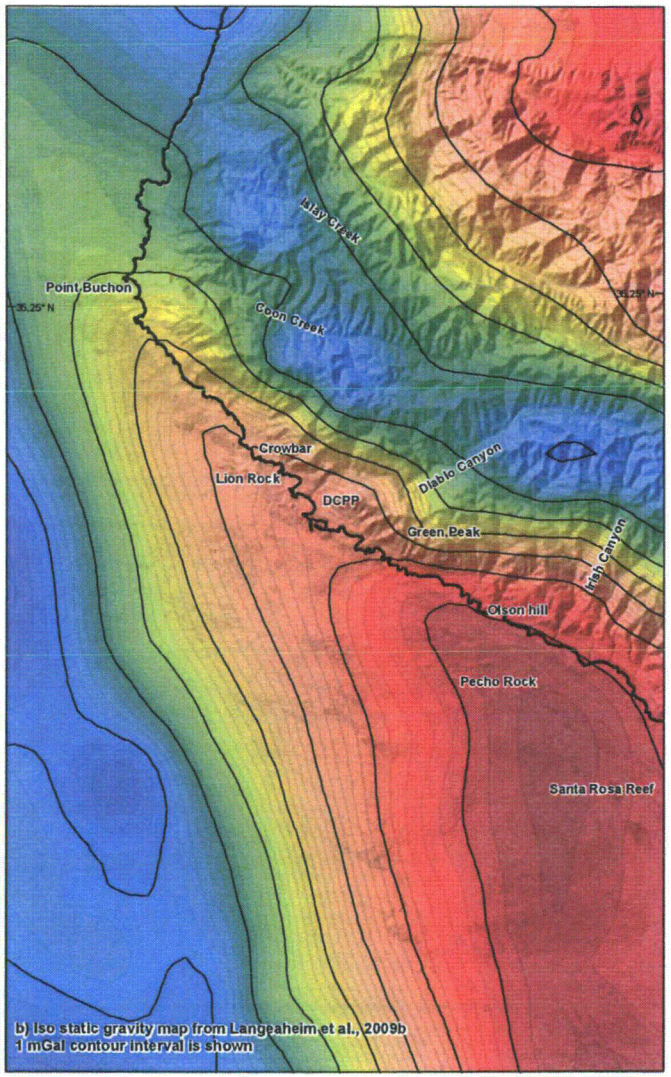

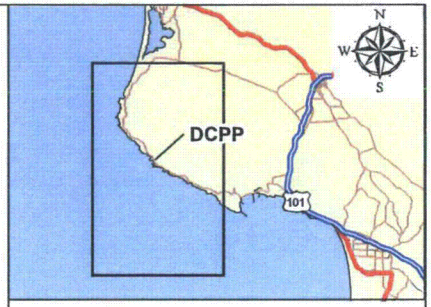

LEGEND

Isostatic Gravity (mGal)

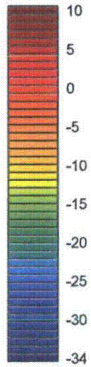

Map scale: 1:100,000
Map projection: NAD 1983, UTM Zone 10 North

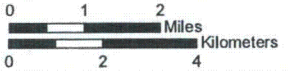

Comparison of 1989 LTSP gravity anomaly map with the 2009 USGS garvity anomaly map

SHORELINE FAULT ZONE STUDY

Pacific Gas and Electric Company | Figure **2-5**

File path: S:\13800\13838\13838.002\Figures\20101112_Report\Figure_2-5.mxd; Date: [12/21/2010]; User: Serkan Bozkurt, AMEC Geomatrix, Inc.

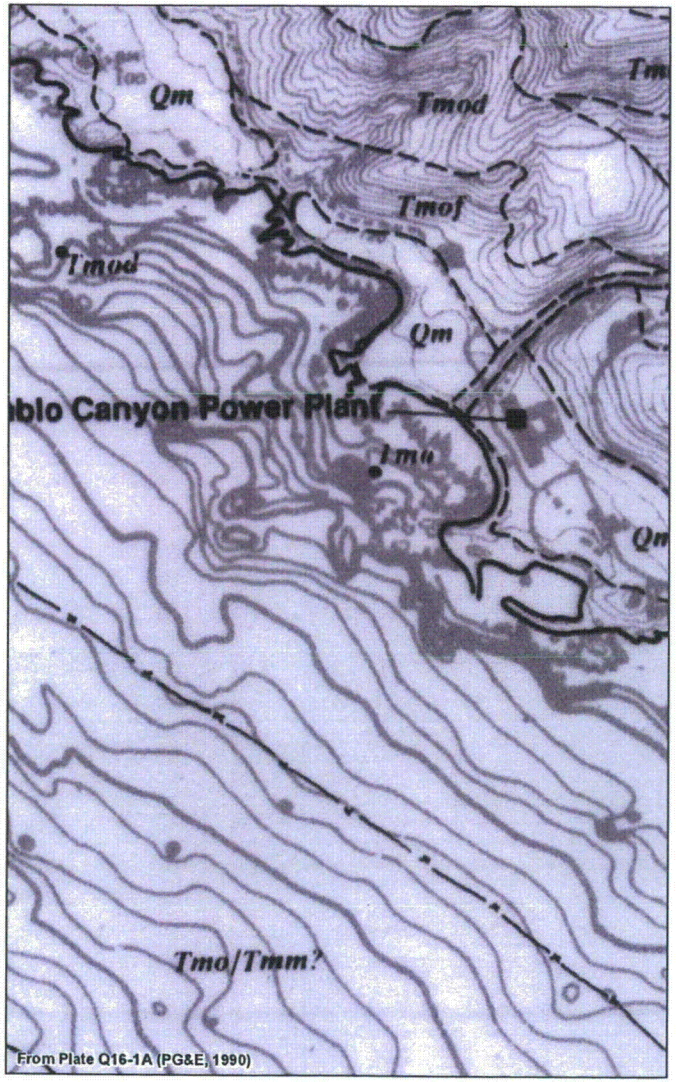

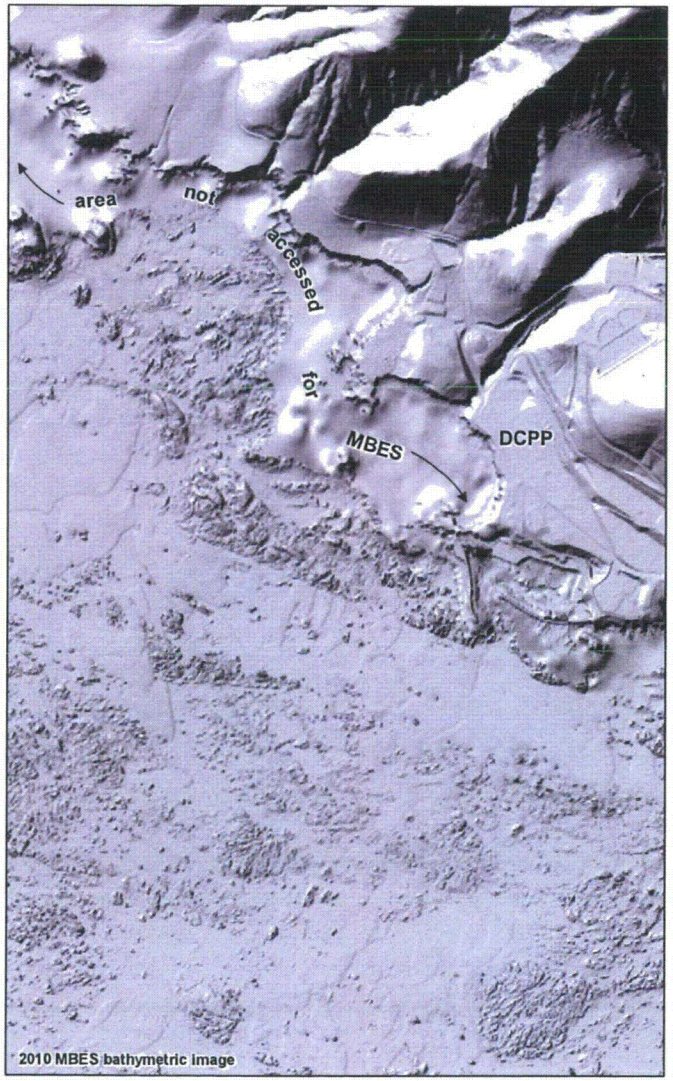

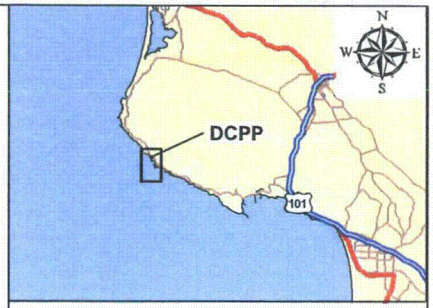

Map scale: 1:15,000
Map projection: NAD 1983, UTM Zone 10 North

0 0.1 0.2 0.3 0.4 0.5 Miles
0 0.2 0.4 0.6 0.8 Kilometers

Comparison of 1990 LTSP bathymetry with the 2009 MBES bathymetry - offshore DCPP area

SHORELINE FAULT ZONE STUDY

Pacific Gas and Electric Company | Figure **2-6**

File path: S:\13800\13838\13838.002\Figures\20101112_Report\Figure_2-6.mxd; Date: [12/21/2010]; User: Serkan Bozkurt, AMEC Geomatrix, Inc.

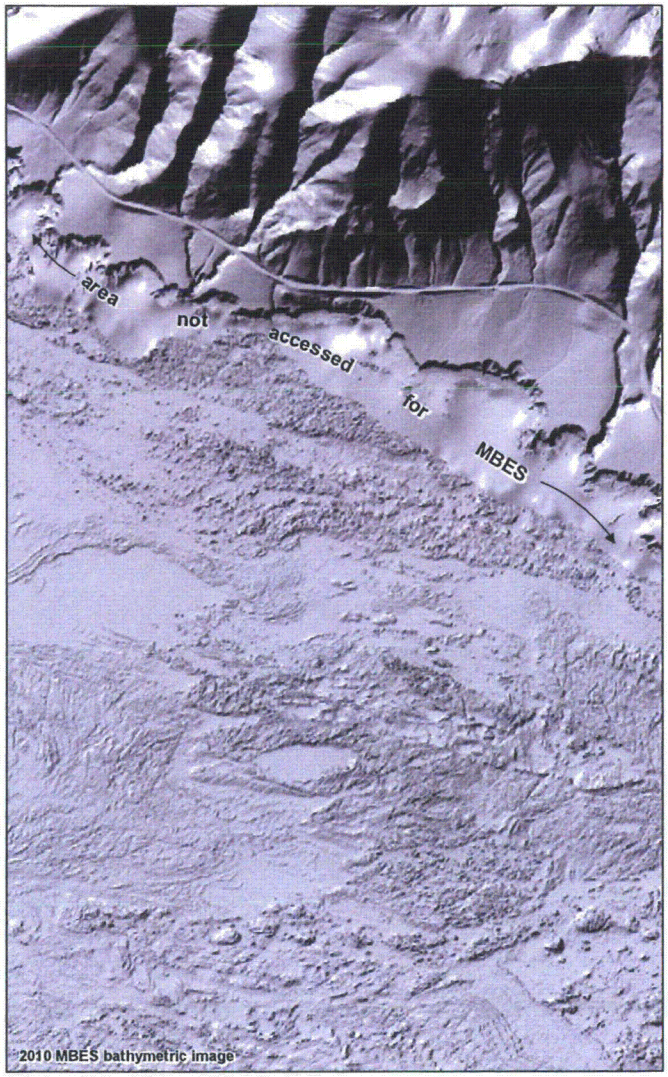

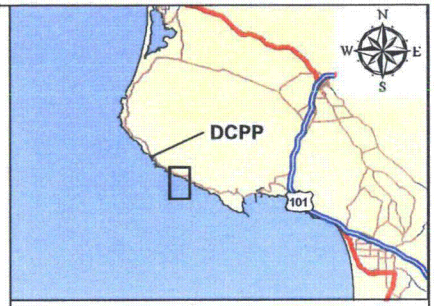

Map scale: 1:15,000
Map projection: NAD 1983, UTM Zone 10 North

0 0.1 0.2 0.3 0.4 0.5 Miles

0 0.2 0.4 0.6 0.8 Kilometers

Comparison of 1989 LTSP bathymetry with the 2009 MBES bathymetry - offshore Olson Hill area

SHORELINE FAULT ZONE STUDY

Pacific Gas and Electric Company | Figure 2-7

File path: S:\13800\13838\13838.002\Figures\20101112_Report\Figure_2-7.mxd; Date: [12/21/2010]; User: Serkan Bozkurt, AMEC Geomatrix, Inc.

3.0 REGIONAL TECTONIC AND SEISMIC SETTING

The following two sections provide descriptions of the regional tectonic setting and the associated patterns of earthquake activity in south-central coastal California. The role of the Shoreline fault zone in the tectonic and seismic setting is discussed in Section 4.

3.1 Regional Tectonic Setting

The Shoreline fault zone is located along the coastal margin of the San Luis Range in south-central California near San Luis Obispo. This region of California is characterized by transpressional deformation between the San Andreas fault zone to the east and the San Gregorio–San Simeon–Hosgri system of near-coastal faults to the west (Figure 3-1). Transpressional deformation in the region appears to be driven by three distinct but interacting processes (Lettis et al., 2009): (1) northward left transfer of slip from the San Andreas fault to the Rinconada and West Huasna faults to the Hosgri–San Simeon fault system; (2) clockwise rotation of the western Transverse Ranges domain, which imparts northerly-directed strain in the region; and (3) possible plate-normal convergence across the region.

This transpressional deformation has produced several distinct but interacting crustal domains and tectonic structures (Figure 3-1; PG&E, 1988). The Los Osos domain is a triangular region consisting of northwest-striking reverse, oblique, and strike-slip faults that border uplifted blocks and subsiding basins within the domain. To the west, the Los Osos domain is bordered by the more northerly trending Hosgri–San Simeon fault system that separates the Los Osos domain from the offshore Santa Maria basin. To the south, the Los Osos domain is bordered by the western Transverse Ranges domain. To the northeast, the Los Osos domain is bordered by the Oceanic–West Huasna fault system that separates the Los Osos domain from the more northerly trending Santa Lucia–San Rafael ranges. The northwest-trending structural grain of the Los Osos domain is transitional between the west-trending structural grain in the Transverse Ranges to the south and the north-northwest-trending structural grain of the Santa Lucia–San Rafael ranges to the northeast, and appears to be abruptly truncated to the west by the more northerly trending Hosgri–San Simeon fault system.

The geomorphology and coastal evolution of south-central California within the Los Osos domain reflects the strong influence of late Quaternary tectonic processes. A well-preserved flight of emergent marine terraces along the coast provides an excellent strain gauge from which Hanson et al. (1994, 2004) have assessed the style, rate, and extent of Quaternary deformation in the region. These studies show that the region has undergone late Pleistocene transpressional deformation accommodated by both strike-slip and dip-slip faulting, and by block uplift and subsidence.

The Hosgri and San Simeon fault zones are characterized by 1–3 millimeters per year (mm/yr) of right-lateral slip, with the rate of slip increasing from south to north along the San Gregorio–San Simeon–Hosgri fault system, ultimately to 6–8 mm/yr on the San Gregorio fault zone to the north in the San Francisco Bay area (Hanson et al., 2004). Whereas the Hosgri fault zone is offshore for its total length, the San Simeon fault zone is onshore between Ragged Point and San Simeon Point for part of its length (Hanson and Lettis, 1994; Hall et al., 1994). Focal mechanisms and the distribution of seismicity along the Hosgri fault zone document nearly pure

strike-slip on a near-vertical to steeply east-dipping fault to a depth of 12 km (McLaren and Savage, 2001; Hardebeck, 2010).

The DCPP is located on the southwestern slope of the Irish Hills (Figure 3-2) in the northern part of the San Luis Range, a prominent west-northwest-trending topographic and structural high that forms the core of one of the more prominent uplifted structural blocks (the San Luis–Pismo block) in the Los Osos domain (Lettis et al., 1990). The range is uplifting as a relatively rigid crustal block bordered by the northwest-trending Los Osos and Southwestern Boundary zone faults. Elevations and ages of the marine terraces on the southwest side of the San Luis Range show that the range is uplifting at rates of between 0.1 mm/yr to the southeast to 0.2 mm/yr to the northwest, with little or no observable internal deformation. Major geologic structures within the range, including the Pismo syncline, which cores the Irish Hills, and the San Miguelito, Edna, and Pismo faults, do not deform Quaternary deposits or landforms and are not active structures in the contemporary tectonic setting. Previously characterized active fault zones bordering the San Luis–Pismo block to the northeast, southwest, and west are the Los Osos, Southwestern Boundary (including the San Luis Bay fault zone), and Hosgri fault zones, respectively (Figure 3-2). As shown on Figure 3-1, the Shoreline fault zone is located along the southwestern margin of the San Luis–Pismo block.

3.1.1 Los Osos Fault Zone

The northeastern margin of the San Luis Range is bordered by the Los Osos fault zone, which separates the uplifting range from the subsiding or southwest-tilting Cambria block to the northeast. The fault zone has had a complex history of both strike-slip and dip-slip displacement (Lettis and Hall, 1990). The fault zone is a 50 km long, 2 km wide system of discontinuous, subparallel, and en echelon fault traces extending from Estero Bay on the north to an intersection with the West Huasna fault southeast of San Luis Obispo. Along the coast, the fault zone truncates a flight of marine terraces, indicating a vertical rate of separation across the fault zone of about 0.2 mm/yr. Preliminary results from new geomorphic mapping, interpretation of reprocessed seismic-reflection data, analysis of seismicity data, and structural analysis suggest that the fault zone dips steeply to the southeast (45 to 70 degrees or possibly steeper), and may be primarily an oblique-slip fault, with a significant component of dip slip to accommodate uplift of the range.

3.1.2 Southwestern Boundary Fault Zone

The southwestern margin of the San Luis Range is bordered by a complex zone of late Quaternary reverse, oblique-slip, and possibly strike-slip faults. Taken as a whole, these faults separate the San Luis–Pismo block from the subsiding Santa Maria Valley block to the southwest. The zone of faults is collectively called the Southwestern Boundary fault zone and is 4–10 km wide and over 60 km long (Lettis et al., 1990, 2004). The faults generally strike west-northwest and dip steeply to moderately to the northeast. Principal structures within this fault zone include the Wilmar Avenue, San Luis Bay, Pecho, Los Berros, Oceano, and Nipomo faults. The cumulative rate of vertical separation across the fault zone, based primarily on deformation of the marine terrace sequence along the coast and southwest side of the range onshore, ranges from about 0.1 to 0.2 mm/yr; the rate for each fault is generally 0.04–0.1 mm/yr.

3.1.3 San Luis Bay Fault Zone

Within the Southwestern Boundary fault zone, the San Luis Bay fault zone lies closest to the DCPP. The general location of the fault zone is well constrained onshore but is less well constrained offshore both to the east in San Luis Obispo Bay and to the west toward the Hosgri fault zone. Onshore a strand of the fault zone is exposed along Avila Beach Road, where it juxtaposes Franciscan basement over the Squire Member of the Pismo Formation and displaces an overlying marine wave-cut platform and associated marine terrace deposits (PG&E, 1990). A fault strand also displaces fluvial deposits at the mouth of San Luis Obispo Creek before extending offshore to the east into San Luis Obispo Bay. Farther east, the fault zone is interpreted to extend to a location offshore of Mallagh Landing, where it either dies out or intersects the offshore projection of the San Miguelito fault (Plate 1). The fault zone does not extend onshore east of Mallagh Landing, confirming that this is the eastern end of the fault zone.

To the northwest of Avila Beach, the San Luis Bay fault zone crosses a topographic saddle north of Point San Luis where the fault is blind, but beneath the onshore coastal terraces the fault diverges into two distinct traces or zones that deform the marine terraces. The southern trace is named the Rattlesnake fault and has a vertical separation rate of about 0.08 mm/yr. The northern trace is named the Olson fault in the LTSP documents (PG&E, 1990) and the Olson Hill deformation zone in this report (Plate 1). The Olson Hill deformation zone appears to form a monoclinal warp in the marine terraces with a total vertical separation of about 0.06 mm/yr. In contrast to the better-defined Rattlesnake fault, the deformation of marine terraces near Olson Hill cannot be attributed to any specific bedrock fault (Appendix B). The cumulative rate of vertical separation across these two parts of the San Luis Bay fault zone along the outer coast is about 0.14 mm/yr. Offshore to the west, the fault zone is interpreted to extend either to an intersection with the Shoreline fault zone (for a total fault length of 8 km) or across the Shoreline fault zone to an intersection with the Hosgri fault zone (for a total fault length of 16 km) (Appendix B).

3.1.4 Hosgri Fault Zone

The Hosgri fault zone is the southern portion of the larger 410 km long San Gregorio–San Simeon–Hosgri fault system. It is an active transpressional, convergent right-slip fault zone that extends southeastward approximately 110 km from a location 6 km offshore of Cambria to a point 5 km northwest of Point Pedernales (Hanson et al., 2004). The Hosgri fault zone lies offshore for its total length. As described above, the fault zone separates two tectonic domains of contrasting styles and rates of crustal deformation: the offshore Santa Maria basin on the western side of the fault zone and the onshore Los Osos domain on the eastern side (PG&E, 1988, 1990; Lettis et al., 2004). To the east, the fault zone truncates a marine bedrock platform associated with uplift of the San Luis–Pismo block.

The Hosgri fault zone was mapped along its entire length using petroleum industry multichannel seismic-reflection data that imaged the traces to depths of 1.5–3 km beneath the seafloor (PG&E, 1988, 1990). Part of the fault zone is remapped for this study using single-channel, high-resolution USGS sparker data (Appendix H). The USGS data set provides better near-surface resolution of the fault traces and associated structures but with limited depth of penetration. An approximate 33 km long section of the Hosgri fault zone is shown on the geologic map of the

Shoreline fault zone study area (Plate 1). The remainder of the Hosgri fault zone extends both northwest and southeast of the area on Plate 1.

Offshore of DCPP the Hosgri fault zone trends approximately N25°W to N30°W and appears to control the break between the inner and outer continental shelves. It also forms the western termination of the offshore Islay and Santa Rosa reef bedrock shelves (Appendix I) and many of the geologic structures in the Los Osos domain. As mapped from the high-resolution USGS seismic reflection data set, the Hosgri fault zone consists of multiple traces, with individual traces that are continuous for as long as 18 km. The fault zone itself is up to 2.5 km wide and contains both active and inactive traces as well as en echelon conjugate faults and folds. The fault traces appear vertical to steeply dipping in the upper few hundred meters of the sediment section. On the multichannel data, with several seconds of signal penetration, some of the traces dip steeply to the east below about 1 km depth.

3.2 Regional Seismicity Setting

Figure 3-2 shows the regional seismicity patterns (a) and focal mechanisms (b) from 1987 to 2008 from Hardebeck (2010). Earthquake activity west of the San Andreas fault zone is concentrated in several areas: (1) within the Santa Lucia Range: (2) west of the San Simeon area within the active offshore Piedras Blancas anticlinorium; (3) along and east of the Hosgri fault zone within the Los Osos domain; and (4) in the southwestern offshore region, broadly west of Pt. Arguello. The dense cluster of earthquakes along the Santa Lucia Range contains primarily aftershocks from the 2003 M_w 6.5 San Simeon earthquake (McLaren et al., 2008). The San Simeon earthquake is the largest event recorded in the region since the 1927 M_w 7.2 Lompoc earthquake. The Lompoc earthquake occurred in the southern offshore region, southwest of Point Conception.

Within the Los Osos domain, earthquakes occur primarily within the San Luis–Pismo, Casmalia, and western Los Osos blocks (Figures 3-1 and 3-2), and they extend to a depth of 12–15 km. The San Luis–Pismo and Casmalia block activity is consistent with active uplifting blocks. There is a relative lack of seismic activity within the eastern half of the Los Osos block and within the onshore Santa Maria basin. The lower rates of seismic activity in these areas suggest low rates of deformation within the down-dropped blocks of the Los Osos domain. However, the seismic activity in Estero Bay (western half of the Los Osos block) is an exception to this generalization and suggests locally active deformation within this down-dropped block.

Relatively few earthquakes have occurred west of the Hosgri fault zone from about the north end of Estero Bay to Pt. Sal (Figure 3-2a), consistent with its regional role as a significant tectonic boundary. The Hosgri fault zone as a tectonic boundary is also consistent with the truncation of the Los Osos domain by the Hosgri fault zone and the lack of mapped Quaternary faults directly west of the Hosgri.

Focal mechanisms of the region are predominantly reverse and strike-slip (Figure 3-2b) and are consistent with dextral transpressional deformation. Mechanisms beneath the Santa Lucia Range from the San Simeon aftershock zone to the area northeast of the San Simeon fault zone show predominantly reverse motion along west-northwest-trending fault planes. Along and west of the San Simeon fault zone in the Piedras Blancas anticlinorium, mechanisms are predominantly

strike-slip. Strike-slip mechanisms are also prevalent south of the San Simeon aftershock zone and along the West Huasna fault zone.

There are numerous strike-slip mechanisms along the Hosgri fault zone between Estero Bay and Pt. San Luis, and directly east of the Hosgri in Estero Bay, along the Shoreline fault zone, and onshore within the Irish Hills. Generally, the Hosgri mechanisms have nodal planes that strike more north-northwesterly compared to the northwesterly striking focal mechanisms directly east of the Hosgri fault zone. Strike-slip mechanisms along the West Huasna fault zone change from nearly north-south-striking nodal planes east of San Luis Obispo to west-northwest-striking nodal planes north of San Luis Obispo to the southern end of the 2003 San Simeon earthquake aftershock zone.

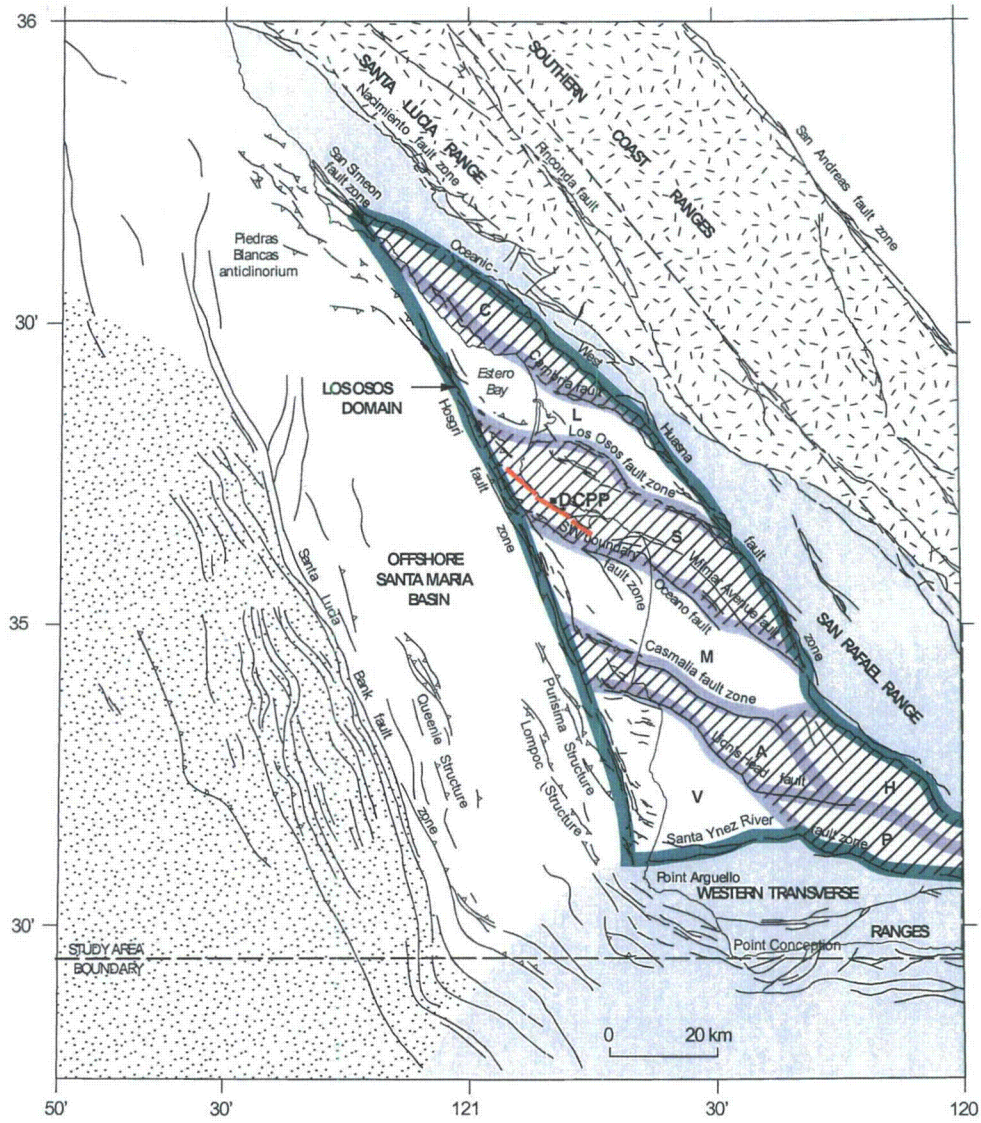

From PG&E, 1988.

- Salinian Terrane
- Stanley Mountain Terrane
- San Simeon Terrane
- Patton Terrane

} Sur-Obispo Composite (McCulloch, 1987)

Note: Orange line is schematic of the Shoreline fault zone.
Green line outlines the Los Osos domain.
Hash marks are uplifted structural blocks within the Los Osos domain.

Structural blocks within the Los Osos domain

A = Casmalia
C = Cambria
H = Solomon Hills
L = Los Osos
M = Santa Maria Valley
P = Purisima
S = San Luis/Pismo
V = Vandenberg/Lompoc

Los Osos domain

SHORELINE FAULT STUDY

Pacific Gas and Electric Company | Figure **3-1**

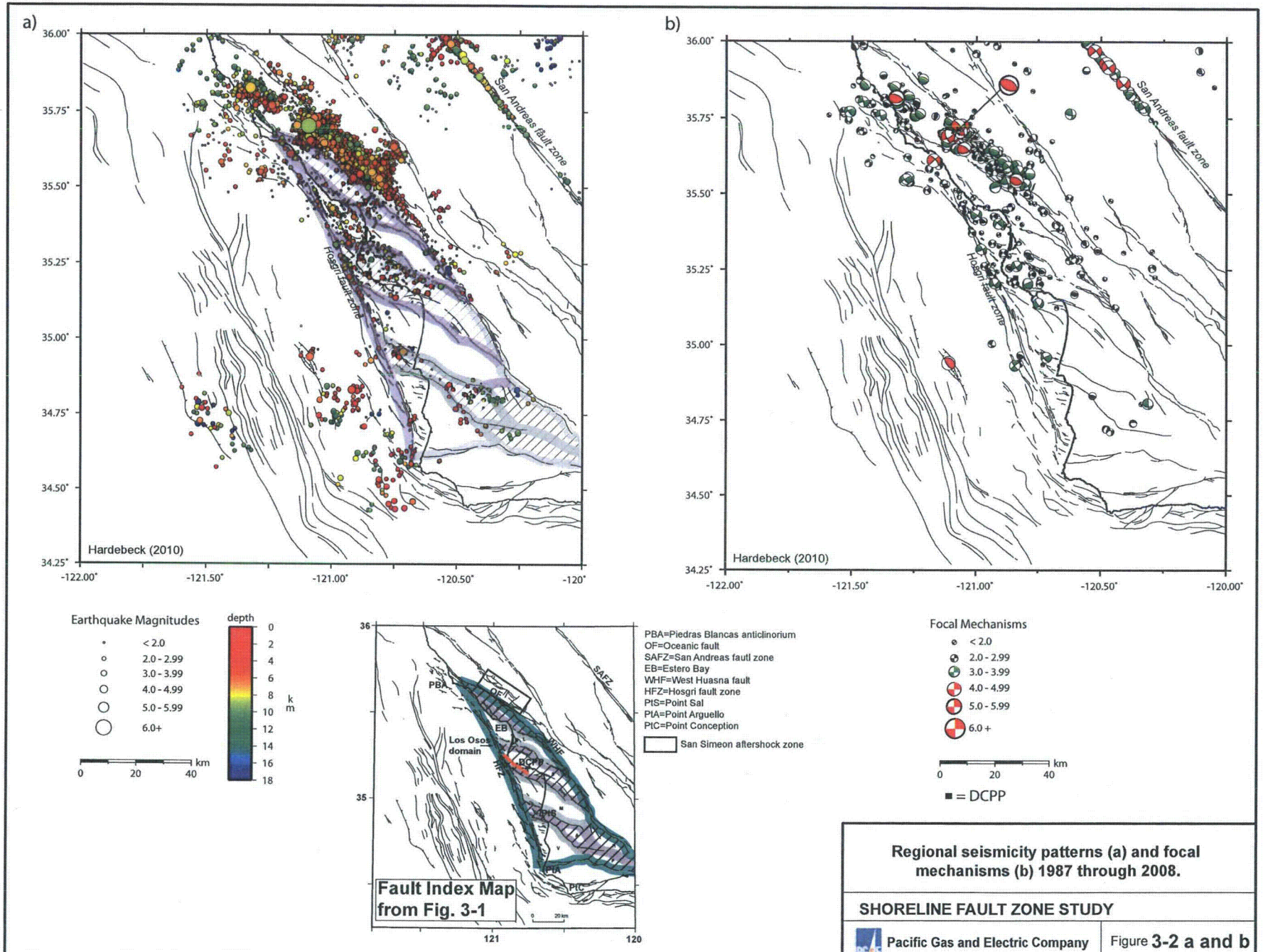

Regional seismicity patterns (a) and focal mechanisms (b) 1987 through 2008.

SHORELINE FAULT ZONE STUDY

Pacific Gas and Electric Company | Figure **3-2 a and b**

4.0 SHORELINE FAULT ZONE

The purpose of this section is to provide a detailed description of the seismic characteristics of the Shoreline fault zone as developed from extensive geologic, geophysical, and seismological data bases and analyses summarized in the previous sections. This description includes data and results considered in the Progress Report (PG&E, 2010a) and developed subsequently. The current understanding of the Shoreline seismicity lineament is discussed in Section 4.2, and the geological and geophysical characteristics of the Shoreline fault zone are discussed in Section 4.3. Section 4.4 presents the current understanding of the recency of fault activity and maximum slip rate of the Shoreline fault zone, and Section 4.5 discusses the kinematic relationship between the Shoreline fault zone and the Hosgri and Southwestern Boundary fault zones.

4.1 Introduction

Following identification of the Shoreline seismicity lineament in 2008 (published in Hardebeck, 2010), an extensive program to acquire and interpret new geological, geophysical, and bathymetric data was performed in 2009 and 2010, as described in Section 2. Based on these studies, a coast-parallel, near-shore bedrock fault zone was identified that lies within the epicentral uncertainty of the seismicity lineament. Given the close spatial association of the fault zone to the seismicity lineament, PG&E interprets that this fault zone, called the Shoreline fault zone, is producing the observed seismicity.

Plate 1 shows the location of the Shoreline fault zone in relation to the observed seismicity and the interpreted onshore and offshore geology. The earthquake data are from Hardebeck (2010) and are used as a primary basis for analysis. The onshore and offshore geologic mapping is presented in more detail in Appendix B.

The Shoreline fault zone is divided into three segments based on differences in the geologic and geomorphic expression of surface and near-surface faulting, intersections with other mapped structures, features observed in the high-resolution magnetic field data, and variations in the continuity, trend, and depth of the seismicity along the lineament. The segments of the Shoreline fault zone are named the North, Central, and South segments (Figure 4-1a). Similarly, the Shoreline seismicity lineament is divided into three distinct, en echelon sublineaments, referred to as the Northern, Central, and Southern seismicity sublineaments (Plate 1, inset). The three Shoreline fault zone segments correspond spatially in both length and location to the three seismicity sublineaments, supporting the segmented nature of the fault zone. These fault zone segments are considered as possible rupture segments in the seismic source characterization discussed in Section 5 of this report.

There are two important differences between the discussion in the Progress Report (Figure 4-1b; PG&E, 2010a) and the present report. First, the current North segment was previously referred to as the "Northern Seismicity Lineament" because at that time the evidence of faults in the bedrock using the 2008 seismic reflection data had not been seen. Second, the current N40W fault was previously referred to as the Northern Segment and was included as an inactive segment of the Shoreline fault zone in the Progress Report. Although a submerged wave-cut platform estimated to be at least 75,000 year old does not appear to be vertically offset by the N40W fault, the fault's proximity to the Northern seismicity lineament and its similarity to the

South and Central segments of the Shoreline fault zone are the basis for considering it to be an alternative northern continuation of the Shoreline fault zone in the seismic source characterization (Section 5).

The following sections provide a discussion of the Shoreline seismicity lineament (Section 4.2) and a description of the characteristics of the Shoreline fault zone (Section 4.3). Table 4-1 summarizes these characteristics and compares them to the characteristics described in the Progress Report (PG&E, 2010a).

4.2 Shoreline Seismicity Lineament

The Progress Report (PG&E, 2010a) concluded that the Shoreline seismicity lineament (Figure 4-2a) is based on accurately located microearthquakes. This conclusion was based primarily on the tests of the relative relocations by Hardebeck (2010) by independent reviewers Dr. Clifford Thurber using the tomoDD program (Zhang and Thurber, 2003) (which Hardebeck also used) and Dr. Felix Waldhauser using hypoDD (Waldhauser and Ellsworth, 2000). The results of the tests by Drs. Thurber and Waldhauser are presented in Appendix C (C-1 and C-2). Thurber performed two tests using Hardebeck's phase data and waveforms. The first test used tomoDD and Hardebeck's 3-D velocity model (Hardebeck, 2010) to successfully replicate her relocations. The second test relocated the 49 earthquakes that comprise the Shoreline seismicity lineament using tomoDD and his preferred velocity model and input parameters. Waldhauser used Hardebeck's phase data and waveforms and tested the McLaren and Savage (2001) 1-D model and the Hardebeck 3-D model in hypoDD, and Hardebeck's 3-D model in a hybrid version of his program. The results from both reviewers also showed a lineament (Figure 4-2, parts a through c, and Appendix C), although Thurber's locations are generally shifted about 0.5 km farther offshore than Hardebeck's. The pattern of Waldhauser's locations is slightly more diffuse than the patterns that the Hardebeck and Thurber locations exhibit. These comparisons show that most of the 49 earthquakes as processed by the three researchers exhibit essentially the same evidence for the interpreted seismicity lineament.

Cross sections of the three sublineaments for Hardebeck, Thurber, and Waldhauser are shown on Figure 4-2, parts d through f. Thurber's locations are approximately 1 km shallower than the Hardebeck locations. The Waldhauser hypocenter depths are quite similar to Hardebeck's. These results were used to establish the ± 0.5 km epicentral and ± 1.3 km depth uncertainties of the earthquakes comprising the seismicity lineament (PG&E, 2010a). (See Section 4.2.2 below for additional details.)

The Hardebeck (2010) seismicity lineament parallels the coast and extends for a distance of approximately 23 km from an uncertain intersection with the Hosgri fault zone on the north to south of Point San Luis on the south (Plate 1 inset). The sublineaments are separated by en echelon offsets of approximately 0.5–1 km. The Southern sublineament is the least well defined and consists of eight earthquakes, although one of these earthquakes is the largest (M_L 3.5) in the entire lineament. The Southern sublineament trends slightly more westerly than the geologically defined South segment of the Shoreline fault zone (Figure 4-2a). In cross-section view, the hypocenters form a vertical alignment to a depth of about 8 km (Figure 4-2d). The Central sublineament is well defined, both in map and cross-section views and contains 16 earthquakes (Figure 4-2, parts a and d). It forms a vertical alignment to a depth of 8–10 km and closely

aligns with the geologically and geomorphologically well-defined Central segment of the Shoreline fault zone. The Northern sublineament contains up to 26 earthquakes and is defined by more diffuse and deeper seismicity (up to 13–15 km) compared to the Central sublineament and may reflect a complex intersection with the Hosgri fault zone, as discussed in Section 4.2.4. In map view, the Northern sublineament aligns with the North segment of the Shoreline fault zone, and trends more westerly than the adjacent N40W fault, an alternative but less preferred structural association for the Northern Shoreline seismicity sublineament, as discussed in Sections 4.2.4 and 4.3.

In the following sections, additional analyses and details of the Shoreline seismicity lineament are provided, including earthquake statistics and earthquake location uncertainties, analyses of epicentral and hypocentral patterns, and an analysis of the association of the Northern seismicity sublineament with the Hosgri fault zone. A description of pre-1988 historical earthquakes within the Shoreline fault zone study area is also provided.

4.2.1 Seismicity Lineament Data Statistics

A total of 49 earthquakes occurred between 1988 and 2008 within the seismicity lineament as defined by Hardebeck (2010). The magnitude range is 0.8 to 3.5 and the depth range is 2–15 km. The magnitude 3.5 earthquake occurred on 10 August 2000 at the southern end of the Southern seismicity sublineament. This earthquake is reported as a local magnitude (M_L) event, and the other earthquakes ($M \leq 2.9$) are reported as duration magnitudes (M_d). The M_L 3.5 event is classified as a small event, whereas the smaller earthquakes are classified as microearthquakes (Lee and Stewart, 1981).

Thurber's preferred data set contains 43 earthquakes (Appendix C). The 6 earthquakes not used by Thurber are either (1) earthquakes that relocated away from the lineament formed by most of the earthquakes or (2) earthquakes that were removed from the final data set because their computed locations were unstable. An example is the M_L 3.5 event, which was not included in Thurber's final run because its location was above the ground surface. In contrast, Hardebeck's relocation for this event was stable and converged at a depth of 3.7 km depth using her parameters in tomoDD.

The earthquakes that comprise the seismicity lineament have occurred fairly uniformly over time between 1987 and 2008 (Figure 4-3a) at an average rate of about 2.3 earthquakes per year. Figure 4-3b is a log-linear plot of the cumulative number of Shoreline lineament earthquakes versus magnitude. From this plot, the magnitude level of completeness is approximately 1.3. A *b*-value of 0.93 is estimated using the method of Weichert (1980). This value is consistent with the *b*-value of 0.91 from Reasenberg and Jones (1994) for their Southern California recurrence model.

4.2.2 Earthquake Location Uncertainties

There are three key factors considered in estimating earthquake location uncertainties for the offshore earthquakes of the Shoreline seismicity lineament, as discussed in the following two subsections. The three factors are the effect of limited azimuthal distribution of the on-land seismographic stations in the effort to triangulate the offshore earthquake locations, the level of accuracy of the velocity model, and the proximity of the closest stations to the epicenter. In the

third subsection, the method used to estimate the average location errors for the 49 earthquakes that comprise the lineament is explained.

Offshore Earthquake Locations

The accuracy of earthquake locations is directly related to seismographic station numbers and spacing. Figure 2-2 shows that the seismographic coverage in the central coast region has evolved and improved with time (McLaren and Savage, 2001). The main network design factors that contribute to robust earthquake locations are seismographic station spacing, azimuthal coverage, and accurate S-wave and P-wave arrival times. The closest station distance controls the depth accuracy, and azimuthal coverage controls the epicentral accuracy. The integrated PG&E–USGS station spacing is about 10–15 km within about 30 km from the coast. This station distribution translates to fairly good depth control for onshore earthquakes in the depth range of 5–10 km. Offshore earthquakes, such as those occurring along the Shoreline seismicity lineament 0–3 km offshore, have the inherent problem of lack of adequate station distribution, resulting in gaps of azimuthal coverage generally greater than 180 degrees and reduced depth control as the distance offshore increases. The five PG&E 3-component analog stations that have been in operation since 1987 have compensated somewhat for the lack of station distribution by improving the accuracy of picking S-wave arrivals. Since 2006, the PG&E station upgrades have improved data quality, but the basic geometry of monitoring the offshore has not changed.

Accuracy of the Velocity Model

An accurate velocity model is also important for accurate absolute locations of earthquakes. Traditionally, inverting arrival time data for catalog locations has been accomplished using a 1-D velocity model and applying it across a region with station corrections that compensate for path effects (e.g., *Hypoinverse*; Klein, 2002). Three-dimensional velocity modeling is used to account for lateral variations in structure, and relative arrival times from waveform cross-correlation and double-difference methods are used to image seismicity features more sharply, such as was done by Hardebeck (2010).

For Hardebeck's San Luis Obispo subregion, which includes the Shoreline and Hosgri fault zones, her velocity modeling results in a reduction in the root mean square (RMS) of the cross-correlation relative arrival times from 0.39 seconds from the 3-D starting model to 0.005 seconds for the final 3-D model. Hardebeck performed a validation of the model by relocating known blasts from a 1986 reflection/refraction program. The blasts occurred both onshore and offshore. The offshore blasts were located about 10 km north and south of the Shoreline seismicity lineament, in Estero Bay and San Luis Bay (Hardebeck, 2010, Fig. 5). The RMS shift from the true shot locations is 1.2 km horizontally and 1.3 km vertically, with the largest shift in the offshore shot locations. The location errors in the offshore blasts are an indication that as long as the earthquakes and blasts are occurring outside the network, there will be an inherent error or uncertainty in their locations.

Uncertainties from Comparing Earthquake Locations Using Different Location Methods

Earthquake location uncertainty is estimated using Hardebeck's, Thurber's, and Waldhauser's uncertainty estimates and the uncertainties based on the average horizontal and vertical shifts of the earthquake locations within the lineament that were obtained from the Hardebeck and Thurber relocations. Table 4-2a lists the absolute and relative uncertainty estimates for the three

results. Table 4-2b lists the average and median differences between the various location methods, 1-D, 3-D, and tomoDD.

Hardebeck (2010) estimated the absolute earthquake location uncertainty by relocating shots with known locations. For 13 shots located inside her 3-D velocity model, the RMS shift from the true location was 0.9 km horizontal and 1.3 km vertical. She concluded that the absolute uncertainty of the earthquake locations, which should be better located than the shots, was ≤ 0.9 km horizontal and ≤ 1.3 km vertical. She acknowledges that the offshore shot location errors are larger.

Hardebeck also estimated uncertainties for her San Luis Obispo region based on the stability of the locations determined using various location methods. The median absolute shift between her hypoDD and 3-D locations is 470 m horizontal and 450 m vertical. The median absolute location shift between her hypoDD and tomoDD locations is 390 m horizontal and 510 m vertical.

In a similar approach, the location results are compared between 1-D, 3-D, Waldhauser's hypoDD, and Thurber's preferred tomoDD locations specifically for the earthquakes that comprise the Shoreline seismicity lineament. The averages and standard deviations are described in Table 4-2b. The average and median shift values between the two tomoDD runs are similar. For this report, the more conservative average horizontal shift of 0.51 km and average vertical shift of 1.33 km were chosen for use in evaluating the significance of location uncertainties.

4.2.3 Relation of the Shoreline Seismicity Lineament to Earthquakes Prior to 1988

Earthquake records prior to the deployment of the PG&E seismic network in 1988 were searched to evaluate whether additional earthquakes have occurred on the Shoreline seismicity trend. The search can be broken down into two time intervals: earthquakes prior to 1970 and earthquakes between 1970 and 1987.

Earthquakes Prior to 1970

A search of the historical database prior to 1970 and prior to local seismic networks (NCEDC, 2010; McLaren and Savage, 2001) showed two M 5 earthquakes that occurred in 1913 and 1916 in the vicinity of the seismicity lineament in the past 100+ years. Considering the location uncertainty of 10–20 km (PG&E, 1988; McLaren and Savage, 2001) for these events, it is possible that they could have been associated with the South segment of the Shoreline fault zone or one of the faults in the Southwestern Boundary fault zone. The 10 km radius circles of uncertainty are shown on Figure 4-4 for the two events. These earthquakes are discussed in the following paragraphs.

- 20 October 1913: This earthquake was located by Toppozada (1987) in the offshore region near Pismo Beach and Arroyo Grande. It was strongly felt in Pismo Beach and Arroyo Grande and as far south as Santa Barbara and Carpenteria. McLaren and Savage (2001) noted that it could have occurred on a fault within the Southwestern Boundary fault zone. The published location is about 5 km southeast of the easternmost seismicity in the Shoreline seismicity lineament.

- 1 December 1916: This earthquake occurred north of the 1913 event. Bolt and Miller (1975) located it directly offshore of Avila Beach in San Luis Obispo Bay, although the published coordinates place it north of Avila Beach. Some of the Union Oil refinery smokestacks toppled over. Landslides were reported in the canyon behind Avila and in Dairy Canyon, 2 miles north of Avila, and the event was strongly felt in San Luis Obispo (McLaren and Savage, 2001). A local newspaper article also reported, "... an upheaval of the waters in the Bay of San Luis Obispo, as the trembling continued out to sea" (McLaren and Savage, 2001). Avila Beach is about 4 km northeast of the southern end of the Shoreline seismicity lineament.

Earthquakes from 1970 to 1987

The USGS catalog data from 1970 to 1987 shows 3–5 microearthquakes in the vicinity of the Shoreline fault zone (Figure 4-5a), allowing for possible large errors in their routine locations. Hardebeck relocated these earthquakes using hypoDD and the 3-D velocity model she developed using the post-1987 data (Hardebeck, 2010). Her results showed that only one of these microearthquakes is likely to have occurred within the Shoreline seismicity lineament (in the Southern sublineament) during this time period (Figure 4-5b).

4.2.4 Data Interpretation

This section discusses the relationship between the seismicity patterns and other features of the Shoreline seismicity lineament and the geologic structure of the Shoreline fault zone. The interpretation of the relationship between the Hosgri fault zone and the Shoreline fault zone is also discussed.

Comparison of Lineament Patterns

A comparison of Hardebeck's relocations to those of Thurber and Waldhauser (Figure 4-2) show that although the earthquake patterns between the results vary somewhat, they are consistent within the bounds of the ± 0.5 km epicentral location uncertainty and the ± 1.3 km vertical uncertainty estimated for the Hardebeck locations. Figures 4-2a-c show quite similar seismicity lineaments in map view among the three different relocation efforts, particularly along the Central and Southern sublineaments. The cross-section views (Figures 4-2d-f) show similar hypocentral patterns of scattered activity between about 2 and 10 km depth in the Southern and Central sublineaments, a fairly abrupt deepening of seismicity to 12–15 km at the south end of the Northern sublineament, and a diffuse zone of deep earthquakes along the Northern sublineament as it approaches the Hosgri fault zone. A general result of this comparison is that, while there are slight differences in the detailed patterns of each of the three maps and sets of vertical sections, such as variations in depth groupings and slight differences in the locations of offsets of epicenters along the mapped alignments, there are no compelling reasons not to accept all the relocations as defining (within the selected uncertainty bounds) a vertical surface that is deeper to the northwest and gently sinuous in map view.

As stated in the Progress Report (PG&E, 2010a), a pronounced seismicity lineament along the southern Irish Hills coast was not previously identified using 1-D catalog locations, as shown on Figure 4-6a. What was visible was a scattering of earthquake epicenters between the coastline and the Hosgri fault zone and staying within about 4 km of the coastline toward Point San Luis to the southeast. Previously, PG&E interpreted this diffuse pattern as due to scattered activity

along small faults that likely branched off the Hosgri fault zone (Plate 3, PG&E, 1988), and possible seismicity related to the Olson Hill deformation zone. On Figure 4-6b, Hardebeck's 3-D locations also show scattered events within the same broad swath as Figure 4-6a; Figure 4-6b also shows the narrow, linear feature now called the Shoreline seismicity lineament.

In general, the results of both 1-D and 3-D absolute location methods often yield seismicity maps that do not resolve seismicity lineaments and other features that can be associated with active geologic structures, especially in an offshore region and outside spatially restricted seismic networks (see Thurber's review, Appendix C). The sophisticated earthquake relocation techniques such as those developed and applied by Thurber, Waldhauser, and Hardebeck are intended to provide more highly resolved relationships between microearthquake and larger earthquakes and the geologic structure of active tectonic and volcanic regimes. For example, McLaren et al. (2008) used hypoDD to relocate the 22 December 2003 San Simeon earthquake and aftershocks. Their results were able to resolve the relationship of the main shock to the main fault plane and backthrust plane defined by the aftershocks.

Compared to the 1-D locations, most of the 3-D offshore epicenters, including the earthquakes on the Hosgri fault zone, shift about 0.5 km to the east (Figure 4-6a–b). This systematic change in a group of relocated earthquakes is a normal product of the application of advanced relocation technology, including better-calibrated 3-D seismic velocity models. While such relocations usually provide better resolution of possible geometric or structural features of the seismicity, the locations may still have systematic biases largely due to remaining errors in the velocity model used in the relocations. Therefore, it is important to use high-resolution geophysical and geological techniques to attempt to constrain the location and geometry of the geologic structure in the vicinity of the structures that have been resolved in the seismicity data. In particular, the absolute locations of geologic structures such as the Shoreline fault zone are determined by other investigations discussed in this report, not by the seismicity. The spatial features of the Shoreline seismicity lineament (including consideration of the hypocentral location uncertainties) that are inferred to reflect structural features at depth are evaluated with respect to the geometry and other characteristics of the independently determined surface and subsurface geologic structures. In combination, these data are used to assess the potential for the geologically defined Shoreline fault zone to be the structure that is releasing the observed seismicity and possibly larger future earthquakes.

Shoreline Seismicity Lineament Focal Mechanisms

The focal mechanisms shown on Figure 4-7 are from Hardebeck (2010) using the program HASH (Hardebeck and Shearer, 2002) and from the USGS catalog using the algorithm FPFIT (Reasenberg and Oppenheimer, 1985) that uses P-wave first-motion data from earthquakes located with a 1-D velocity model. HASH computes P-wave first-motion focal mechanisms using takeoff angles observed from ray tracing in the 3-D seismic velocity model. FPFIT is a grid-search algorithm that finds the best double-couple solution. The FPFIT mechanisms have been filtered to include only those earthquakes with unique, good-quality solutions that use 25 or more P-wave first motions and that have converged to the solution by finding the minimum misfit solution.

HASH assigns mechanism quality (A, B, C, and D) based on the solution stability with respect to the uncertainty in the take-off angles and polarity observations. Quality D mechanisms are from

those earthquakes that did not meet the criteria of Quality A to C earthquakes, but were considered adequate upon examination of the polarity data (at least 6 P-wave first motions) and the computed focal mechanisms (Hardebeck, 2010). Hardebeck (2010) also computed composite focal mechanisms for selected sets of earthquakes in the offshore and southern parts of the study area where there was limited azimuthal coverage. She grouped together earthquakes that were clustered in space (Figure 4-7).

Due to the stringent nature of the acceptance parameters, including robust azimuthal station distribution, Hardebeck's highest quality focal mechanisms (Qualities A to C) are all onshore (Figure 4-7). The offshore focal mechanisms thus include her Quality D and composite focal mechanisms and the FPFIT mechanisms from the USGS Northern California Earthquake Data Center catalog (http://www.ncedc.org/ncedc/catalog-search.html).

The offshore focal mechanisms on Figure 4-7 show predominantly strike-slip motion, particularly along the Hosgri fault zone and the Central sublineament of the Shoreline seismicity lineament. Scattered throughout are reverse and oblique-reverse focal mechanisms, and a few normal mechanisms. Focal mechanisms near the Northern sublineament are predominantly strike-slip and oblique-reverse. Mechanisms along the Central sublineament, including the composites, show consistent right-lateral, strike slip along northwest-trending fault planes, consistent with the orientation of the Central sublineament. Mechanisms along the Southern sublineament show normal and oblique-normal fault motion. The northeast-trending nodal planes of the pure normal mechanism at the south end of the Southern seismicity lineament, which is a Quality D focal mechanism, are not consistent with either the mapped orientation of the northwest-trending southern sublineament, or with Hardebeck's composite mechanism (Figure 4-7). The HASH mechanism for the M_L 3.5 event near the end of the Southern sublineament shows normal-oblique motion along a northwest-trending fault plane and is consistent with the mapped lineament orientation. The nearly pure strike-slip FPFIT mechanism for the M_L 3.5 event and Hardebeck's strike-slip composite mechanism for the small group of earthquakes near the M_L 3.5 event is evidence that the Southern sublineament is dominantly strike-slip, but with some normal-oblique fault motion.

Association of the Northern Seismicity Sublineament with the Hosgri Fault Zone
As described in the previous subsections of Section 4.2, the seismicity characteristics of the Southern and Central sublineaments have the following attributes:

- Earthquake epicenters are located along a nearly straight-line segment within the horizontal location uncertainty of 0.5 km.
- Earthquake hypocenters are distributed nearly vertically beneath the nearly straight line of the sublineament.
- The deepest earthquakes associated with either sublineament are no deeper than 10 km (8 km for the Southern sublineament).
- The predominant style of faulting as exhibited by focal mechanisms is right slip along a plane parallel to the strike of the lineament; however, there are outliers in each segment.

The pattern of the Northern seismicity sublineament, however, varies over its length. Beginning at its southeast end, the lineament exhibits the same characteristics as the Central and Southern

sublineaments, with the exception that the southeastern half of the Northern sublineament does not have any focal mechanism data.

However, as the projected Northern sublineament approaches the Hosgri fault zone, the following changed characteristics are observed:

- Earthquake epicenters diffuse outside of the collinear pattern defined by 0.5 km uncertainty (Plate 1 and Figure 4-8a), and it is not clear where the seismicity associated with the lineament ends and the seismicity associated with the Hosgri fault zone begins.
- Focal mechanisms include greater diversity than predominantly strike-slip (Figure 4-8a).
- Focal mechanisms at the western end have planes rotated closer to the strike of the Hosgri.
- The trend of the Northern sublineament is more northerly than the other two sublineaments, and appears to be bending northward.

This interaction is ultimately significant to interpreting the relationship between the Shoreline fault zone and the Hosgri fault zone, so it is extensively explored. To begin, the seismicity and focal mechanisms are projected onto cross sections perpendicular to the Hosgri fault zone and the Shoreline seismicity lineament, A-A′ and B-B′ on Figures 4-8a and 4-8b. The earthquakes that define the Northern seismicity sublineament are plotted in red in both cross sections for comparison. Also shown on cross section A-A′ are (1) the projection of an interpreted nearby common-depth point (CDP) seismic-reflection profile (Comap profile GSI-85; PG&E, 1988) showing the two steeply east-dipping branches of the Hosgri fault zone (cross section K-K′), and (2) linear projections of four possible average dip angles of the Hosgri fault zone ranging from 90 to 70 degrees to the northeast. Overall, the seismicity projected normal to the Hosgri fault zone (cross-section A-A′) fit reasonably well along an 80- to 85-degree east-dipping fault zone, especially when the red earthquakes of the Shoreline seismicity lineament are included below depths of 11 km. This pattern is consistent with the steeply east-dipping faults interpreted from the 1986-vintage CDP seismic reflection profile, and suggests that a viable alternative explanation for at least some of the earthquakes along the Northern seismicity sublineament is that they are part of the Hosgri fault zone, and not part of a separate Shoreline fault zone.

More detailed interpretations of the Hosgri fault zone at depth based on the seismicity data are ambiguous. For example, it is not clear whether the locations and focal mechanisms of the shallow earthquakes between about 3 and 8 km deep at the west side of cross section A-A′ are showing a vertically dipping west branch of the Hosgri fault zone or a steeply east-dipping west branch that connects with the central and east branches of the Hosgri fault zone below about 7 km depth. However, the strike-slip focal mechanisms of these shallow earthquakes are consistent with a vertically dipping west branch. Also, whereas the seismicity is not consistent with a Hosgri fault zone dipping approximately 70 degrees northeast or less to depth, the data cannot distinguish between a steeply (approximately 80 degrees) northeast-dipping Hosgri fault zone to depth and a northeast-dipping fault zone in the upper few kilometers (as interpreted from the CDP seismic reflection profile) that steepens to subvertical at depth.

In comparison to the diffuse seismicity projected normal to the Hosgri fault zone (cross section A-A′), the red earthquakes attributed to the Shoreline seismicity lineament plot in an aligned,

vertical pattern in cross section B-B′. The earthquakes between about 11 and 13 km that provide a reasonable fit to an 80- or 85-degree northeast-dipping Hosgri fault show a distinct vertical pattern on the Shoreline cross section B-B′. The earthquakes between about 4 and 9 km depth show an overall subvertical alignment, and in detail suggest a zigzag pattern that may indicate along-strike structural complexity. Also, focal mechanisms in this depth range show reverse and reverse-oblique fault motion along varying fault planes. As there are no earthquakes located shallower than about 4 km, the updip projection of the causative fault zone is unclear. Alternatives include (1) a buried fault that does not penetrate the upper few kilometers of crust; (2) an emergent, subvertical fault that coincides with the North segment of the Shoreline fault zone; and (3) an emergent fault that coincides with the more northerly striking N40W fault (Plate 1 and Section 4.3.1). Thus, whereas much of the seismicity along the Northern sublineament may record activity on the Hosgri fault zone, the overall pattern supports the preferred interpretation that the seismicity is associated with a distinct subvertical fault, the North segment of the Shoreline fault.

4.3 Geological and Geophysical Characterization of the Shoreline Fault Zone

Additional investigations completed since the Progress Report (PG&E, 2010a) have led to an improved understanding of the fault, including information on fault location, geometry, segmentation, slip rate, and relationship to the Hosgri fault zone, Southwestern Boundary fault zone, and older Tertiary structures.

The nomenclature used in this report for the Shoreline fault zone is presented in Table 4-1 and Figure 4-1. The characteristics of the Shoreline fault zone were developed from the following:

- Geologic and geomorphic interpretation of MBES bathymetric imagery (Appendix B).
- Assessment of submerged marine terraces from MBES bathymetric imagery and high-resolution seismic-reflection profiles (Appendix I).
- Correlation of geologic units and structures onshore and offshore (Appendix B) using a low-tide LiDAR base map (Appendix G).
- Reinterpretation of offshore diver and core samples from the LTSP and collection of 50 additional samples (Appendix B).
- Interpretation of high-resolution seismic-reflection profiles acquired in 2008 and 2009 (Appendix H) and seismic-reflection profiles from the LTSP (PG&E, 1988).
- Analysis of magnetic-field data from helicopter and ship-born measurements (Appendix D).
- Evaluation of the earthquakes associated with the Shoreline seismicity lineament (Section 4.2).

This section describes the location, length, faulting style, dip, activity, slip rate and relationship of the Shoreline fault zone to other faults in the region. The Shoreline fault zone is presented in its entirety on Plate 1 at 1:35,000 scale. Several comparative maps illustrate the interpretations of geology and submerged marine terraces with the MBES bathymetric imagery along the N40W fault and the Central and South segments of the Shoreline fault zone at key locations at a more detailed 1:12,000 scale. These comparative maps highlight the following areas: (1) west of Lion Rock, (2) directly west of DCPP, (3) directly south of DCPP, (4) southwest of Olson Hill, (5) west of Rattlesnake Creek, and (6) southwest of Point San Luis (Figures 4-9 to 4-15). In this

section, the alternative interpretations and uncertainties in the fault characteristics are explicitly discussed to provide the rationale for establishing the range of fault parameters in the logic tree characterization presented in Section 5.

The Shoreline fault zone appears to be a locally reactivated preexisting fault. Although the preexisting fault is not reflected in the regional gravity data (Figure 4-16), this older fault is associated with a distinct, linear magnetic anomaly as seen in the high-resolution helicopter magnetic field data (Appendix D and Figure 4-17). The magnetic field associated with the older fault zone is probably from serpentinite or greenstone lenses within Franciscan mélange along the portion of the fault between about Olson Hill and offshore Point San Luis (Figure 4-18). Juxtaposition of magnetic (e.g., greenstone) against nonmagnetic (e.g., sandstone) blocks of pre-Tertiary rock along the older fault zone accounts for the strong contrast in the magnetic field strength. The prior episode of faulting dates to late Miocene and perhaps Pliocene time that probably occurred either during a regionally recognized mid-Miocene to early Pliocene period of transtensional deformation or during a later middle to late Pliocene period of transpressional deformation (PG&E, 1988 and references therein).

The current transpressional deformation regime began in about the middle Pliocene, coincident with reorganization of the Pacific-North America plate boundary (Lettis et al., 2004 and references therein). This reactivated several faults bounding the Irish Hills and the rest of the San Luis Range. Since one to two million years ago, the mode of deformation in the Irish Hills switched from folding to block uplift (Lettis et al., 2004; Hanson et al. 1994). Some but not all of the structures active during the earlier episodes of faulting have been reactivated in the current tectonic regime. Quaternary erosion during periods of lower sea level or during transgressions to sea-level highstands has enhanced the geomorphic expression of preexisting faults formed during the prior episodes of faulting, producing a prominent series of bathymetric lineaments and associated scarps. For example, the prominent escarpment off the coast of Point Buchon that coincides with the N40W fault (Appendix B; Plate 1) appears to be the result of differential erosion rather than late Pleistocene faulting (Section 4.4.2).

The South and Central sublineaments of the Shoreline seismicity lineament align with sections of the preexisting Tertiary fault (within the 0.5 km resolution of the epicenters), indicating that the older fault has been locally reactivated in the current stress regime. Seismicity along the Northern sublineament, however, trends northwest toward the Hosgri fault zone and lies west of the N40W fault (Plate 1). Late Quaternary marine deposits and ephemeral drifting sand sheets on the seafloor mask any geomorphic expression of a fault and any direct surface observation of geologic structure that may be associated with the Northern seismicity sublineament. The origin of the Northern seismicity sublineament and direct linkage to a bedrock fault, therefore, is less certain than for the Central and Southern sublineaments of the seismicity trend. As described in Section 4.2.4, alternative structural origins of the Northern seismicity sublineament include (1) a steeply east-dipping Hosgri fault zone; (2) a subvertical fault (buried or emergent) coincident with the seismicity sublineament; and (3) the N40W fault, with a steeply west-dipping shallow crustal portion to link the surface trace of the fault with the seismicity trend. As discussed in Section 4.2.4, the analysis of the seismicity is the basis for preferring the subvertical fault model.

Three methods are used to evaluate whether a direct structural link can be made between the Hosgri fault zone and a distinct causative fault associated with the Northern seismicity sublineament:

1. Reexamination of the USGS high-resolution seismic-reflection profiles that cross the Northern seismicity sublineament.
2. Reprocessing of three of these high-resolution seismic-reflection profiles to improve data resolution.
3. Reexamination of 1980s-era high-energy Comap CDP seismic-reflection profiles interpreted during the LTSP (PG&E, 1990) that cross the Northern seismicity sublineament and the N40W fault trend.

Reexamination of an earlier Comap CDP seismic-reflection profile (CM-21) collected across the northern end of the Northern seismicity sublineament reveals gently folded Tertiary strata east of the Hosgri fault zone with no evidence of faulting across the Northern seismicity sublineament to the limit of the resolution of the Comap data (Figure 4-19). In contrast, this Comap seismic-reflection profile shows disruptions in reflectors consistent with faulting or tight folding across the nearby N40W fault.

Reprocessed high-resolution seismic-reflection profiles at the northern and southern ends of the Northern seismicity sublineament provide significant improvement in overall data clarity compared to the basic processing by the USGS. Although the seismic-reflection data are still insufficient to resolve definitively the presence or absence of faulting, careful reexamination of the high-resolution profiles crossing the central portion of the Northern seismicity sublineament permits an interpretation of minor vertical separations across subvertical faults in Tertiary strata that are plotted on Plate 1 as two concealed, queried, en echelon faults. The southwestern fault follows the axis of a well-expressed syncline in Tertiary strata and the fault to the northeast is subparallel to the syncline. These faults generally align with the Northern seismicity sublineament. Preliminary estimates of vertical separations are on the order of 5–10 m with the northeast side down. This is opposite to the direction of Quaternary uplift of the Irish Hills. Direct correlation of Tertiary strata across the faults also suggests that the amount of cumulative lateral displacement is also limited to a few tens of meters or less. These faults clearly lie west of the N40W fault, and are named the North segment of the Shoreline fault (Plate 1). Given the minor displacement of Tertiary strata, the North segment of the Shoreline fault zone does not appear to be associated with a well-developed older Tertiary fault similar to the Central and South segments of the Shoreline fault zone.

Based on the above evidence, three alternative interpretations of the North segment of the Shoreline fault zone are considered. The preferred alternative is that the North segment of the Shoreline fault zone coincides generally with the Northern seismicity sublineament as shown on Plate 1. The fault either has produced only minor displacement in the Tertiary strata in the near surface or does not extend to the seafloor (i.e., is not emergent). This location for the fault is preferred because it most closely aligns with the Northern seismicity sublineament. The second alternative locates the North segment along the N40W fault. This alternative is less preferred because the N40W fault departs from the strike of the seismicity lineament, but the N40W fault is a recognized preexisting fault that is associated with microseismicity along its southeastern

trend (i.e., the Central and South segments). The third alternative is that some or all of the Northern seismicity sublineament is associated with an east-dipping Hosgri fault zone, in which case the North segment of the Shoreline fault zone does not exist or is limited to a few kilometers in length beyond the better-defined Central segment. These alternatives and their potential significance to hazard are discussed further in Section 5.

4.3.1 Length and Segments

The Shoreline fault zone, including all three segments, has an overall strike of about N60°W and is up to 23 km long (Plate 1). The total length of individual segments and the continuity and integration of the fault as a whole are discussed in the following subsections.

North Segment

The North segment is up to 8 km long. The uncertainty in the segment length encompasses the range of alternative locations described above ranging between zero length (with seismicity occurring on an east-dipping Hosgri fault zone at depth) and the maximum 8 km length extending southeast from the Hosgri fault zone to south of Lion Rock. The alternative N40W fault trace also yields an 8 km segment length. The North segment is concealed beneath marine sediments and the ephemeral drifting sand sheet on the seafloor, and has no geomorphic expression. The alternative surface trace along the older N40W fault coincides with the mapped trace west of Lion Rock and the linear escarpment accented by erosion that created a composite series of submerged marine strandlines across the fault (Appendix I). West of Lion Rock a late Pleistocene submerged wave-cut platform extends across the N40W fault with no apparent vertical separation within a limit of resolution of 1 m (Figure 4-9).

The two alternative locations of the North segment have different expressions in the magnetic field data (Figure 4-17). The preferred trace that follows the seismicity sublineament does not coincide with a strong magnetic anomaly, although the lack of an anomaly may simply reflect progressively deeper seawater and Quaternary sediments along this trace of the fault. The alternative N40W trace is subparallel to but crosses a magnetic anomaly associated with intrusive diabase (Figure 4-17; Appendix B). The south ends of both the North segment and the N40W fault are obscured by sand sheets, so the connection between the North and Central segments is unclear. The anomalies in the magnetic-field data are not continuous and appear complex; this complexity in the magnetic-field data indicates probable structural complexity at this segment boundary.

Central Segment

The Central segment is approximately 8 km long and follows an older reactivated Tertiary fault that is well expressed in the geology and as a magnetic anomaly (Plate 1; Figure 4-17). The Central segment is further divided into three en echelon subsegments, C-1, C-2, and C-3. These subsegments are not considered to be rupture segments in the seismic source characterization of the Shoreline fault zone (Section 5). Subsegment C-1 merges with a strike change with C-2, and C-2 has a right step to C-3 of 100–200 m. Subsegment C-1 is west of Discharge Cove and appears to die out northward beneath the sand sheet directly south of Lion Rock. The northern end of C-1, however, does not follow the magnetic anomaly high that characterizes the majority of the Central and South segments but transitions into a magnetic trough. Subsegment C-1

forms a very prominent and well-defined bathymetric lineament and, where mapped at the seafloor, juxtaposes Tertiary diabase against Franciscan mélange (Figure 4-10).

Subsegment C-2 also forms a very prominent, well-defined bathymetric lineament and juxtaposes Obispo diabase, Cretaceous sandstone and Franciscan mélange on the east against a thin mobile sand sheet covering Franciscan mélange on the west (Figure 4-11). West of Olson Hill, a moderate to strong, 900 m long geomorphic lineament is evident on the MBES bathymetric image. The lineament lies within a shallow, 2–4 m-deep, 25 m-wide trough in Franciscan mélange and is likely accentuated by differential erosion (Figure 4-12). In this area of subsegment C-2, two small pockmarks in a mobile sand sheet are well expressed on the 2009 bathymetry, but are absent on the 2010 bathymetry (Figure 4-12). If these pockmarks are not data artifacts but are formed by gas or fluid expulsed along the fault zone, their disappearance in the 2010 bathymetry illustrates the mobile, ephemeral nature of the sand deposits that locally veneer the seafloor.

The subsegment C-2 coincides with a linear magnetic anomaly high (Figures 4-17 and 4-18). To the south, subsegment C-2 ends near where the Olson Hill deformation zone (the northern splay of the San Luis Bay fault zone) projects offshore. A direct structural or geomorphic linkage between the Central segment of the Shoreline fault zone and the bedrock faults near Olson Hill has not been established (Figure 4-13). The step-over between subsegments C-2 and C-3 is southeast of Olson Hill where the linear, magnetic anomaly high ends.

Subsegment C-3 also is expressed as a well-defined bathymetric lineament (Plate 1; Figure 4-14). The lineament is primarily in Cretaceous sandstone and Franciscan mélange and is covered by a thin sand sheet. The lineament coincides with a magnetic anomaly high (Figure 4-18). As shown on Figure 4-14, the southern end of subsegment C-3 may bend to the east and follow a lineament (also interpreted to be a paleostrandline) that projects directly toward the Rattlesnake fault (the southern strand of the San Luis Bay fault zone) at the coastline. The apparent connection of the two faults suggests that there may be a kinematic link between these two structures, but analysis of the submerged wave-cut platform associated with the marine oxygen isotope stage (MIS) 5a sea-level highstand (approximately 80,000 years old) indicates that the Shoreline fault zone is probably a separate structure (Appendix I). Alternatively, the south end of the Central segment may continue on strike beneath the mobile sand sheet to the southeast toward a linear magnetic high before ending within a kilometer or so.

South Segment

The South segment is approximately 7 km long and, like the Central segment, follows a reactivated older bedrock fault. It is expressed as a poor to moderate bathymetric lineament inferred to be in a band of mélange covered by a thin mobile sand sheet. Locally, the South segment truncates bedding in Cretaceous sandstone along a low, northeast-facing escarpment (Plate 1; Figure 4-15). It is also associated with a strong linear magnetic anomaly high (Figure 4-18). In detail, the fault trace defined on the MBES bathymetry image follows the west flank of the magnetic high rather than the crest. The northern end of the South segment lies within a broad zone of Franciscan mélange that is covered by a sand sheet, so its exact location is uncertain. The junction between the Central and South segments is interpreted as either a right step-over of 100–500 m, or the two segments meet at the north end of the linear magnetic

anomaly southeast of Rattlesnake Creek. The south end of the South segment projects beneath a sand sheet southwest of Point San Luis and southwest of the southern cluster of seismicity that marks the south end of the Southern seismicity sublineament (Plate 1; Figure 4-1).

4.3.2 Faulting Style

The Shoreline fault zone is inferred to be primarily a right-lateral fault based on focal mechanisms that indicate vertical strike-slip fault motion (Figure 4-7) and the linear geologic expression of the fault on the seafloor along the Central and South segments. However, some focal mechanisms along the North and Central segments show right-oblique or right-reverse motion, and one focal mechanism along the South segment shows right-normal motion. These oblique mechanisms suggest that the fault may accommodate some vertical displacement as well as lateral displacement. However, as discussed in Section 4.4, the vertical component of displacement along the Shoreline fault zone is less than approximately 2 m on submerged wave-cut platforms estimated to be 75,000 years old or older (Figures 4-10, 4-11, 4-13, 4-15, 4-24, and 4-25). These data support a characterization of the Shoreline fault zone as a strike-slip fault with a limited vertical component.

4.3.3 Geometry and Downdip Width

The seismicity defines a nearly vertical fault zone (Figures 4-2 and 4-8). Along the Central and Southern seismicity sublineaments, the hypocentral distribution of seismicity forms a nearly vertical alignment to a depth of about 8–10 km. The vertical alignment of seismicity is consistent with the results of the 2-D magnetic profile modeling discussed in Appendix D. The magnetic data along a southwest-northeast cross section passing south of Olson Hill indicate that the source body associated with the Shoreline fault zone is nearly vertical, with a width on the order of 200 m, and extends from the near-surface to a depth ranging from several hundred meters to several kilometers below the surface (Figure 4-20)

Along the northern seismicity sublineament, the seismicity is more diffuse and forms a nearly vertical alignment to a depth of about 12–15 km. Steep dips for magnetic source bodies along the Northern seismicity lineament are not as well constrained as the Central and Southern sublineaments due to the possible effects of deep water relative to the survey flight elevation (Appendix D). As discussed previously, it is not certain how much of the seismicity along the Northern seismicity sublineament, in particular the deeper seismicity, may be associated with a steeply east-dipping Hosgri fault zone.

4.4 Activity of the Shoreline Fault Zone

Several approaches are used for assessing the recency of activity and the slip rate of the Shoreline fault zone as discussed below. Of primary importance are the identification and dating of offshore late Quaternary marine terraces, which consist of submerged paleostrandlines (ancient shorelines) and associated wave-cut platforms. These are discussed in Section 4.4.1. The geometries and distribution of offshore marine terrace (e.g. Hanson et al., 1994), including direct measurements of late Quaternary vertical separation across the Shoreline fault zone and N40W fault. The assessment of recency of activity and slip rate are discussed in Sections 4.4.2 and 4.4.3, respectively.

4.4.1 Offshore Wave-Cut Platforms and Paleostrandlines

A detailed analysis of ancient offshore marine terraces was performed in the study area (Appendix I, Figure 4-21). The recently acquired high-resolution MBES bathymetric data and USGS high-resolution seismic-reflection profiles allowed the identification and mapping of the submerged marine wave-cut platforms and paleostrandlines. The interpretation of these submerged geomorphic features helped constrain the location and rates of deformation along the Shoreline fault zone and the surrounding continental shelf. The submerged marine terraces were mapped in the entire offshore bedrock platform extending from the coastline between Estero Bay and San Luis Obispo Bay west to the Hosgri fault zone. Results of the study are presented in detail in Appendix I and briefly summarized below.

The offshore marine terraces contain two spatially distinct terrace sequences on the inner continental shelf: one sequence is on the Islay shelf west of Point Buchon and the other sequence is on the Santa Rosa Reef shelf west of Point San Luis (Figure 4-21). The terraces appear to correlate laterally within each shelf, but do not appear to correlate between the two shelves. The submerged terraces on these shelves have not been independently dated, but analysis of possible periods of formation (Appendix I) shows that they are older than the last glacial maximum (LGM) that occurred about 22,000 years ago. The preferred interpretation is that the marine terrace sequence on the Islay shelf is the offshore continuation of the onshore flight of emergent marine terraces near Point Buchon (and are being uplifted at a rate of 0.2 mm/yr; Hanson et al., 1994), and the marine terrace sequence on the Santa Rosa Reef shelf is the offshore continuation of the onshore flight of emergent marine terraces at Point San Luis (and are being uplifted at a rate of 0.06 mm/yr; Hanson et al., 1994). Using this model, the shallower offshore marine terraces generally correlate to MIS 5 stillstand sea levels of approximately 75,000 to 100,000 years ago, and the deeper marine terraces are older than the LGM that occurred about 22,000 years ago and generally correlate to MIS 3 stillstand sea levels approximately 30,000 to 50,000 years ago. Some of the wave-cut platforms on the Islay and Santa Rosa Reef shelves are probably reoccupied and modified from wave-cut platforms developed during stillstand sea levels that occurred prior to the last interglacial (MIS stage 5e; approximately 120,000 years ago).

The submerged paleostrandlines and associated wave-cut platforms have been modified by the last marine transgression, but as discussed in detail in Appendix I, the extent of the modifications are relatively minor and localized. Given the relatively rapid rise in sea level and because the zone of wave erosion (approximately 10–15 m deep) past any one place on the shelf within a period of 1,000–1,500 years, no wave-cut platforms wider that approximately 100 m could have formed, and vertical lowering of the platform is limited to about 1–1.5 m (Appendix I, Sections 7.2.1.2 and 7.2.1.3). Therefore, while wave erosion during the last marine transgression may have locally removed some geomorphic evidence of recent faulting, if present, it would not destroy larger vertical offsets (on the order of multiple meters) or remove significant geomorphic evidence of extensive late Quaternary faulting over the entire reach of the Shoreline fault zone.

Based on the above observations, the submerged wave-cut platforms and paleostrandlines older than about 75,000 years (i.e., Stage 5 stillstands) constrain the rate of vertical separation across the Central and South segments of the Shoreline fault zone and N40W fault (discussed in 4.4.3

below). The Islay and Santa Rosa Reef terrace sequences are separated by a change in uplift rate that occurs in a poorly defined zone that lies west of the Shoreline fault zone.

4.4.2 Evidence of Activity

The seismicity along the Central and Southern sublineaments aligns with the Central and South segments of the Shoreline fault zone within the 0.5 km horizontal uncertainty (Plate 1, Figure 4-1). Because of this direct association with seismicity, PG&E concludes that the Central and South segments of the Shoreline fault zone are active, and infers that the Northern seismicity sublineament is part of the active fault zone. The alternative and less preferable interpretation that the seismicity of the Northern seismicity sublineament may be wholly or in part produced by the Hosgri fault zone is also acknowledged.

No definitive evidence of late-Quaternary displacement has been observed anywhere along the Shoreline fault zone or the N40W fault. Elevation profiles on the late Quaternary wave-cut platforms across the N40W fault and Central and South segments of the Shoreline fault zone do not show systematic vertical separation across the faults (Section 4.4.3 and Figures 4-9, 4-11, and 4-15). The moderate to strong geomorphic lineament in bedrock west of Olson Hill is interpreted to be formed by differential erosion (Section 4.3.1 and Figure 4-12). Similarly, the small scarp and associated geomorphic features imaged in the high-resolution seismic-reflection profiles off Intake Cove (Figure 4-10) are interpreted to be formed by differential erosion (Appendices B and I).

4.4.3 Slip Rate

The Shoreline fault zone lies entirely offshore and thus it is difficult to develop direct quantitative estimates of slip rate. The MBES bathymetric data were extensively probed to identify piercing points (i.e., potentially datable geomorphic features such as paleostrandlines or submerged channels on both sides of the fault zone that could be used to constrain cumulative lateral slip and slip rate). No geomorphic features that could be reliably used as lateral offset markers have been identified. In the absence of more direct information, constraints on slip rate are provided by several qualitative and indirect quantitative estimates of slip rate. These are summarized below.

Comparison to the Hosgri–San Simeon Fault System

The Hosgri–San Simeon fault system has a slip rate of 0.5 to 6 mm/yr, with a preferred rate of 1 to 3 mm/yr (Hall et al., 1994; Hanson et al, 1994; Hanson et al., 2004). Onshore, the San Simeon fault is well expressed geomorphically and clearly displaces late Pleistocene and Holocene deposits at numerous locations. Offshore, the Hosgri fault zone locally produces scarps on the seafloor and, along the reach of the fault directly west of the Irish Hills, abruptly truncates the westward extent of the offshore bedrock platform. In addition, individual strands of the Hosgri fault zone produce linear escarpments in bedrock that appear to be pressure ridges on the seafloor. All of these features on the Hosgri fault zone occur in water depths shallower than 120 m, and thus, if present at the time of the last transgression, were subject to erosion. The Shoreline fault zone is not associated with geomorphic or geologic features similar to those of the Hosgri fault zone offshore or the San Simeon fault zone onshore. Geomorphic features produced by high slip rate faults are lacking, even in locations where the fault zone extends into deeper water where the relatively rapid rise in sea level during the last sea-level transgression

caused sea level to pass more rapidly than in shallow water, shortening the duration that potential fault features would have been exposed to wave erosion, and reducing the likelihood that they would have been significantly eroded (Appendix I).

In addition, if the Shoreline fault zone had a slip rate comparable to the Hosgri–San Simeon fault system, it is likely that it would be part of a longer fault zone with an onshore portion along strike to the southeast (for example, it would likely be a part of a longer and more active Southwestern Boundary fault zone). If this were the case, it would be expected that the Shoreline fault zone would have maintained a seafloor expression southwest of Point San Luis, and evidence of higher slip rate faults in the associated Southwestern Boundary zone would be expressed onshore in the vicinity of San Luis Obispo Bay or the Santa Maria Valley. Despite extensive onshore mapping in this area during both the LTSP and during this study, no onshore faults with comparable geomorphic expression to the San Simeon fault have been identified.

Based on these observations, the slip rate on the Shoreline fault zone is qualitatively estimated to be at least an order of magnitude less that the slip rate on the Hosgri–San Simeon fault zone. This qualitative comparison yields an estimate of horizontal slip rate of 0.05 to 0.6 mm/yr for the Shoreline fault zone.

Estimates of Vertical Separation

Two approaches are used to constrain the amount of vertical separation on the Shoreline fault zone. Along the North segment (associated with the Northern seismicity sublineament), possible displaced Tertiary strata on high-resolution seismic-reflection profiles are interpreted to constrain the cumulative amount of vertical separation on the segment to be about 5–10 m, with a northeast-side down vertical separation. The northeast-side down sense of vertical separation is opposite the expected northeast-side up vertical separation if the fault is partially accommodating uplift of the San Luis–Pismo block. In addition to the apparent limited vertical stratigraphic separation, the similarity in the seismic stratigraphy across the fault zone observed at these two locations probably indicates limited lateral displacement as well. These interpreted faults are similar to several small displacement faults imaged in the MBES bathymetric data that are associated with folds in the Monterey and Pismo Formations west of Point Buchon that probably formed in the Miocene and early Pliocene (Plate 1). However, estimating an onset of deformation at between 1 and 2 million years ago (coinciding with the estimated onset of block uplift recorded by emergent marine terraces on the adjacent coast; Hanson et al., 1994) the vertical separation rate would be less than 0.01 mm/yr.

The second approach to constrain vertical separation rates across the Shoreline fault zone is based on the evaluation of submerged wave-cut platforms that are mapped across the N40W fault and Central and South segments of the fault zone (Appendices B and I). The amounts and estimated rates of vertical separation of wide wave-cut platforms across mapped faults are constrained at the following locations (from north to south):

- The wave-cut platform associated with the –38 m paleostrandline crosses the N40W fault west of Lion Rock (Figure 4-9). The probable timing of the most recent sea-level occupation (and associated significant geomorphic modification of the –38 m paleostrandline on the Islay shelf) was between 49,000 and 60,000 years ago (Appendix

I). Analysis of elevation profiles across the wave-cut platform suggests that there is zero vertical separation across the mapped fault trace with a combined uncertainty of approximately ±2 m (Appendix I, Section 7.3.1). This limits the maximum vertical separation rate across the N40W fault to less than 0.04 mm/yr.

- The wave-cut platform associated with the –25 m paleostrandline crosses the C-1 subsegment of the Central segment of the Shoreline fault zone west of DCPP (Figure 4-10). The estimated vertical separation of the buried wave-cut platform associated with the –25 m paleoshoreline in the step-over region between the C-1 and C-2 subsegments of the Shoreline fault zone is either 0 (from the preferred interpretation that the apparent scarp is due to differential erosion) or 1 ± 2.5 m with the center value having a northeast-side up vertical separation (Appendix I, Section 7.3.2). Using the vertical separation and the estimated minimum age of 75,000 years for the wave-cut platform yields a vertical separation rate of 0 or 0.01 ± 0.03 mm/yr.
- The wave-cut platform associated with the –21 m shoreline crosses the C-2 subsegment of the Central segment of the Shoreline fault zone (Figure 4-11). The –21 m paleostrandline and wave-cut platform are also estimated to be at least 75,000 years old. Analysis of elevation profiles across the wave-cut platform suggests there is zero vertical separation across the mapped fault trace with a combined uncertainty of approximately ±1.5 m (Appendix I, Section 7.3.2), the upper bound of 1.5 m of vertical deformation across the mapped fault trace limits the vertical slip rate to be less than 0.02 mm/yr.
- The wave-cut platform associated with the –31 m paleostrantline crosses the South segment of the Shoreline fault zone near its south end (Figure 4-15). The platform and associated paleostrandline (also estimated to be at least 75,000 years old) extend across the fault zone. Analysis of elevation profiles across the wave-cut platform suggests there is zero vertical separation across the mapped fault trace with a combined uncertainty of approximately ± 1.5 m (Appendix I, Section 7.3.3), constraining the upper bound to be about 1.5 m. This limits the vertical slip rate to less than 0.02 mm/yr.

The results summarized above suggest that the vertical separation rate on the Shoreline fault zone is indistinguishable from zero. In order to estimate a maximum horizontal slip rate from the wave-cut platform data, the maximum vertical separation rates are considered with a fault having an assumed 10:1 horizontal-to-vertical slip ratio. This assumption yields maximum horizontal slip rates on the order of 0.2 to 0.4 mm/yr.

Estimates of Cumulative Right-Lateral Strike-Slip

Toward the northern end of the Central segment of the Shoreline fault zone, directly west of Discharge Cove, two west-northwest-trending, subparallel magnetic anomaly highs show an apparent right-lateral step of about 300 m (Figure 4-22). Although not a unique interpretation, the apparent right-lateral step may occur across a N15°E striking basement fault whose north end aligns with the north-south to N25°W striking fault mapped in the headland at the northwest end of Discharge Cove. This fault, which is referred to as the N15E fault, may cross the Central segment of the Shoreline fault zone. Thus, the N15E fault provides a possible piercing line or strain gauge from which cumulative right-lateral displacement on the Shoreline fault zone can be estimated.

The N15E fault, where mapped onshore and in the rocks at low tide, juxtaposes resistant Obispo Formation tuff against Obispo Formation bedded sedimentary rock in a broad zone of shearing that is associated with hydrothermal alteration. The N15E fault is truncated to the north by an east-west-striking fault that is clearly mapped in the intertidal zone and in the sea cliff (Plate 1; Figure 4-22). This east-west fault does not displace the emergent MIS 5a (approximately 80,000 years old) wave-cut platform exposed in the sea cliff, and illustrates the inactivity of the N15E fault. The inferred right-lateral separation of the magnetic anomalies across the N15E fault is supported by the right-lateral separation of other approximately north-south-striking faults mapped elsewhere in the vicinity of DCPP (Appendix B).

Alternative traces of the N15E fault through the MBES bathymetric data that satisfy the right-lateral separation of the twin magnetic anomaly peaks are shown on Figure 4-22. The alternative traces limit the possible offset of the N15E fault across the Central segment of the Shoreline fault zone to less than 100–200 m right-lateral, and possibly zero (Figure 4-22). Estimating an onset of deformation at between 1 and 2 million years ago (coinciding with the estimated onset of block uplift recorded by emergent marine terraces on the adjacent coast; Hanson et al., 1994) yields an estimated maximum horizontal dextral slip rate of about 0.05 to 0.2 mm/yr for the Shoreline fault zone.

Seismicity

The rate of seismicity on the Shoreline seismicity lineament provides a limited constraint on the slip rate on the Shoreline fault zone. Figure 4-3c shows the maximum likelihood fit of the Shoreline seismicity (empirical fit) in comparison to mean characteristic recurrence models for characteristic magnitudes of 5.8 (single segment rupture), 6.0 (two segment rupture) and 6.5 (total fault rupture) using the qualitative slip rates of 0.01 and 0.3 mm/yr reported in the Progress Report (PG&E, 2010a). The Shoreline seismicity rate is most consistent with the recurrence model having a mean characteristic magnitude 5.8 earthquake (single segment rupture) with a slip rate of 0.3 mm/yr rather than the lower slip rate of 0.01mm/yr. Extrapolating the slope of the empirical data based on a *b*-value of 0.93 out to M 6.0 results in an estimated annual recurrence of about 0.0002 events/yr and a return period of about 5,000 yrs.

San Luis Bay Fault Zone

An alternative structural interpretation of the Shoreline fault zone is that it is kinematically linked to the San Luis Bay fault zone such that the slip on the North and Central segments of the Shoreline fault zone continues onshore and follows the Rattlesnake fault of the San Luis Bay fault zone and forms part of a strike-slip restraining bend (Plate 1; Figure 4-14). In characterizations based on this linked structural model the slip rate on the San Luis Bay fault zone can be used to provide information on the slip rate of the Shoreline fault zone. The San Luis Bay fault zone has a cumulative rate of vertical separation of 0.14 mm/yr as recorded in the emergent marine terraces at the coast, with about half of that vertical rate occurring on the Rattlesnake fault (PG&E, 1990; Hanson et al., 1994). In addition, detailed mapping along the coastline shows steeply (approximately 70 degrees) north-dipping beds of Cretaceous sandstone and siltstone across the Rattlesnake fault (Figure 4-25).

Tentative correlation of an approximately 35–40 m thick sequence of resistant sandstone beds on the modern wave-cut platform across the Rattlesnake fault yields an estimate of about 70 ± 20 m

of apparent right-lateral separation across the fault, indicating that the Rattlesnake fault does not have significant cumulative deformation across it. Because the beds dip steeply to the north, the apparent right-lateral separation is consistent with pure north-side-up dip-slip motion on a vertical fault of about 190 m. Oblique motion of the Rattlesnake fault would yield horizontal displacements of less than approximately 70 m. An estimated onset of deformation of 1 to 2 million years ago and a maximum horizontal displacement of 70 m yields a limiting lateral slip rate of about 0.14 to 0.07 mm/yr. Considered very unlikely, the absolute maximum lateral slip rate on the fault would consider the limiting horizontal offset of 70 m and a minimum age of 120,000 years, the age of the MIS 5e marine terrace that records the offset of the Rattlesnake fault. This extreme maximum lateral slip rate would be about 0.6 mm/yr. Given the roughly equal distribution of vertical separation between the Rattlesnake fault and Olson Hill deformation zone, the lateral slip rate can be assumed to also be equally distributed, giving a cumulative absolute maximum lateral slip rate for the entire San Luis Bay fault zone of 1.2 mm/yr. As described earlier, given the absence of geomorphic expression onshore along the San Luis Bay fault zone similar to the San Simeon fault, a slip rate of over 1 mm/yr is not credible. Thus this analysis is used to conclude that a maximum lateral slip rate of up to 1 mm/yr may branch from the San Luis Bay fault zone onto the Shoreline fault zone.

Conclusion

Given the above five lines of reasoning, slip rate on the Shoreline fault zone is interpreted to range from 0.05 mm/yr to possibly 1 mm/yr, with a preferred range of 0.2 to 0.3 mm/yr. The slip rate could also be zero.

4.5 Relationship to Other Structures

The Shoreline fault zone lies between the active Hosgri fault zone on the west, the Los Osos fault zone on the north and east, and faults of the Southwestern Boundary fault zone on the south and southeast. Three alternatives are considered for the kinematic relationship of the Shoreline fault zone to these nearby structures.

One alternative is that the Shoreline fault zone is an independent strike-slip fault within the San Luis–Pismo structural block. In this model, the Southwestern Boundary fault zone is a system of reverse faults and the Shoreline fault zone is a minor strike-slip fault accommodating differential slip in the hanging wall of the fault zone. Uplift of the San Luis–Pismo block is accommodated by reverse or reverse-oblique slip on both the Los Osos and Southwestern Boundary fault zones and oblique slip on the Hosgri fault zone. This alternative is most consistent with the structural model proposed in the LTSP (PG&E, 1988; Lettis et al., 1994, 2004).

In the second and third alternatives, the Shoreline fault zone is part of the Southwestern Boundary fault zone that borders the southwestern margin of the uplifting San Luis–Pismo structural block. In these alternatives, the Shoreline fault zone is kinematically linked to the San Luis Bay fault zone, and potentially other faults of the Southwestern Boundary fault zone (i.e., Wilmar Avenue, Los Berros, Oceano, Pecho, and Nipomo faults [PG&E, 1988]). In the second alternative, the Shoreline fault zone is a strike-slip fault linked to the Southwestern Boundary fault zone via left-restraining step-overs in a strike-slip fault system. Uplift of the San Luis–Pismo block is accommodated primarily by reverse or oblique slip on the Los Osos fault zone,

oblique slip on the Hosgri fault zone, and possibly transpressional oblique slip on a Southwestern Boundary strike-slip fault zone.

In the third alternative, the Shoreline fault zone is an integral part of a Southwestern Boundary fault zone system of reverse- and oblique-slip faults. In this model, the Shoreline fault zone is kinematically linked to and may be, in part, the offshore continuation of the San Luis Bay fault zone. Uplift of the San Luis–Pismo block is accommodated by the Los Osos fault zone and by oblique slip on the Shoreline fault zone as part of the overall Southwestern Boundary fault zone.

All three alternatives were considered in the logic tree characterization of seismic source parameters for the Shoreline fault zone (Section 5). Alternative one is considered in an "independent" Shoreline fault zone branch, and alternatives two and three are combined into a single "linked" Shoreline fault zone branch.

4.5.1 Independent Shoreline Fault Zone Model

Determining whether the San Luis Bay fault zone is truncated by the Shoreline fault zone or whether it crosses the Shoreline fault zone is important for assessing the relative merits of the alternative kinematic models presented above. In the scenario where the strike-slip Shoreline fault zone is kinematically independent and separate from the reverse-slip San Luis Bay fault zone, the San Luis Bay fault zone may cross the Shoreline fault zone and extend to the Hosgri fault zone to accommodate uplift of the San Luis–Pismo block. Although the exact location and western limit of the San Luis Bay fault zone in the offshore is uncertain, several lines of evidence support the concept that the onshore San Luis Bay fault zone crosses the inner continental shelf west of the Shoreline fault zone as a deformation zone, possibly as a fold. If so, this structural relationship supports an independent Shoreline fault zone.

The first line of evidence comes from the west-northwest trend of bedrock structures (Appendix B) and the subparallel trending magnetic anomaly (Appendix D) in the offshore. Specifically, there is a broad geologic boundary west of Olson Hill in the offshore geologic map (Plate 1) that places Obispo Formation on the south-southwest against pre-Tertiary rocks on the north-northeast. This north-side up structural relief is similar to the sense of displacement across the San Luis Bay fault zone documented by the emergent marine terraces. The west-northwest trending structural grain in the MBES bathymetric data across this zone do not show a throughgoing fault zone at the seafloor, but a south-southwest-facing monoclinal warp or flexure above a blind fault is permissible. A folding style of deformation (as opposed to surface fault offset) would be similar to the broad deformation of the emergent MIS 5e terrace (approximately 120,000 years old) across the Olson Hill deformation zone (PG&E, 1989c). The San Luis Bay fault zone thus may be partially blind at the coastline and offshore with only some strands (such as the Rattlesnake fault) locally intersecting the surface.

The second line of evidence that the San Luis Bay fault zone crosses the Shoreline fault zone comes from the analysis of the MIS 5a (approximately 80,000 years old) marine terrace and wave-cut platform across the San Luis Bay fault zone (Appendix I). The MIS 5a terrace is observed as a deformed emergent terrace onshore across the Olson Hill deformation zone and in the hanging wall (north side) of the Rattlesnake fault (PG&E, 1989c; Hanson et al., 1994). In the offshore, the MIS 5a wave-cut platform is locally reoccupied but recognizable on either side of

the Rattlesnake fault and on the footwall (south) side of the Olson Hill deformation zone (Appendix I, Section 7.1). Analysis of the offshore marine terraces that reoccupy the MIS 5a wave-cut platform west of Rattlesnake Creek indicates that the vertical deformation of the MIS 5e terrace documented onshore across the Rattlesnake fault continues offshore along strike of the Rattlesnake fault (Figures 4-24 and 4-25; Appendix I). The deformation crosses the southern end of the Central segment of the Shoreline fault zone without evidence of displacement on the Central segment.

The third line of evidence for a San Luis Bay fault zone that crosses the Shoreline fault zone comes from the preferred correlation of the paleostrandlines between the Islay and Santa Rosa Reef shelves (Appendix I, Section 7.1). This preferred correlation includes a deformation zone that trends offshore between Diablo Creek and Rattlesnake Creek along the westward continuation of the San Luis Bay fault zone, seaward of the MIS 5a wave-cut platform. Although the specific location of the uplift rate boundary between the Islay and Santa Rosa Reef shelves is not well defined, it is consistent with the general location of the south-southwest-facing monoclinal warp or flexure suggested from the offshore geologic map (first item above).

4.5.2 Linked Shoreline Fault Zone Model

In the alternative models where the Shoreline and San Luis Bay fault zones are kinematically linked as part of the Southwestern Boundary fault zone, one model prediction is that the San Luis Bay fault zone proper may merge with the Shoreline fault zone and will not extend farther west to the Hosgri fault zone. Partial support of this model is the observation that the Rattlesnake fault mapped at the coastline appears to continue offshore as a lineament that merges with the Shoreline fault zone (Plate 1; Figure 4-14). In addition, the uplift rate boundary west of the Shoreline fault zone between the Islay and Santa Rosa Reef shelves is not unique, and thus it is permissible that alternative structures other than a westward continuation of the San Luis Bay fault zone accommodate the differential uplift rate. In the linked fault alternatives listed above, alternative three includes the Shoreline fault zone as a relative uplift rate boundary as part of the margin of the San Luis–Pismo structural block. As described above, our evaluation of submerged marine terraces has documented evidence suggesting a low to zero vertical displacement rate across the Shoreline fault zone (Figures 4-9 to 4-11 and 4-15; Appendix I). This evidence does not support the third alternative wherein the Shoreline fault zone accommodates differential uplift.

4.6 Location of the Shoreline Fault Zone with Respect to DCPP

The mapping based on high-resolution MBES bathymetric data clearly shows a sharp, well-defined lineament that lies offshore and west of the DCPP. This lineament is interpreted as the surface expression of the Shoreline fault zone. Immediately offshore of DCPP, the Central segment of the Shoreline fault zone is located 300 m southwest of the intake structure and 600 m southwest of the power block (Figure 4-10). Onshore geologic mapping documents the absence of late Quaternary deformation within the DCPP site that may be associated with the Shoreline fault zone (Section 7).

Table 4-1 Comparison of Characteristics of the Shoreline Fault Zone presented in the Progress Report (PG&E, 2010a) with this Report

PARAMETER	PROGRESS REPORT (PG&E, 2010a)	THIS REPORT (2011)
FAULT LENGTH	Total Length: 13 to 14 km Two segments: Central and Southern Northern Seismicity Trend considered a separate structure	Total Length: up to 23 km Three segments: North, Central, and South Overall Strike:N60° to 70°W
SEGMENTATION	Three segments w/ lengths (Figure 4-1 this report) Northern Seismicity Trend, 8 to 9 km Central segment, 8 km Southern segment, 5 to 5½ km	Three segments w/ lengths (Figure 4-1 this report): North segment, ~8 km Central segment, ~8 km South segment, ~ 7 km
FAULT DIP	90° based on seismicity	90° based on seismicity and magnetic potential field data
DOWN DIP WIDTH	10 to 15 km from the surface	10 to 15 km from the surface
FAULTING STYLE	Right-lateral strike slip based on linear surface expression of bathymetric lineaments and focal mechanisms.	Right-lateral strike slip based on linear surface expression of bathymetric lineaments and focal mechanisms.
RELATIONSHIP TO OTHER STRUCTURES	Hosgri fault zone (HFZ) • Rupture is inhibited from branching from the HFZ to the Shoreline fault San Luis Bay fault zone (SLBFZ) • Not addressed	Hosgri fault zone (HFZ) • Rupture is inhibited from branching from the HFZ to the Shoreline fault • North Segment dies out before or terminates at the HFZ. • HFZ dips 80 to 85 degrees east, hence some of the deeper seismicity in the North Segment may be on the HFZ San Luis Bay fault zone (SLBFZ) • Relationship to late Quaternary deformation on the SLBFZ uncertain
SLIP RATE	0.01 to 0.3 mm/yr Used Hosgri and San Luis Bay fault zones for comparison	Preferred maximum slip rate: 0.2 to 0.3 mm/yr based on • Comparison with geomorphic/structural expression of the HFZ: 0.05 to 0.6 mm/yr. • Offshore paleo-wave-cut platforms (vertical): <0.02 mm/yr (at 10/1 lateral = < 0.2 mm/yr) • Limited offset of basement fault: 0.05 to 0.2 mm/yr • Seismicity rate: 0.2 to 0.3 mm/yr • Association with SLBFZ: ~0.1 mm/yr
DISTANCE FROM DCPP	600 m southwest of power block 300 m southwest of Intake Structure	600 m southwest of power block 300 m southwest of Intake Structure
SECONDARY DEFORMATION AT DCPP SITE	Negligible Calculation indicates negligible deformation (DCPP.GEO.10.01, R0)	None. Documented absence of late Quaternary primary or secondary surface faulting or other forms of late Quaternary tectonic deformation within the DCPP site that may be associated with a maximum earthquake on the nearby Shoreline fault zone.

Table 4-2a. Absolute and Relative Location Uncertainty Estimates

Analyst	Absolute		Relative	
	Horizontal (km)	Vertical (km)	Horizontal (km)	Vertical (km)
Hardebeck (2010)	0.9	1.3	1.0	0.93
Thurber (2009)	0.5	0.5	0.17	0.28
Waldhauser (2009))	NA	NA	0.2	0.7

Table 4-2b. Average and Median Shifts in Epicenters and Depths between Location Methods for the Shoreline Earthquakes (H=Hardebeck; T=Thurber)

	Horizontal Shifts (km)				Vertical Shifts (km)			
	1D vs 3D	3D vs H-tomoDD	1D vs H-tomo DD	H-tomoDD vs T-tomoDD	1D vs 3D	3D vs H-tomoDD	1D vs H-tomoDD	H-tomoDD vs T-tomoDD
Median	1.499	0.496	1.045	0.450	0.66	0.302	0.779	1.293
Average	1.469	0.603	1.273	**0.510**	0.880	0.411	1.126	**1.329**
StdDev	0.743	0.381	0.901	0.328	0.761	0.363	0.955	0.842

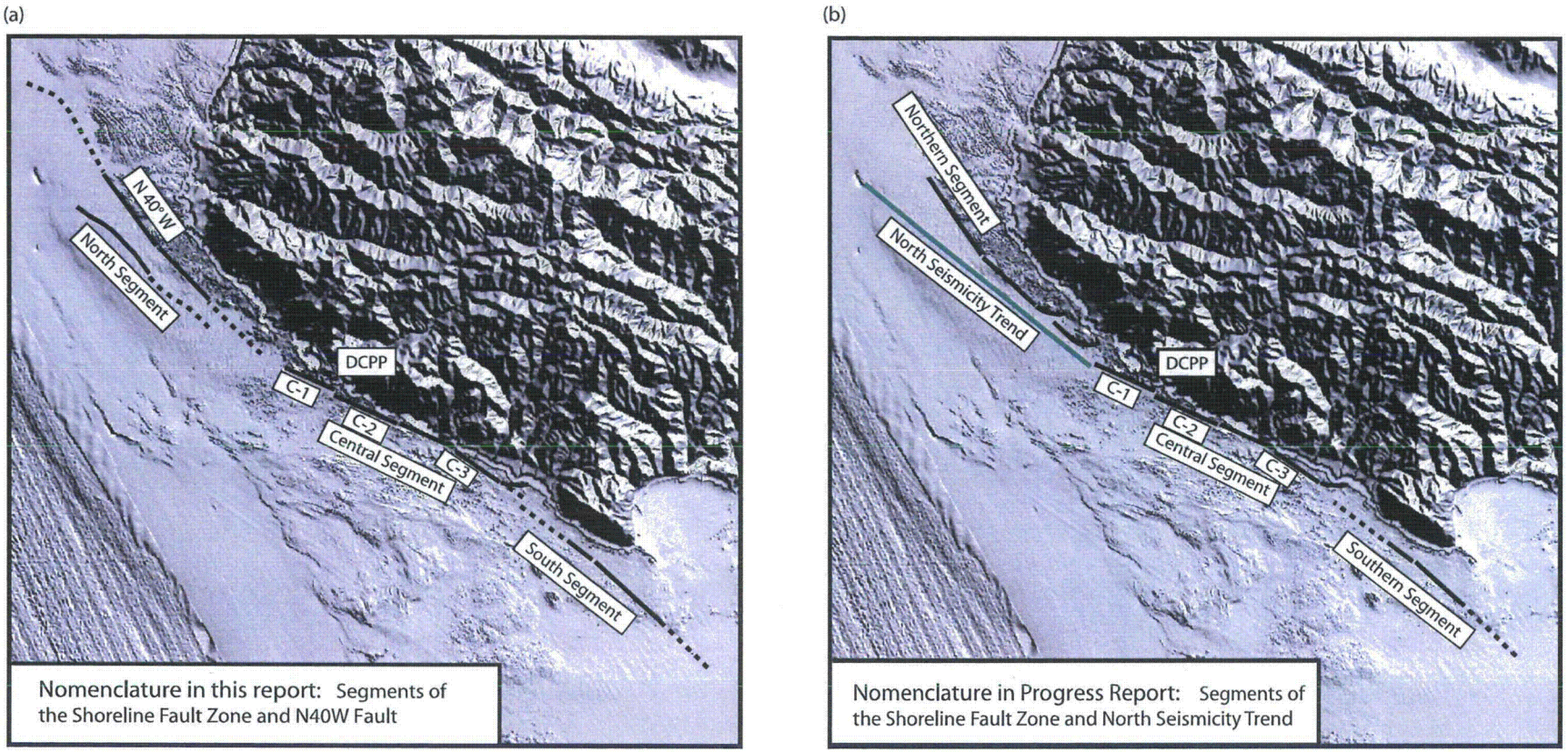

Map projection: NAD 1983, UTM Zone 10 North

0 2.5 5 Miles

0 2.5 5 Kilometers

File path: S:\13800\138381383838.002\Figures\20101112_Report\Figure_4-1.ai; Date: [12/21/2010]

Comparison of nomenclature for (a) the Shoreline fault zone in this report and (b) the Progress Report (PG&E, 2010a)

SHORELINE FAULT ZONE STUDY

Pacific Gas and Electric Company | Figure **4-1**

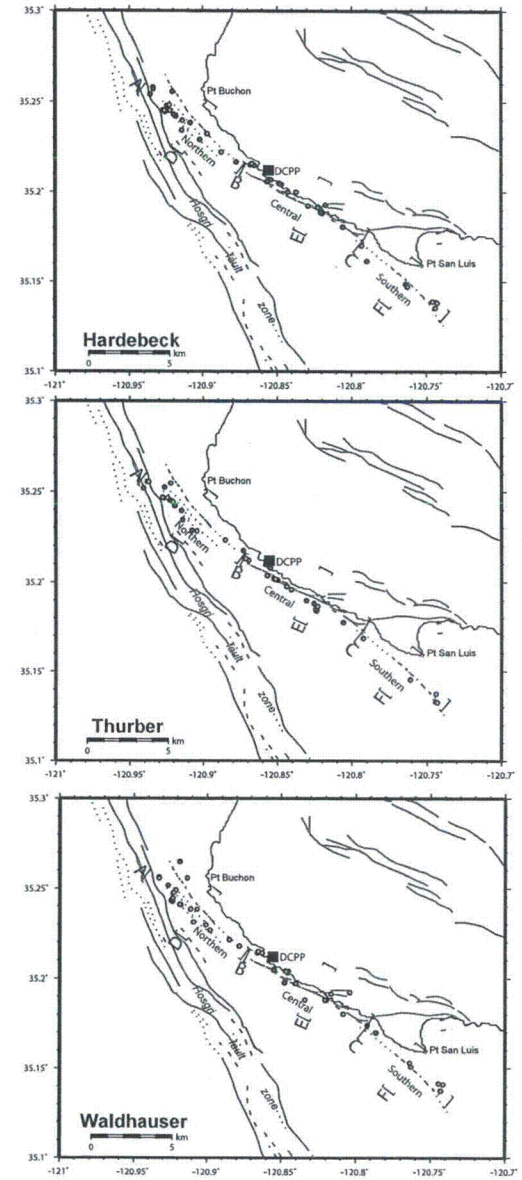

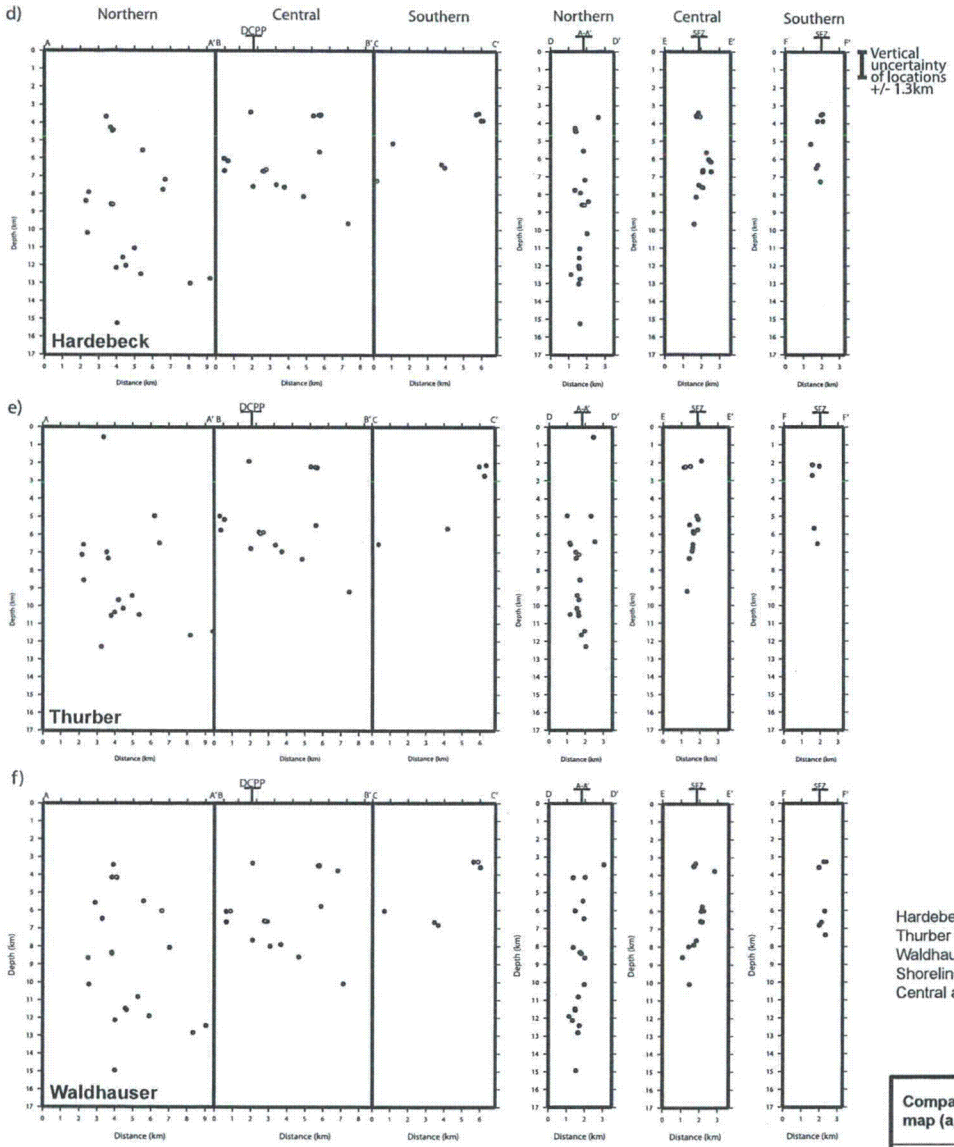

Hardebeck =TomoDD (Hardebeck, 2010),
Thurber = TomoDD (Thurber, 2009),
Waldhauser= HypoDD (Waldhauser, 2009).
Shoreline seismicity sub-lineaments, Northern, Central and Southern, are labeled.

Comparison of shoreline seismicity relocations in map (a, b, c) and cross section (d, e, f) views.

SHORELINE FAULT STUDY

Pacific Gas and Electric Company | Figure **4-2**

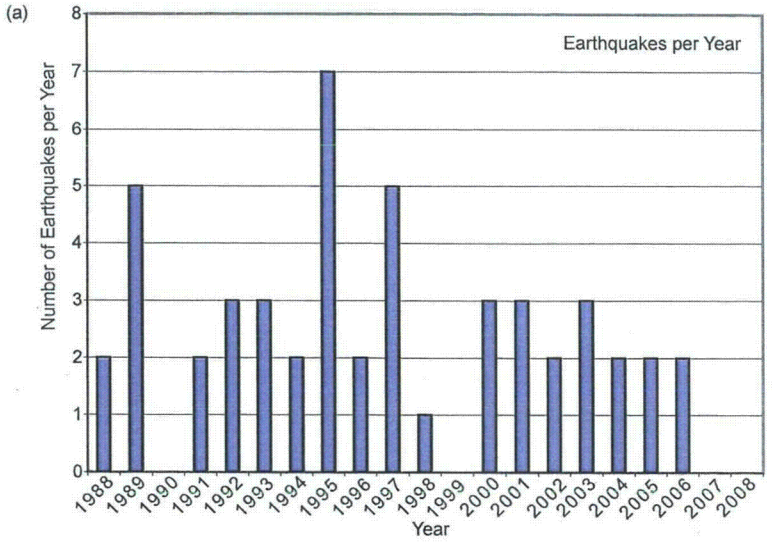

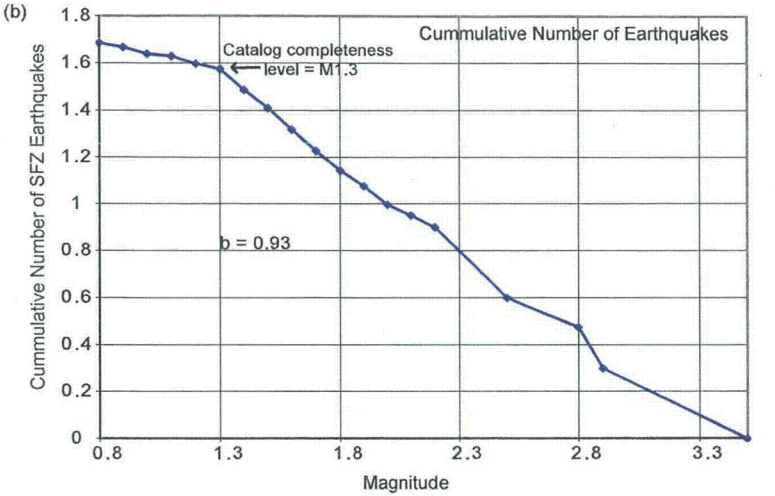

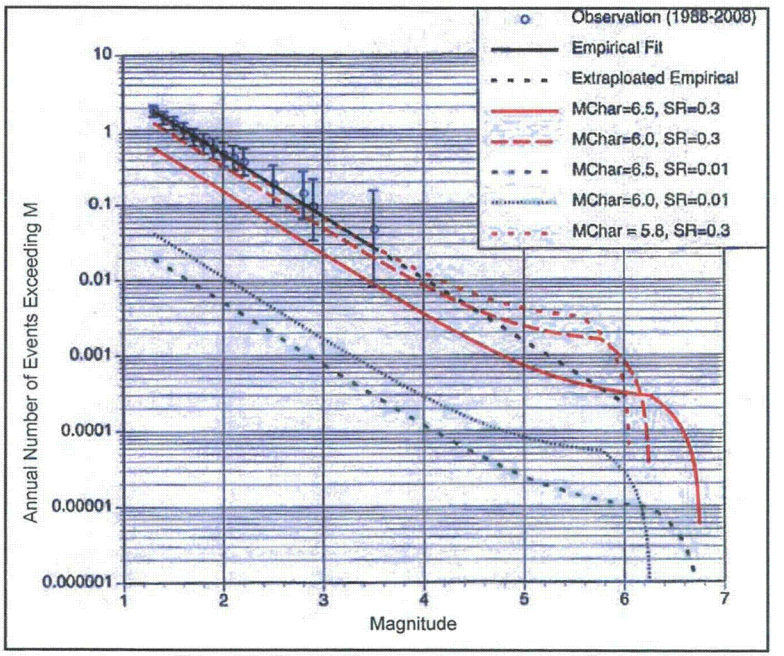

Shoreline seismicity lineament statistics, 1987 to 2008; (a) histogram of earthquakes per year, (b) cummulative number of earthquakes, (c) annual frequency of occurrence plot of Shoreline seismicity (Observation) and Empirical Fit to selected characteristic magnitudes (MChar) and slip rate (SR) mm/yr

SHORELINE FAULT ZONE STUDY

Pacific Gas and Electric Company Figure **4-3**

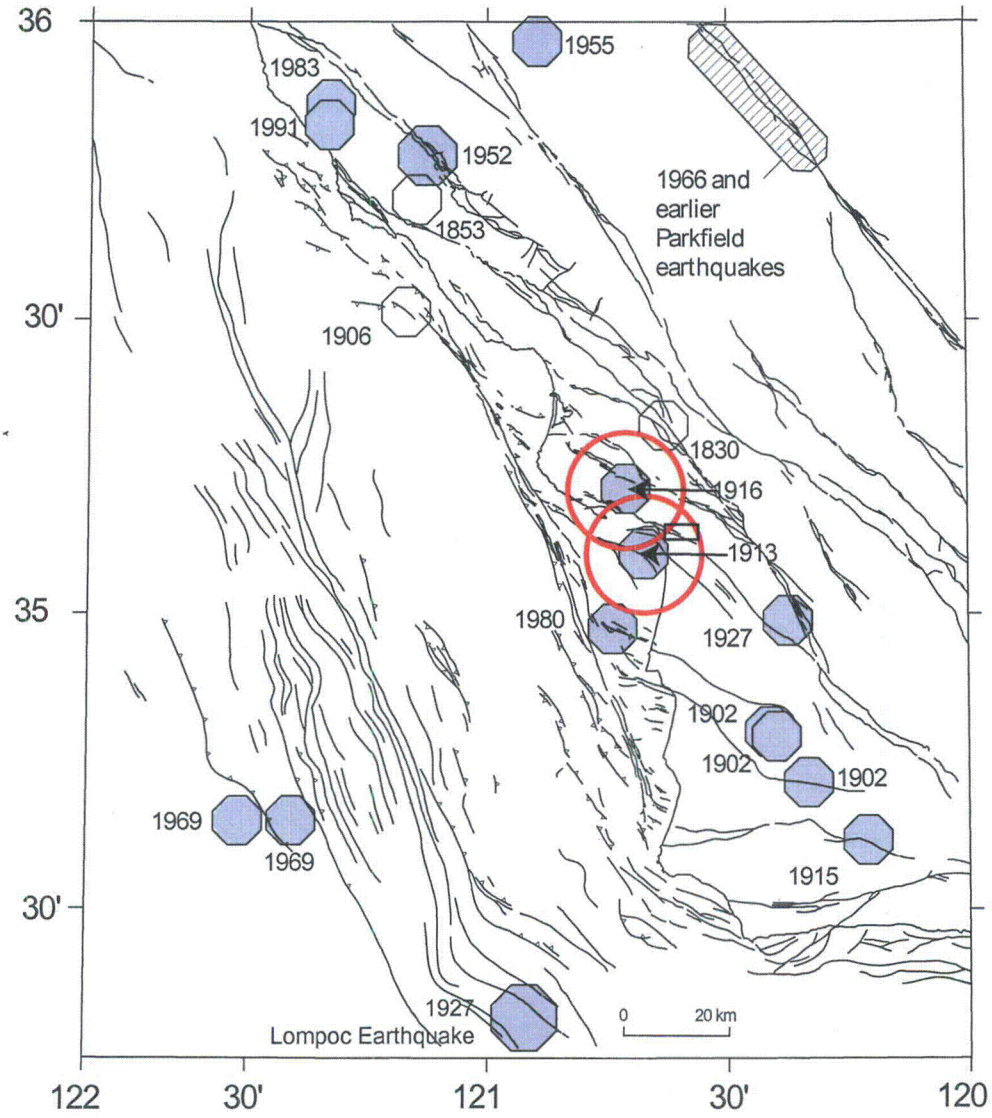

Figure from McLaren and Savage, 2001

EXPLANATION

Event location that is poorly constrained

Event location that is within 20 km and generally within 10 km

10-km radius of uncertainty

Pismo Beach/Arroyo Grande area northeast of the 1913 earthquake

MAGNITUDES

5.0 - 5.9

6.0 - 6.9

7.0 - 7.9

Magnitude 5 and greater pre-1987 historical earthquakes

SHORELINE FAULT ZONE STUDY

Pacific Gas and Electric Company | Figure **4-4**

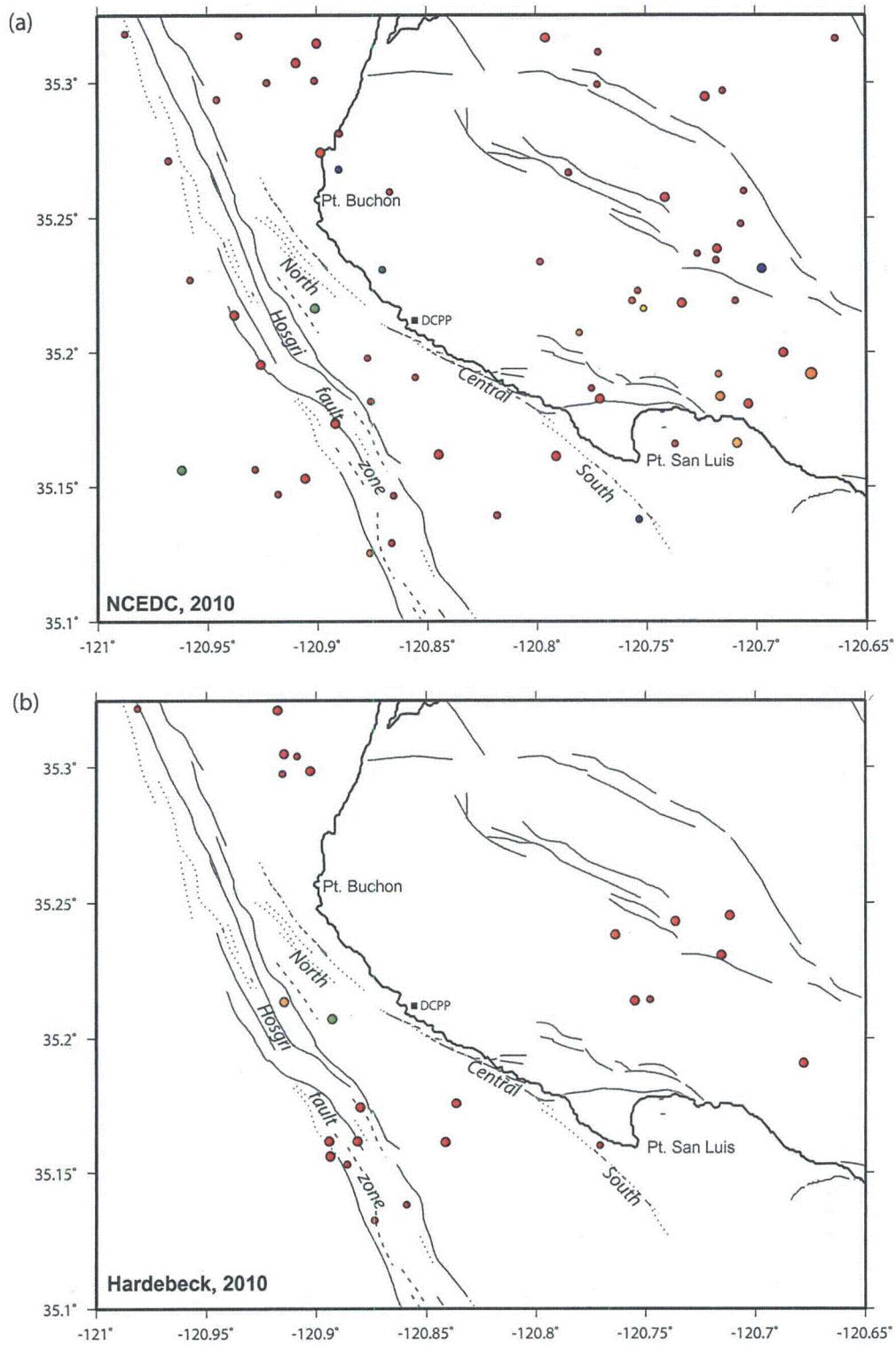

Comparison of 1970 to 1987 earthquake locations (a) 1-D USGS absolute locations and (b) Hardebeck hypoDD relocations.

SHORELINE FAULT ZONE STUDY

Pacific Gas and Electric Company | Figure **4-5**

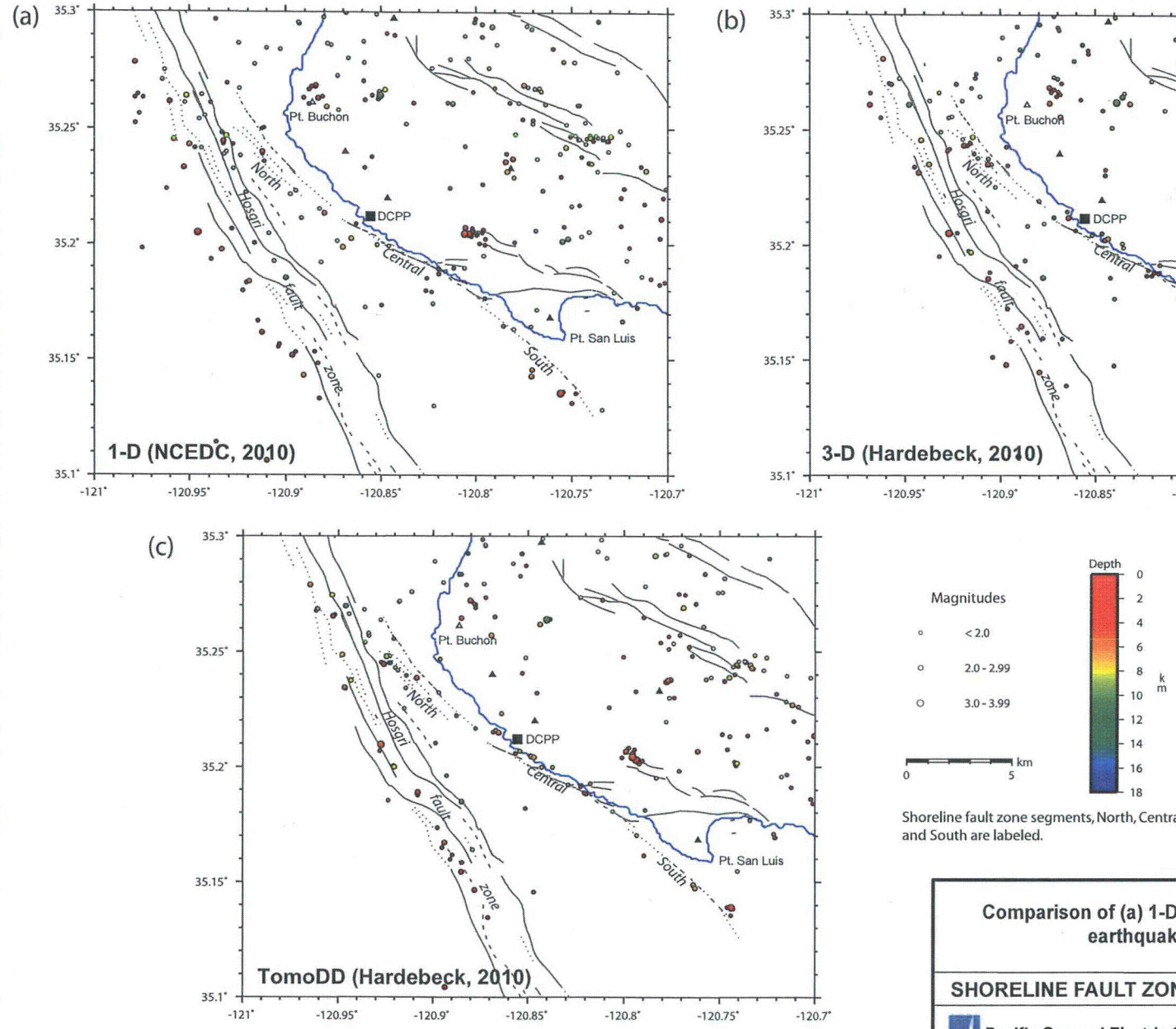

Shoreline fault zone segments, North, Central and South are labeled.

Comparison of (a) 1-D, (b) 3-D and (c) TomoDD earthquake locations.

SHORELINE FAULT ZONE STUDY

Pacific Gas and Electric Company | Figure **4-6**

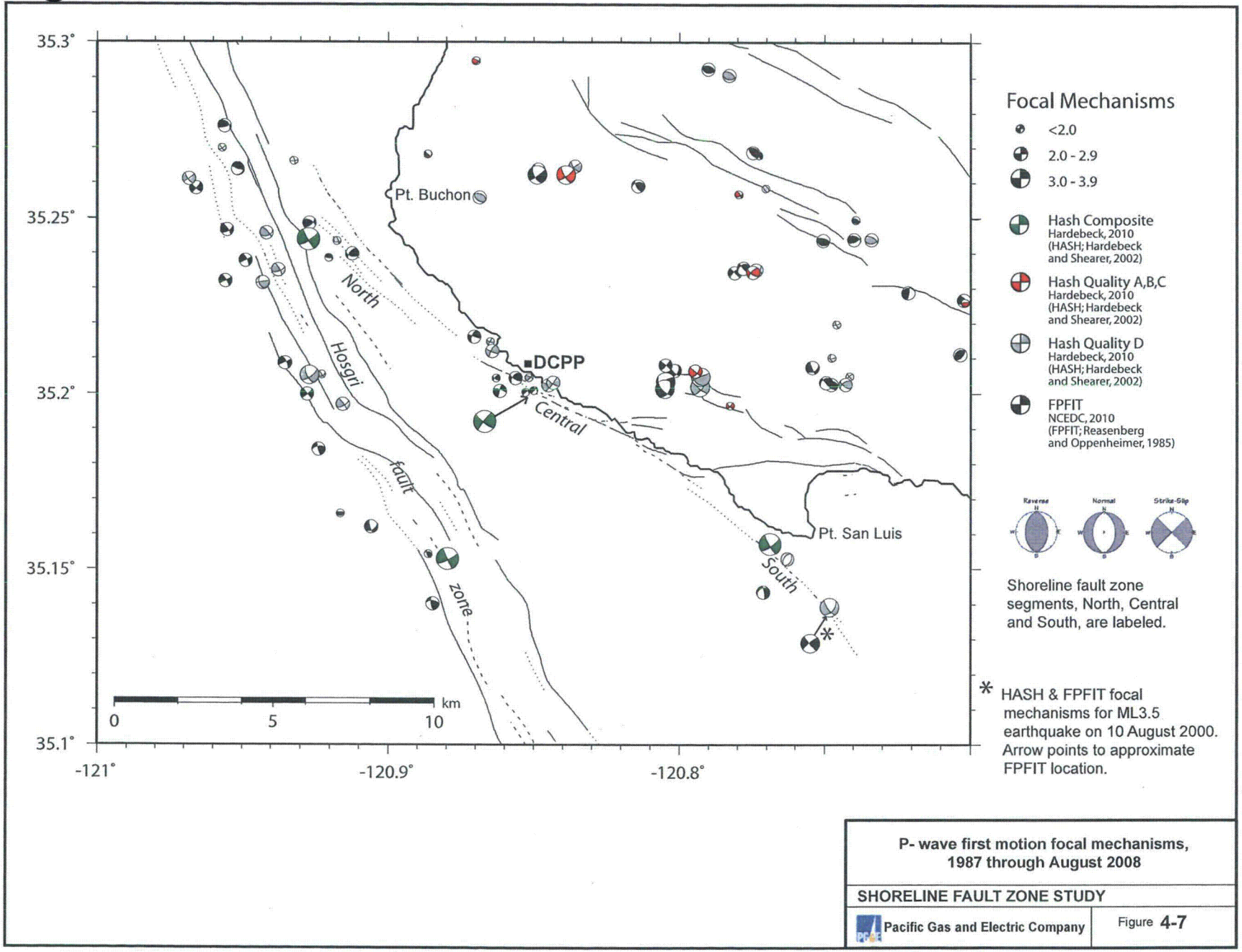

P- wave first motion focal mechanisms, 1987 through August 2008

SHORELINE FAULT ZONE STUDY

Pacific Gas and Electric Company | Figure **4-7**

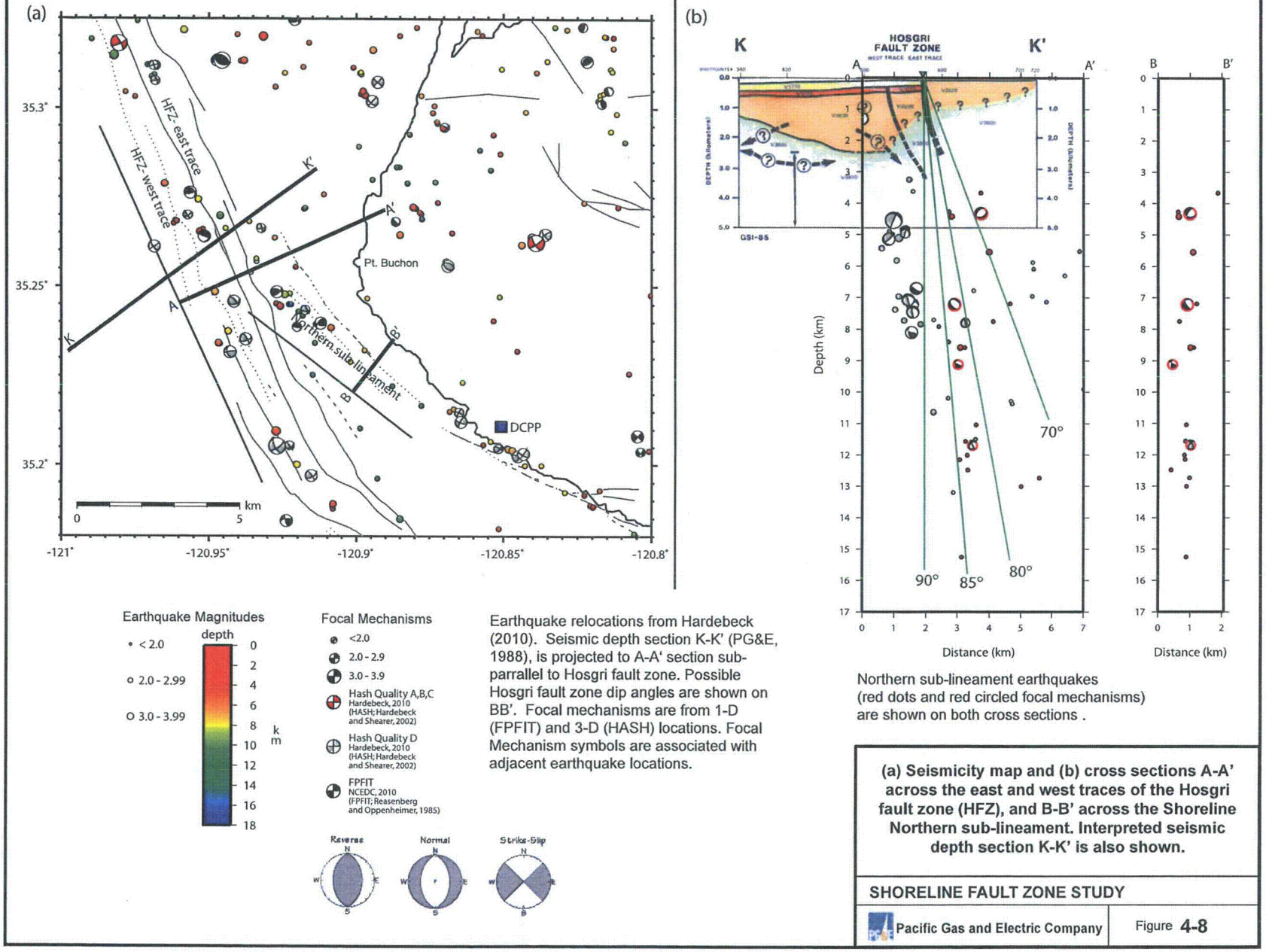

Earthquake relocations from Hardebeck (2010). Seismic depth section K-K' (PG&E, 1988), is projected to A-A' section sub-parrallel to Hosgri fault zone. Possible Hosgri fault zone dip angles are shown on BB'. Focal mechanisms are from 1-D (FPFIT) and 3-D (HASH) locations. Focal Mechanism symbols are associated with adjacent earthquake locations.

Northern sub-lineament earthquakes (red dots and red circled focal mechanisms) are shown on both cross sections .

(a) Seismicity map and (b) cross sections A-A' across the east and west traces of the Hosgri fault zone (HFZ), and B-B' across the Shoreline Northern sub-lineament. Interpreted seismic depth section K-K' is also shown.

SHORELINE FAULT ZONE STUDY

Pacific Gas and Electric Company | Figure **4-8**

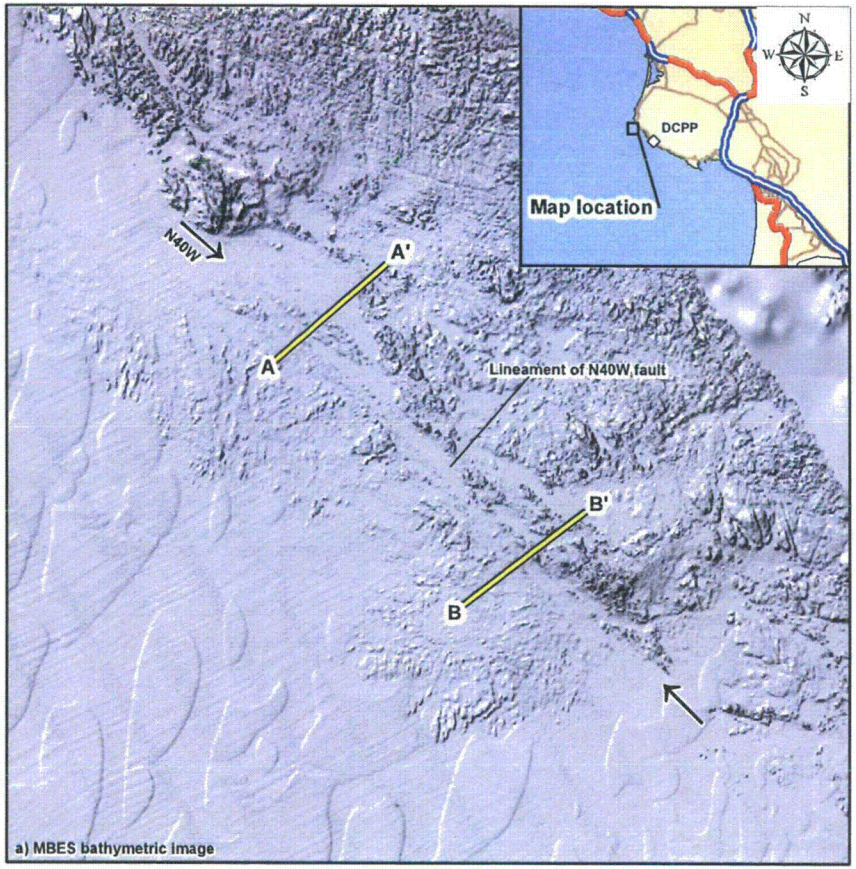

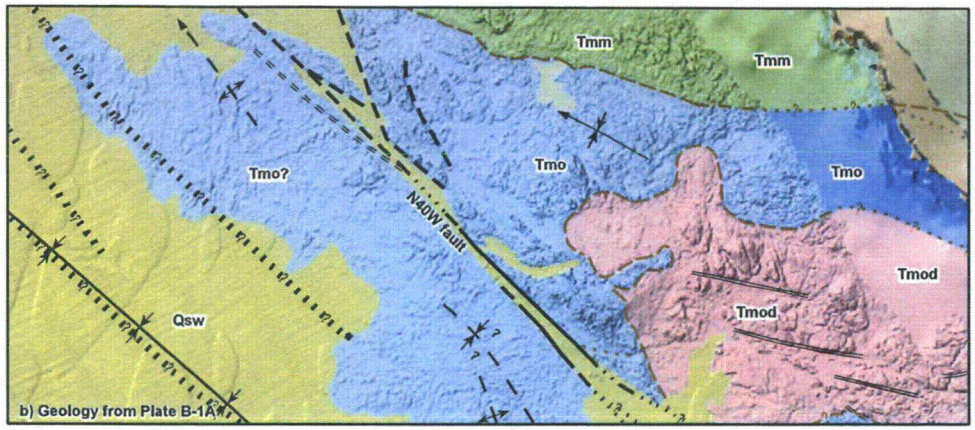

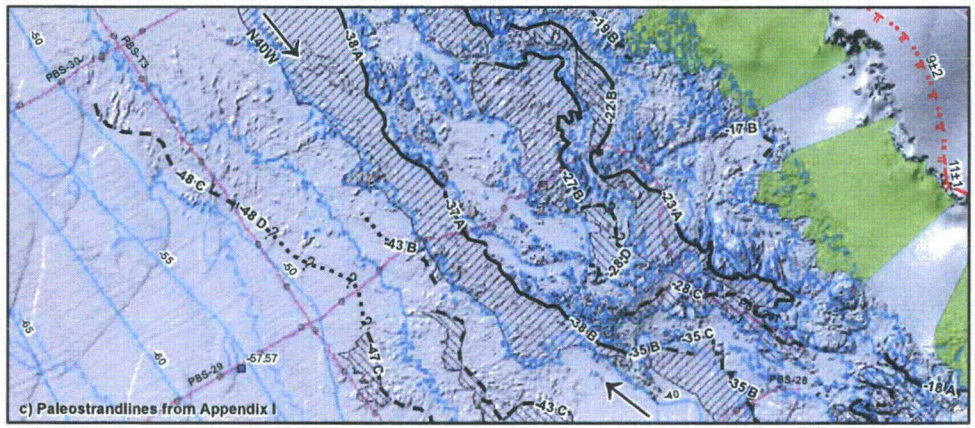

Note: See legend on Plate 1 for geology and Appendix I Plate I-1A for paleostrandlines

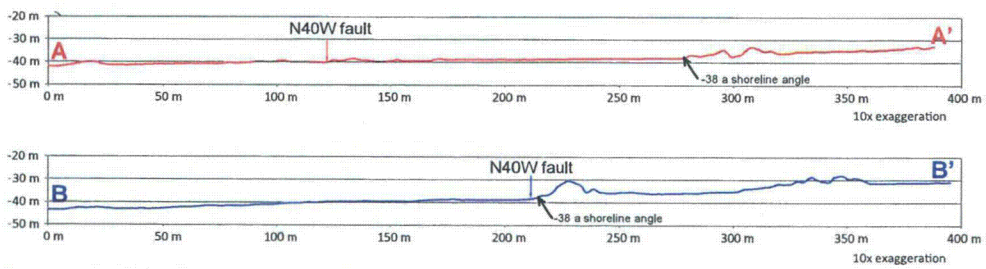

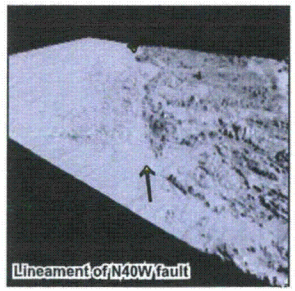

Map scale: 1:12,000
Map projection: NAD 1983, UTM Zone 10 North
0 500 1,000 Feet
0 100 200 300 Meters

Comparison of (a) MBES bathymetric image with (b) the interpreted geology and (c) paleostrandlines across the N40W fault

SHORELINE FAULT ZONE STUDY

Pacific Gas and Electric Company | Figure **4-9**

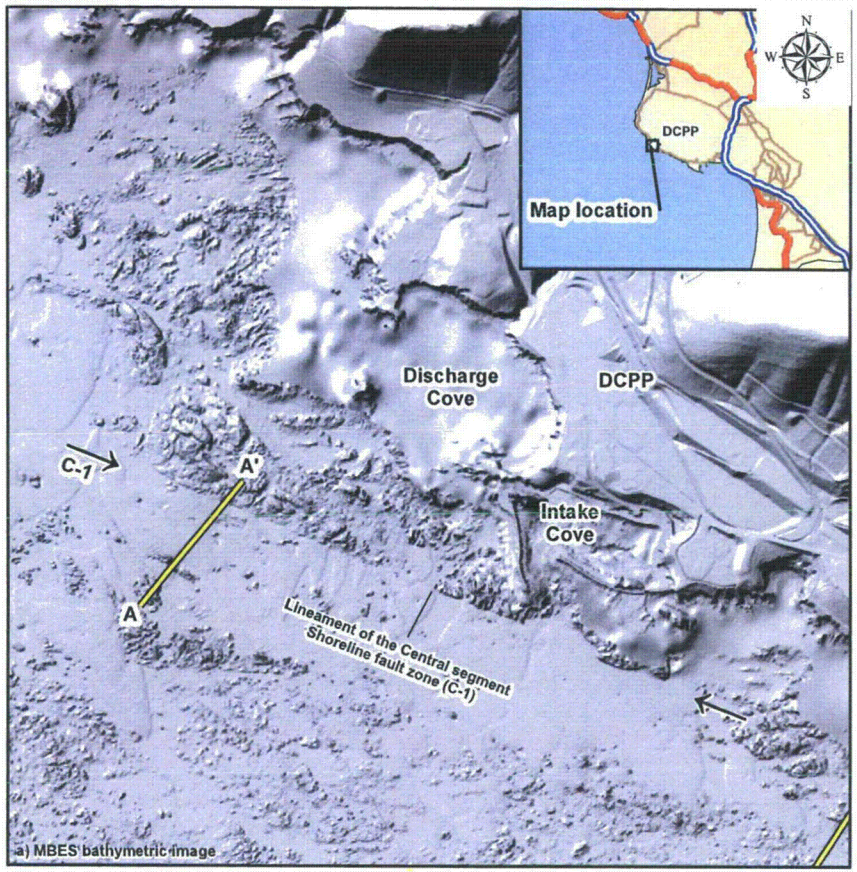

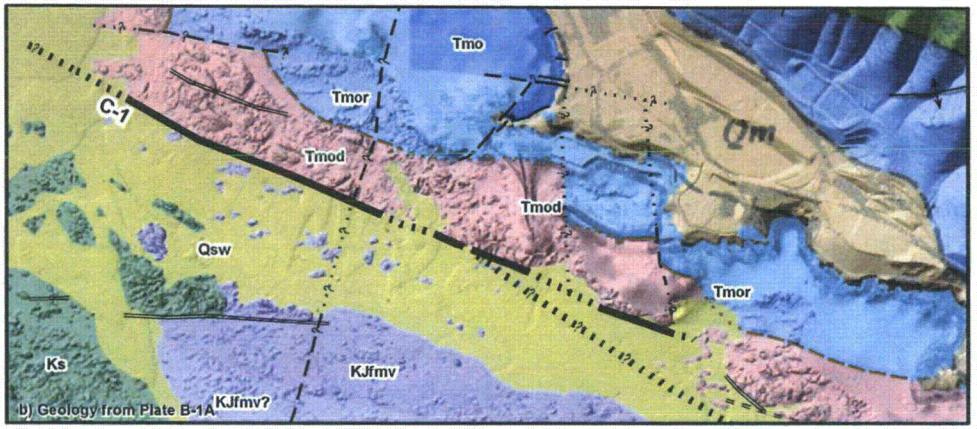

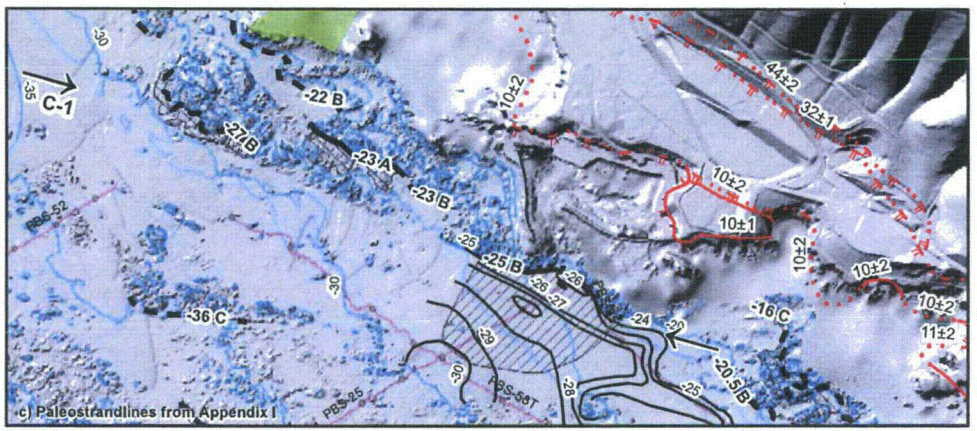

Note: See legend on Plate 1 for geology and Appendix I Plate I-1A for paleostrandlines

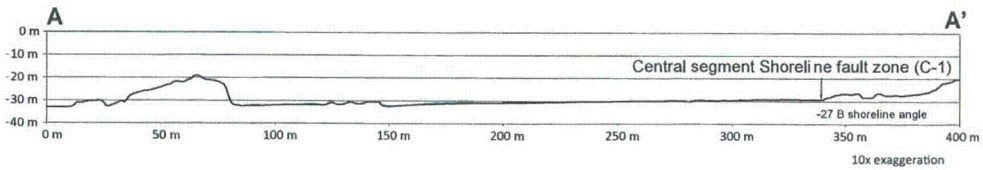

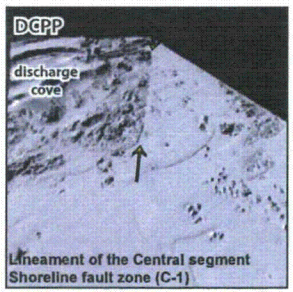

Map scale: 1:12,000
Map projection: NAD 1983, UTM Zone 10 North
0 500 1,000 Feet
0 100 200 300 Meters

Comparison of (a) MBES bathymetry with (b) interpreted geology and (c) paleostrandlines across the Central Segment (C-1) Shoreline fault zone west of DCPP

SHORELINE FAULT ZONE STUDY

Pacific Gas and Electric Company | Figure **4-10**

File path: S:\13800\138381383838.002\Figures\20101112_Report\Appendix_B\Figure_B-5-5.mxd; Date: [12/20/2010]; User: S. Bozkurt

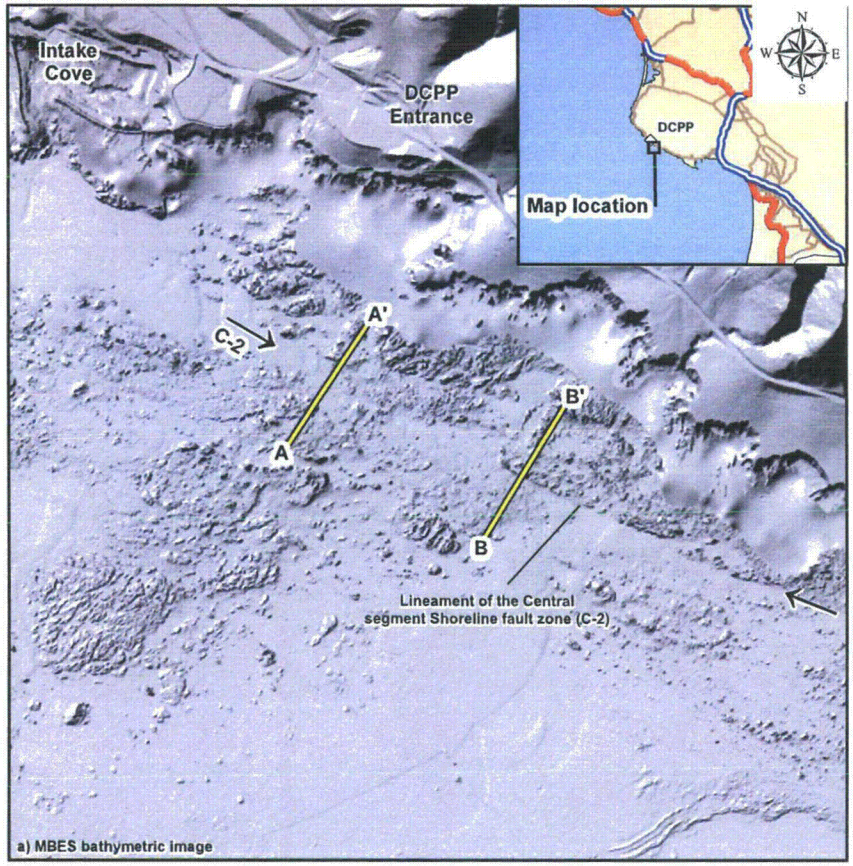

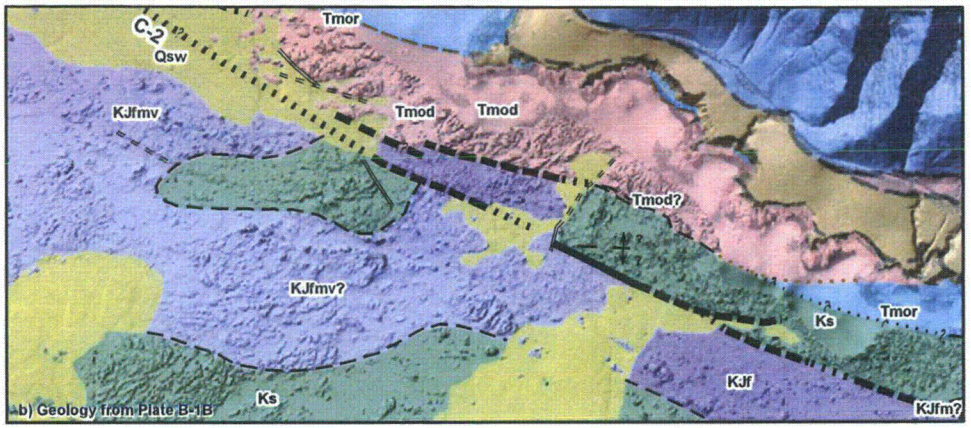

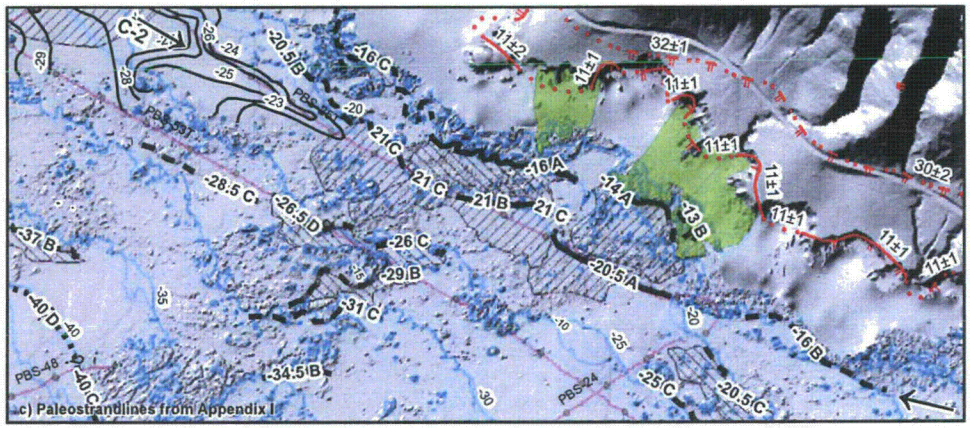

Note: See legend on Plate 1 for geology and Appendix I Plate I-1A for paleostrandlines

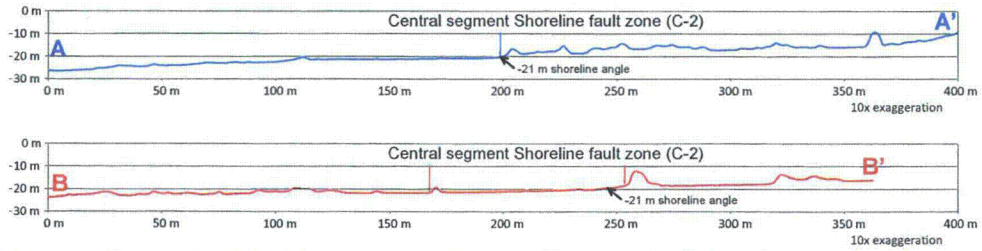

Map scale: 1:12,000
Map projection: NAD 1983, UTM Zone 10 North
0 500 1,000
Feet
Meters
0 100 200 300

Comparison of (a) MBES bathymetry with (b) interpreted geology and (c) paleostrandlines across the Central segment (C-2) Shoreline fault zone southwest of DCPP entrance

SHORELINE FAULT ZONE STUDY

Pacific Gas and Electric Company | Figure **4-11**

File path: S:\13800\138381138838.002\Figures\20101112_Report\Appendix_B\Figure_B-5-6.mxd; Date: [12/20/2010]; User: S. Bozkurt

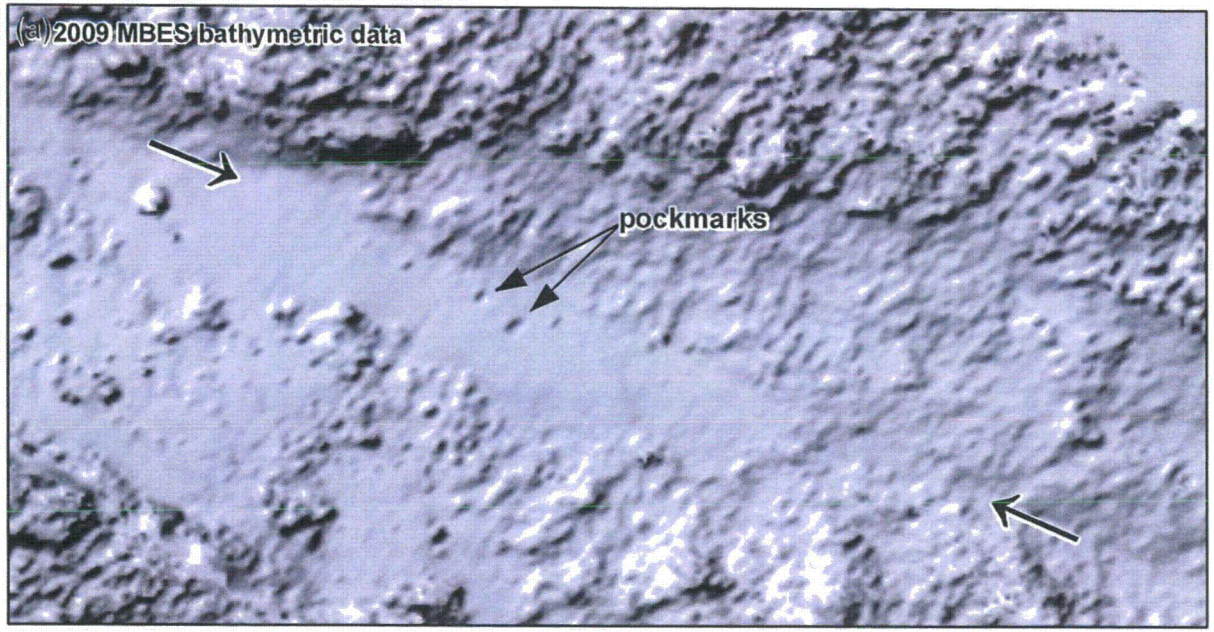

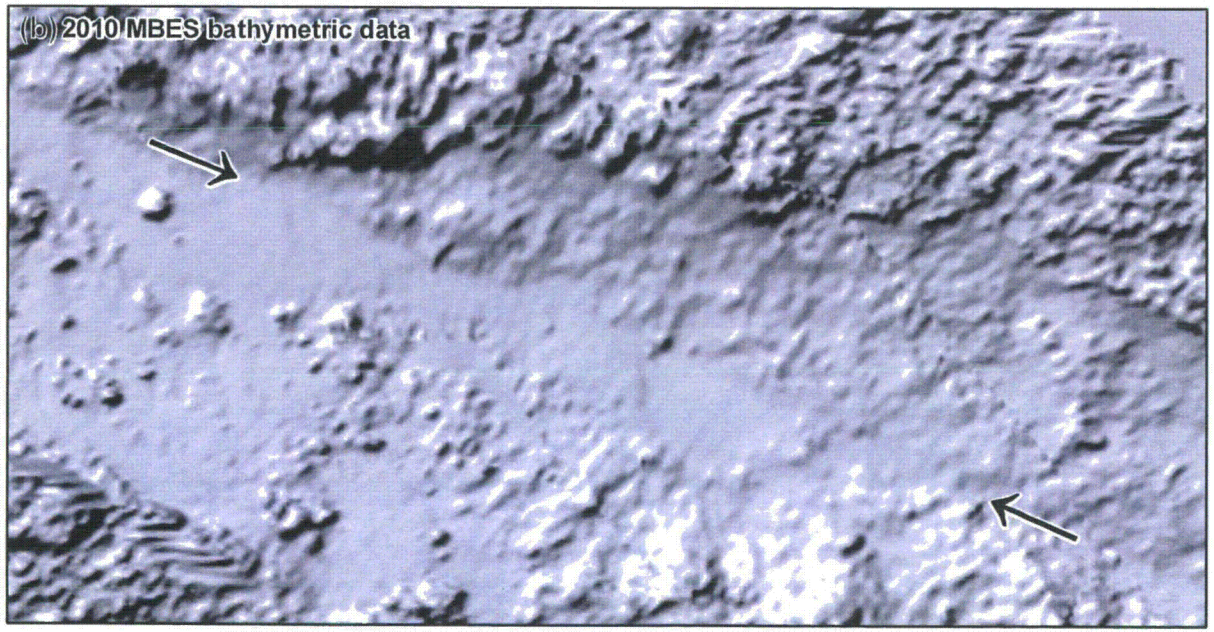

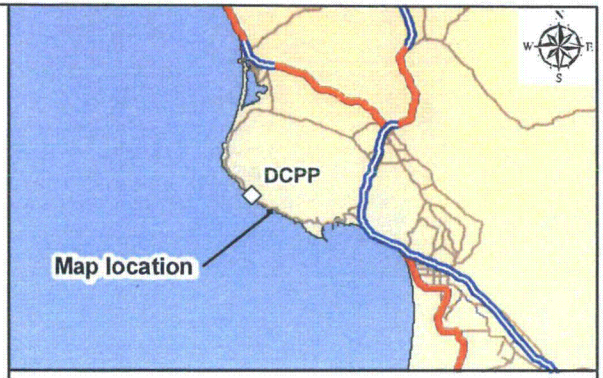

LEGEND

Lineament of Central segment (sub-segment C-2) of the Shoreline fault zone

Notes:
a) The 2009 MBES bathymetric image shows two small pockmarks in the sand sheet that may have been formed by gas or fluid release along the Central segment of the Shoreline fault zone.
b) 2010 MBES bathymetric image of the same area shows the loss of the pockmarks and thinning of the sand sheet, with more bedrock exposed along the fault at the sea floor.

Map scale1:2,000
Map projection: NAD 1983, UTM Zone 10 North

0 200 400 Feet
0 50 100 Meters

Migration of sand sheet along the Central segment (C-2) of the Shoreline fault zone between (a) the 2009 and (b)2010 MBES surveys northwest of Olson Hill

SHORELINE FAULT ZONE STUDY

Pacific Gas and Electric Company | Figure 4-12

File path: S:\13800\13838\13838.002\Figures\20101112_Report\Appendix_B\Figure_B-3-5.mxd; Date: [12/22/2010]; User: Serkan Bozkurt, AMEC Geomatrix, Inc.

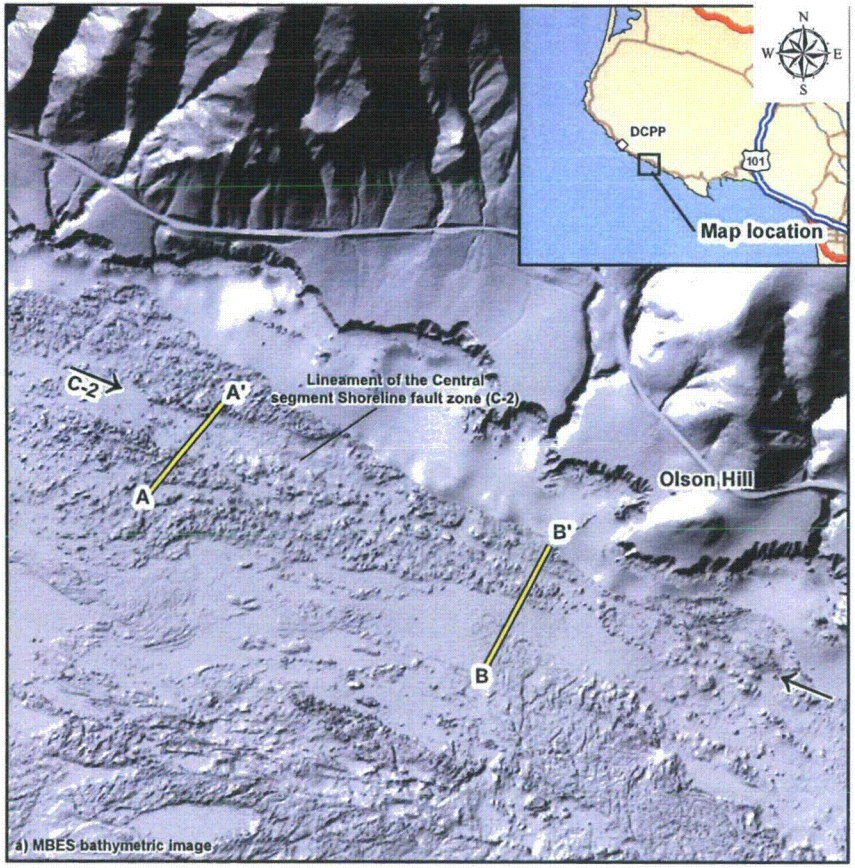

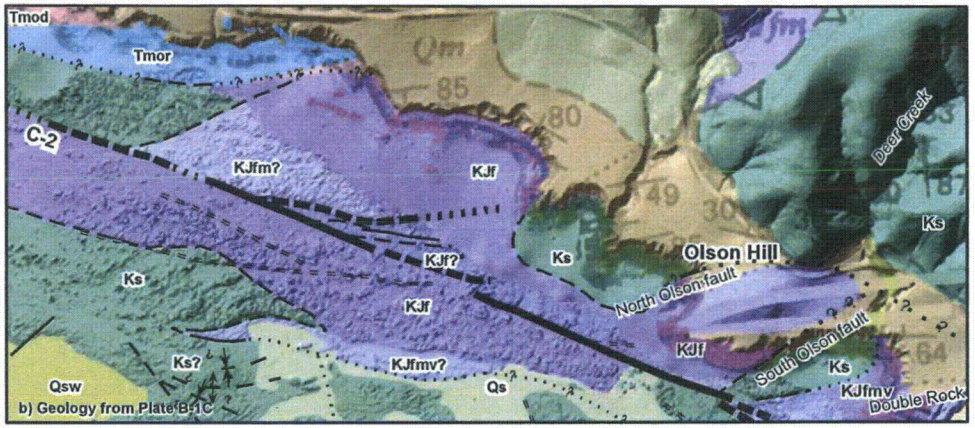

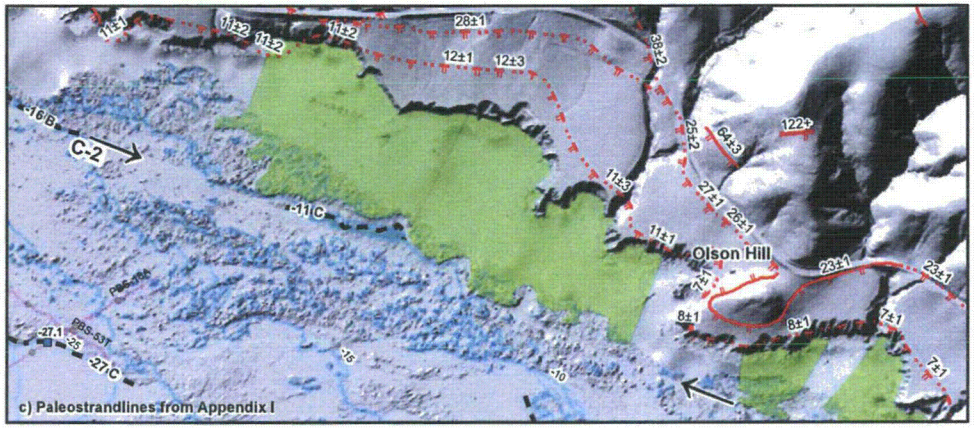

Note: See legend on Plate 1 for geology and Appendix I Plate I-1A for paleostrandlines

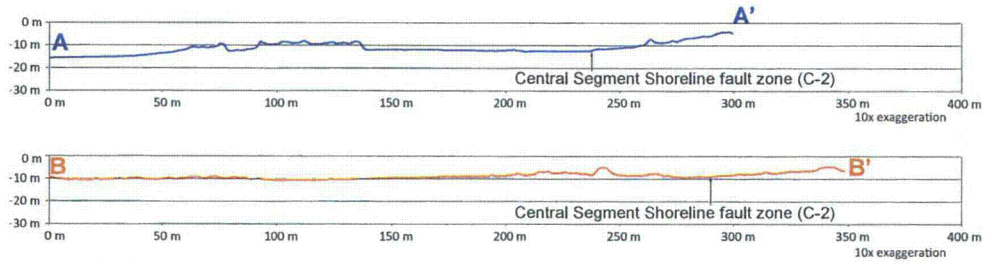

Map scale: 1:12,000
Map projection: NAD 1983, UTM Zone 10 North
0 500 1,000
Feet
Meters
0 100 200 300

Comparison of (a) MBES bathymetry with (b) interpreted geology and (c) paleostrandlines across the Central segment (C-2) Shoreline fault zone west of Olson Hill

SHORELINE FAULT ZONE STUDY

Pacific Gas and Electric Company | Figure **4-13**

File path: S:\13800\113838\13838.002\Figures\20101112_Report\Appendix_B\Figure_B-5-8.mxd; Date: [12/20/2010]; User: S. Bozkurt

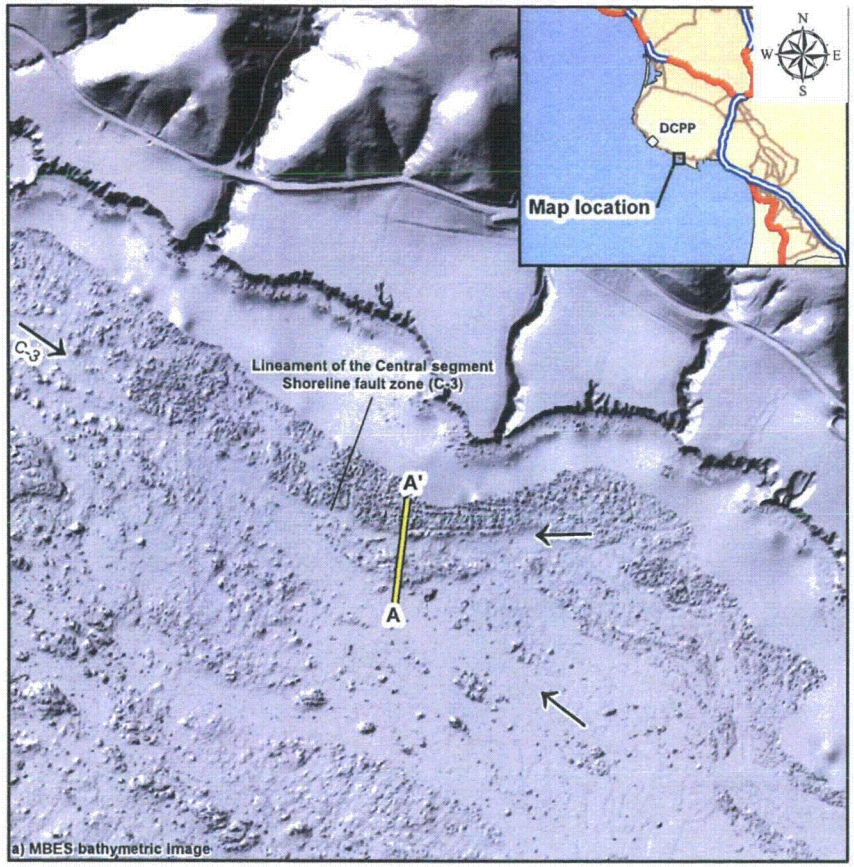

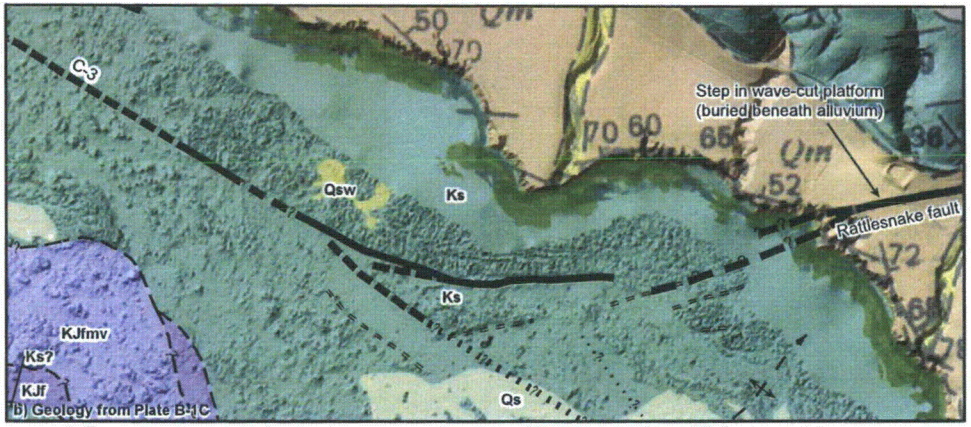

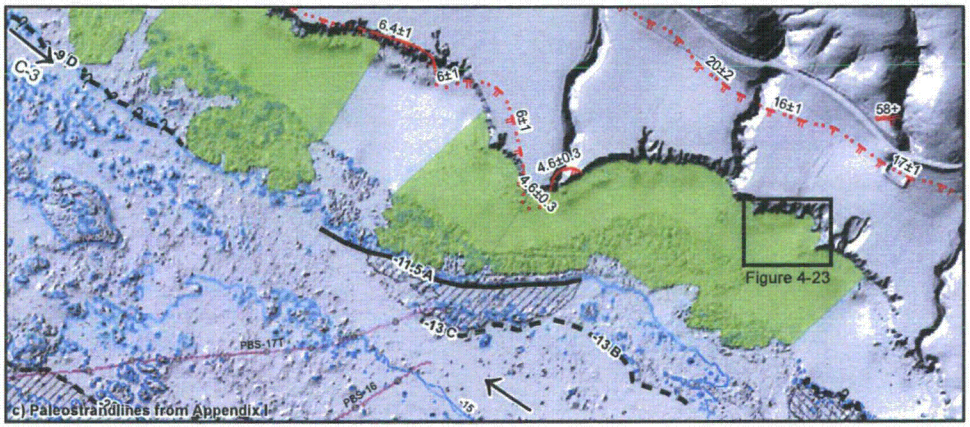

Note: See legend on Plate 1 for geology and Appendix I Plate I-1A for paleostrandlines

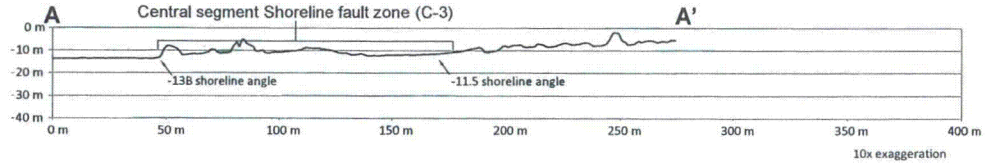

Map scale: 1:12,000
Map projection: NAD 1983, UTM Zone 10 North
0 500 1,000
Feet
Meters
0 100 200 300

Comparison of (a) MBES bathymetry with (b) interpreted geology and (c) paleostrandlines across the Central segment (C-3) of the Shoreline fault zone west of Rattlesnake Creek

SHORELINE FAULT ZONE STUDY

Pacific Gas and Electric Company | Figure **4-14**

File path: S:\13800\13838\13838.002\Figures\20101112_Report\Appendix_B\Figure_B-5-9.mxd: Date: [12/20/2010]; User: S. Bozkurt

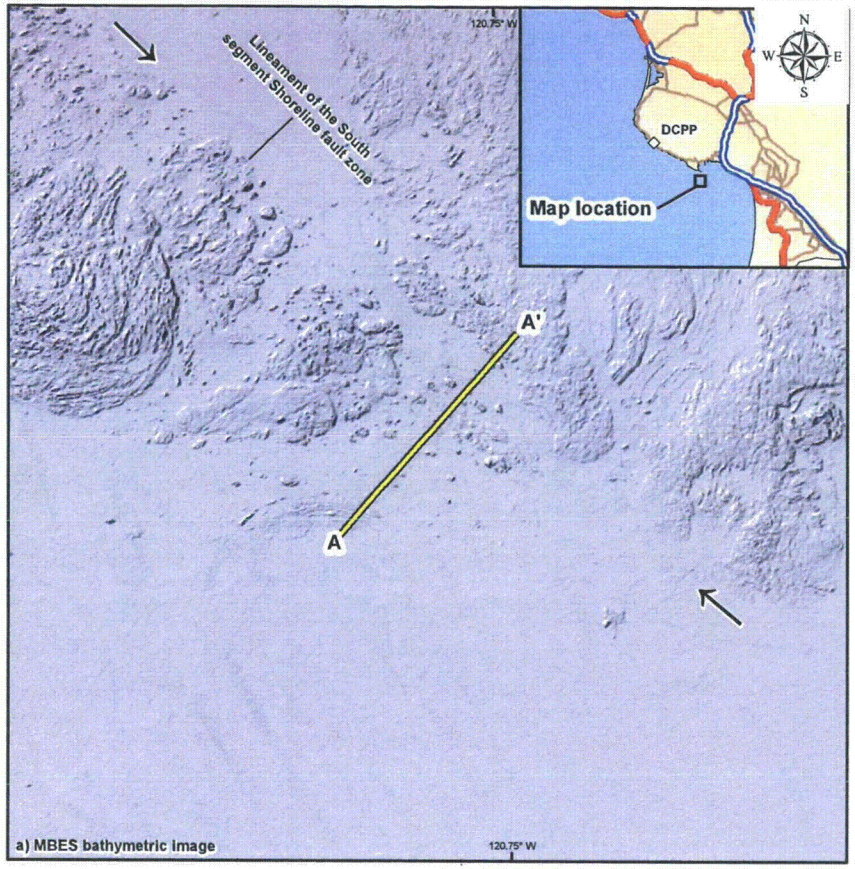

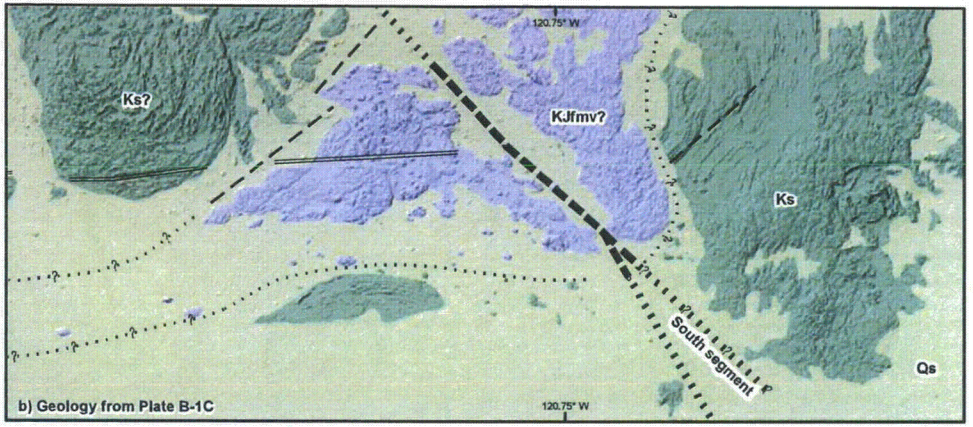

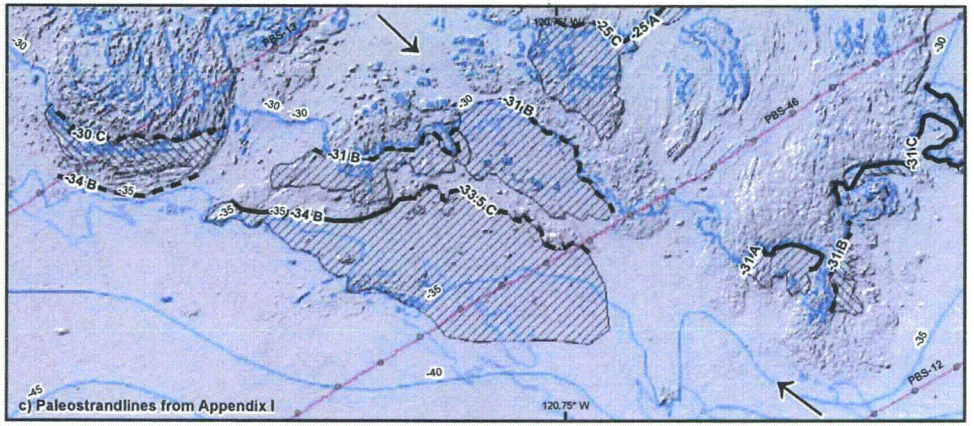

Note: See legend on Plate 1 for geology and Appendix I Plate I-1A for paleostrandlines

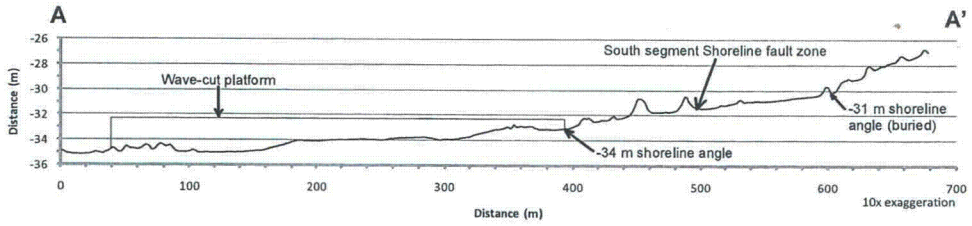

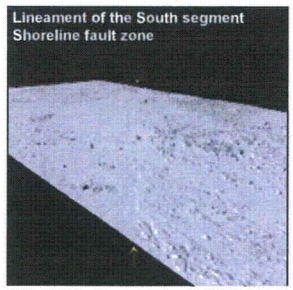

Map scale: 1:12,000
Map projection: NAD 1983, UTM Zone 10 North
0 500 1,000 Feet
0 100 200 300 Meters

Comparison of (a) MBES bathymetry with (b) interpreted geology and (c) paleostrandlines across the South segment of the Shoreline fault zone south of Point San Luis

SHORELINE FAULT ZONE STUDY

Pacific Gas and Electric Company | Figure **4-15**

File path: S:\13800\138381138381138.002\Figures\20101112_Report\Appendix_B\Figure_B-5-10.mxd; Date: [12/21/2010]; User: S. Bozkurt

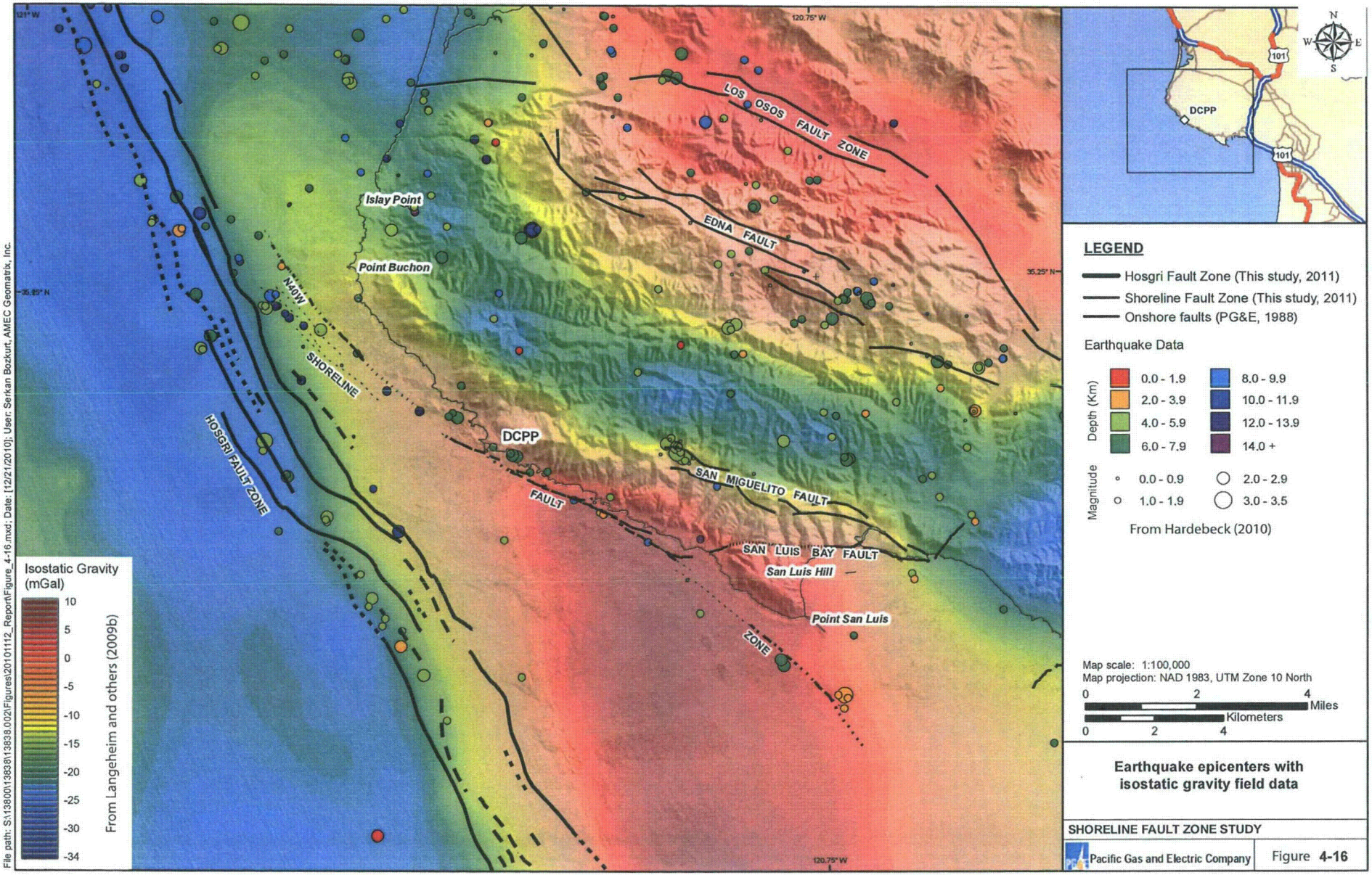
LOS OSOS FAULT ZONE
Islay Point
EDNA FAULT
Point Buchon
N40W
SHORELINE
HOSGRI FAULT ZONE
DCPP
FAULT
SAN MIGUELITO FAULT
SAN LUIS BAY FAULT
San Luis Hill
Point San Luis
ZONE
120.75° W
35.25° N
35.85° N
121° W
Isostatic Gravity (mGal)
10
5
0
-5
-10
-15
-20
-25
-30
-34
From Langeheim and others (2009b)
DCPP
101
101
N
W
E
S
LEGEND
Hosgri Fault Zone (This study, 2011)
Shoreline Fault Zone (This study, 2011)
Onshore faults (PG&E, 1988)
Earthquake Data
Depth (Km)
0.0 - 1.9
2.0 - 3.9
4.0 - 5.9
6.0 - 7.9
8.0 - 9.9
10.0 - 11.9
12.0 - 13.9
14.0 +
Magnitude
0.0 - 0.9
1.0 - 1.9
2.0 - 2.9
3.0 - 3.5
From Hardebeck (2010)
Map scale: 1:100,000
Map projection: NAD 1983, UTM Zone 10 North
0 2 4 Miles
0 2 4 Kilometers
Earthquake epicenters with isostatic gravity field data
SHORELINE FAULT ZONE STUDY
Pacific Gas and Electric Company
Figure 4-16
File path: S:\13800\13838\13838.002\Figures\20101112_Report\Figure_4-16.mxd; Date: [12/21/2010]; User: Serkan Bozkurt, AMEC Geomatrix, Inc.

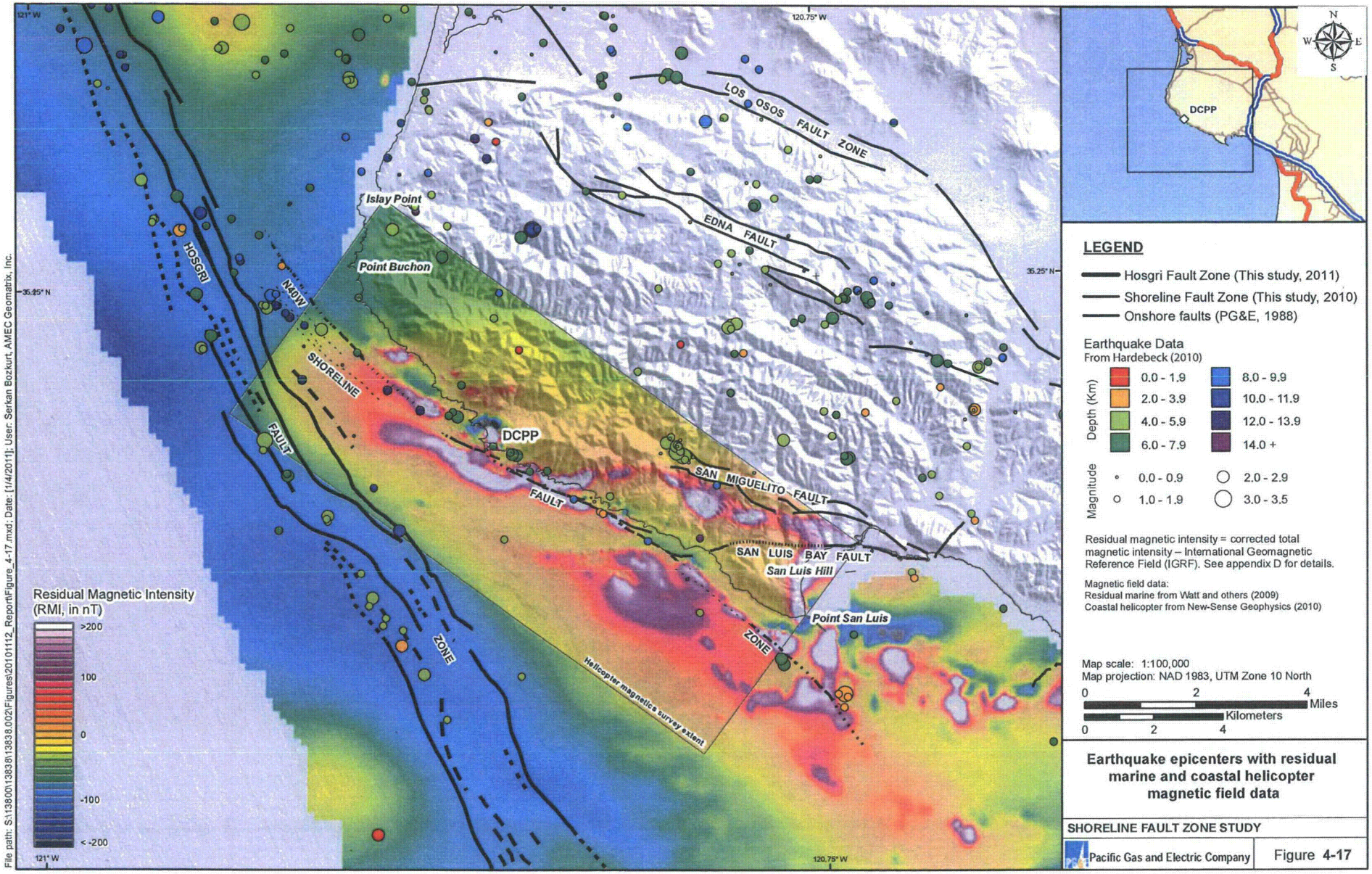

Earthquake epicenters with residual marine and coastal helicopter magnetic field data

SHORELINE FAULT ZONE STUDY

Pacific Gas and Electric Company | Figure 4-17

File path: S:\13800\13838\13838.002\Figures\20101112_Report\Figure_4-17.mxd; Date: [1/4/2011]; User: Serkan Bozkurt, AMEC Geomatrix, Inc.

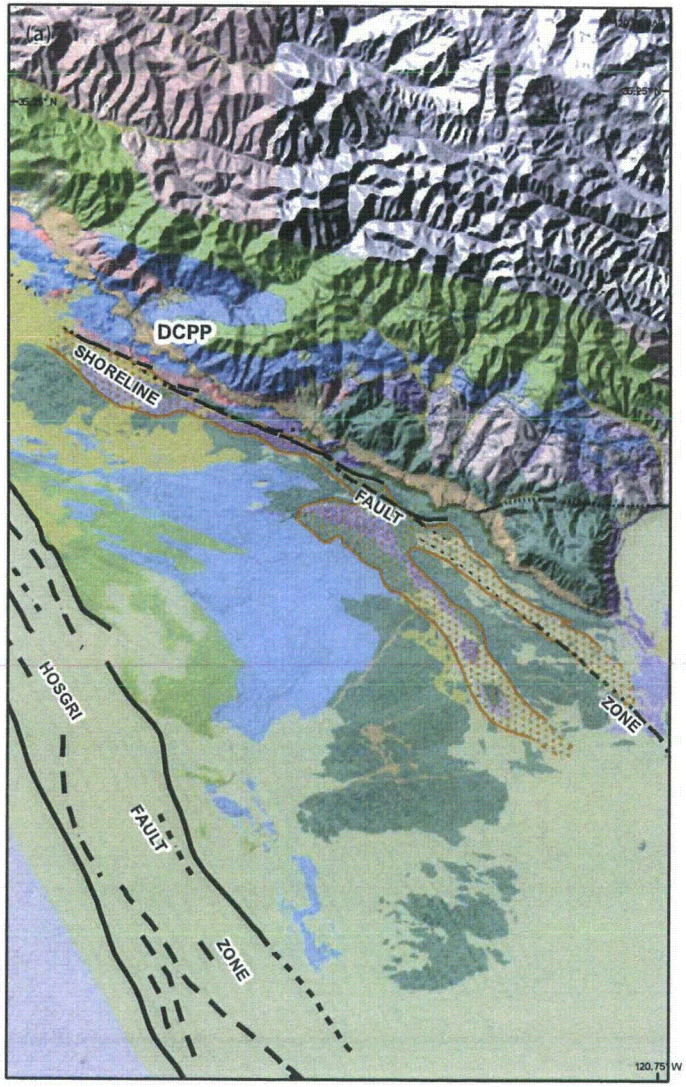

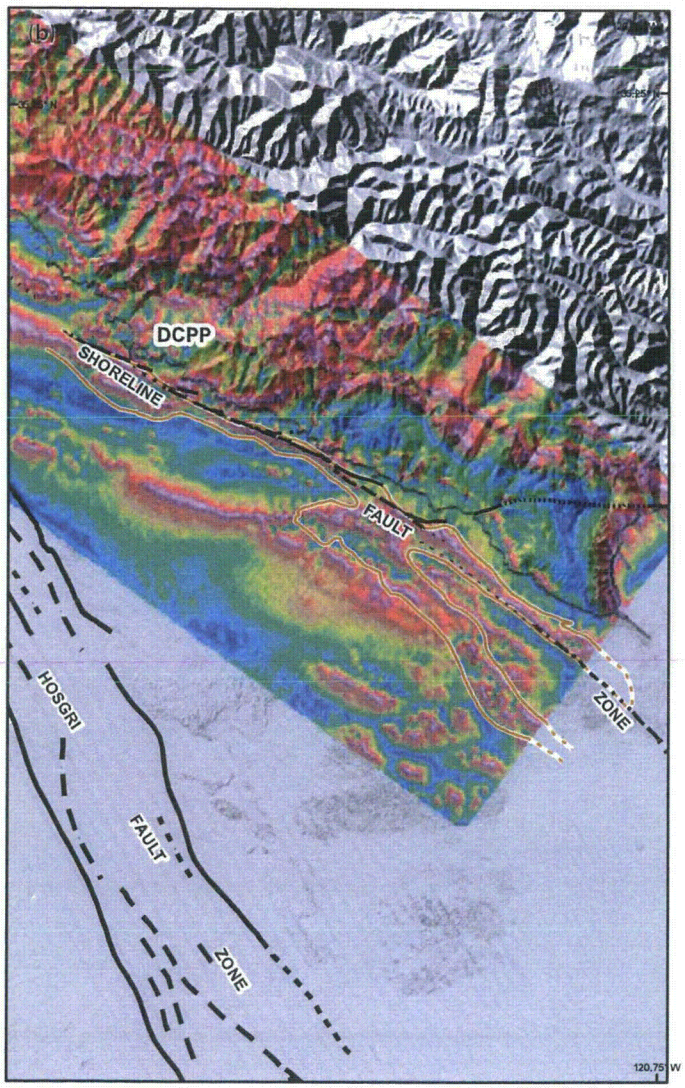

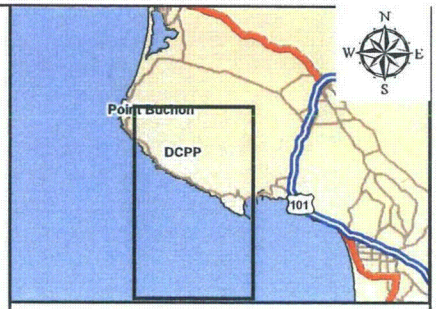

LEGEND

Area of Franciscan mélange interpreted from geology at sea floor or beneath thin sand sheet

Mélange bounding line from geologic map on magnetic image

Faults (This study, 2011)

2010 Helicopter Magnetic Survey

45
21
-1
-21
-39
-55
-67
-78

Tilt angle of RTP is shown in degrees

See Appendix D for discussion of magnetic data

Notes:
See Plate 1 for geology legend.
The Central and Southern segments of the Shoreline fault zone lie within the Franciscan mélange and generally follow magnetic highs.

Map scale: 1:90,000
Map projection: NAD 1983, UTM Zone 10 North

0 1 2 Miles
0 2 4 Kilometers

Generalized area of (a) Franciscan mélange offshore compared to (b) magnetic-field anomalies

SHORELINE FAULT ZONE STUDY

Pacific Gas and Electric Company | Figure **4-18**

File path: S:\13800\13838\13838.002\Figures\20101112_ReportAppendix_BI\Figure_B-4-4.mxd; Date: [12/20/2010]; User: Serkan Bozkurt, AMEC Geomatrix, Inc.

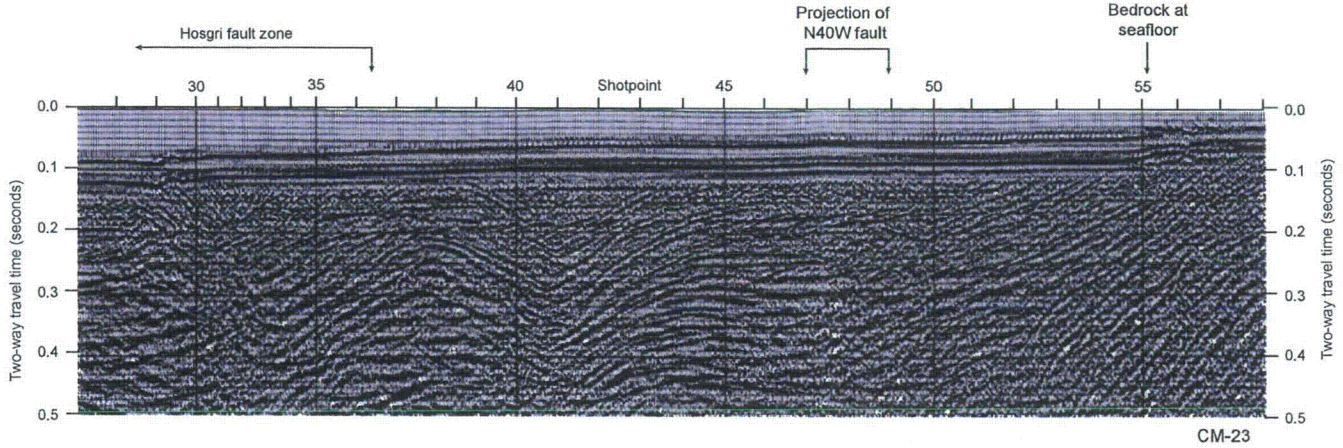

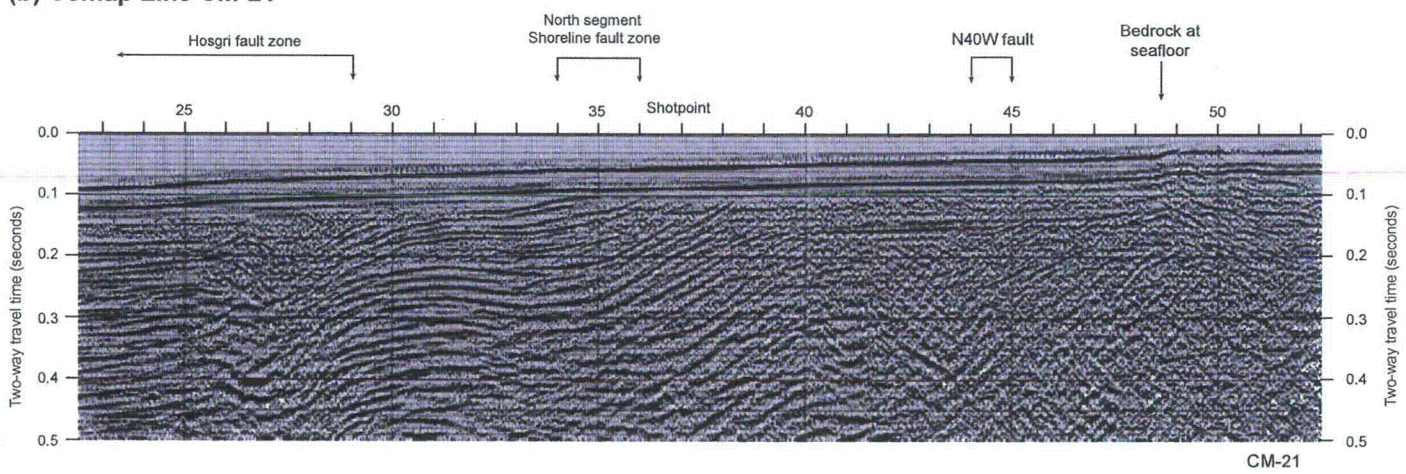

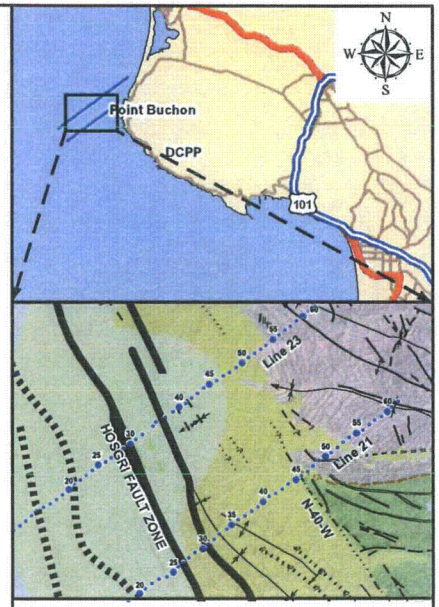

Note: Comap profiles (upper 0.5 seconds) (PG&E, 1988). CM-23 images the eatern part of the Hosgri fault zone but not the N40W fault. CM-21 images the eastern part of the Hosgri fault zone and the N40W fault. No fault is detected in the seismic-reflection profile across the northern Shoreline seismicity lineament.

Comap seismic-reflection profiles (a) CM-23 and (b) CM-21 across the Hosgri fault zone, North segment of the Shoreline fault zone and the N40W fault.

SHORELINE FAULT ZONE STUDY

Pacific Gas and Electric Company | Figure **4-19**

File path: S:\113800\138381838.002\Figures\20101112_Report\Appendix_B\Figure_B-5-3.ai; Date: [12/21/2010]; User: S. Bozkurt

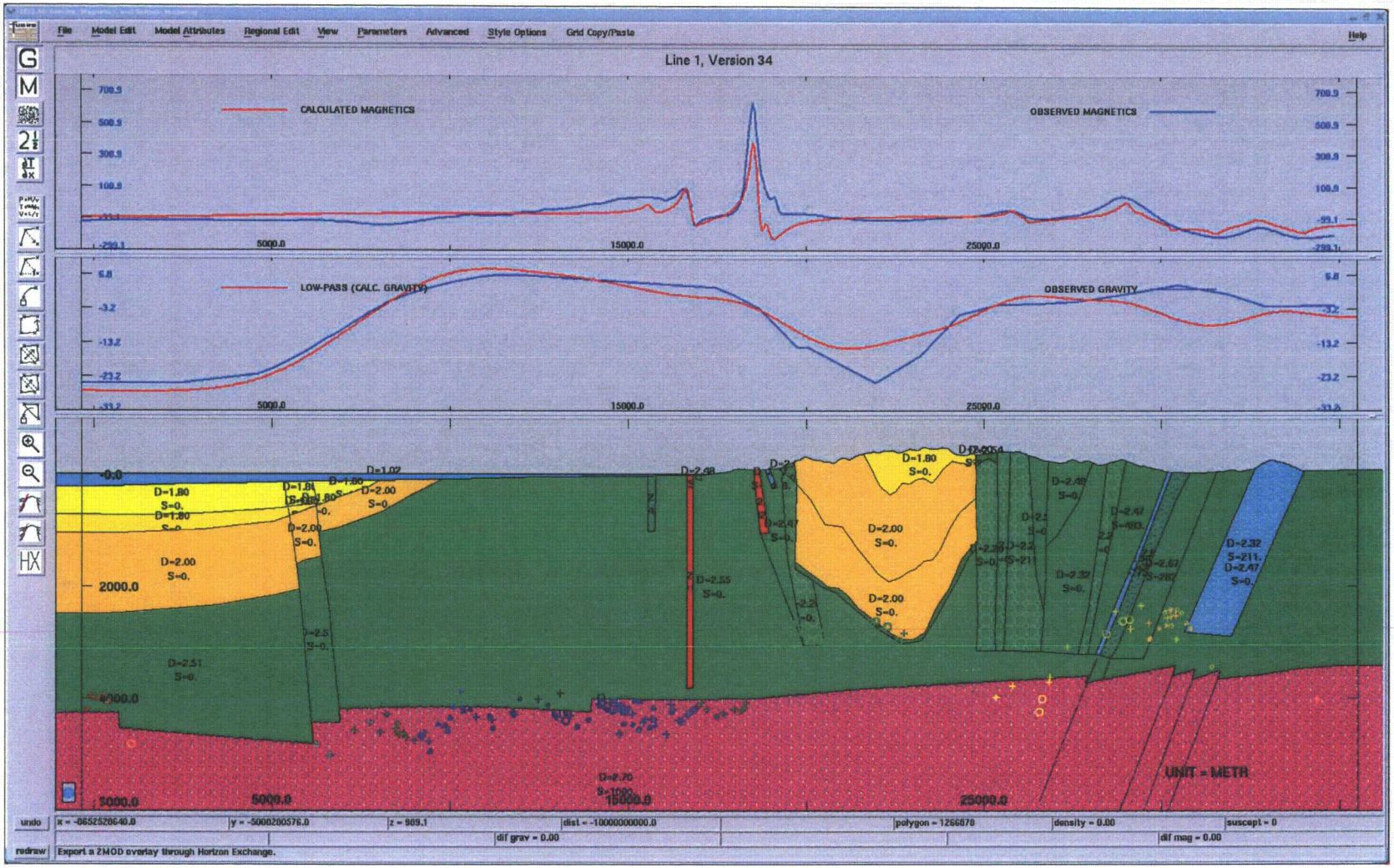

Cross Section of geology, magnetic inversion and gravity through Olson Hill

SHORELINE FAULT ZONE STUDY

Pacific Gas and Electric Company | Figure **4-20**

File path: S:\13800\13838\13838.002\Figures\20101112_Report\Figure_4-20.ai; Date: [12/21/2010]; User: S. Bozkurt

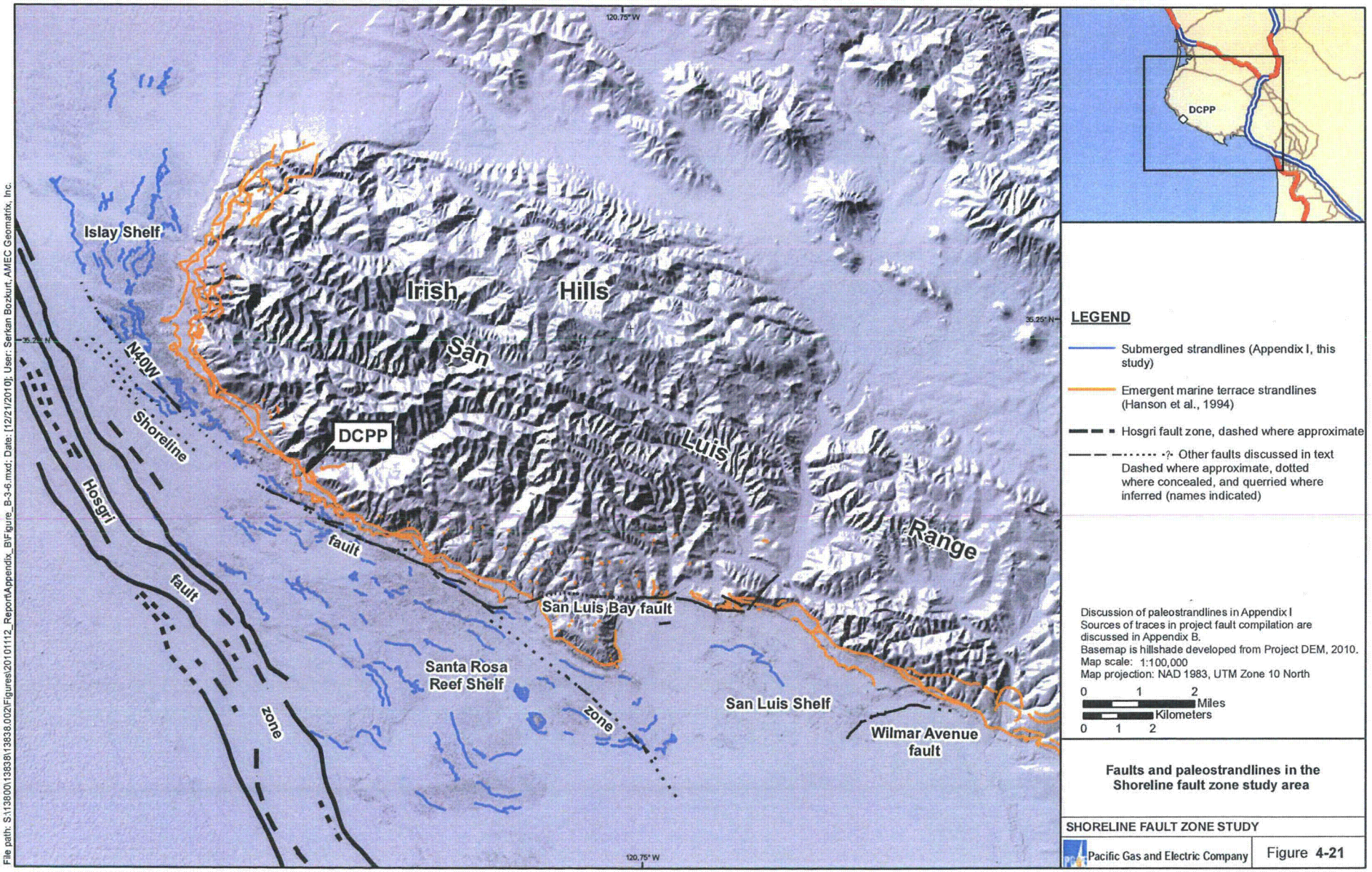

File path: S:\13800\113838\113838.002\Figures\20101112_ReportAppendix_B\Figure_B-3-6.mxd; Date: [12/21/2010]; User: Serkan Bozkurt, AMEC Geomatrix, Inc.

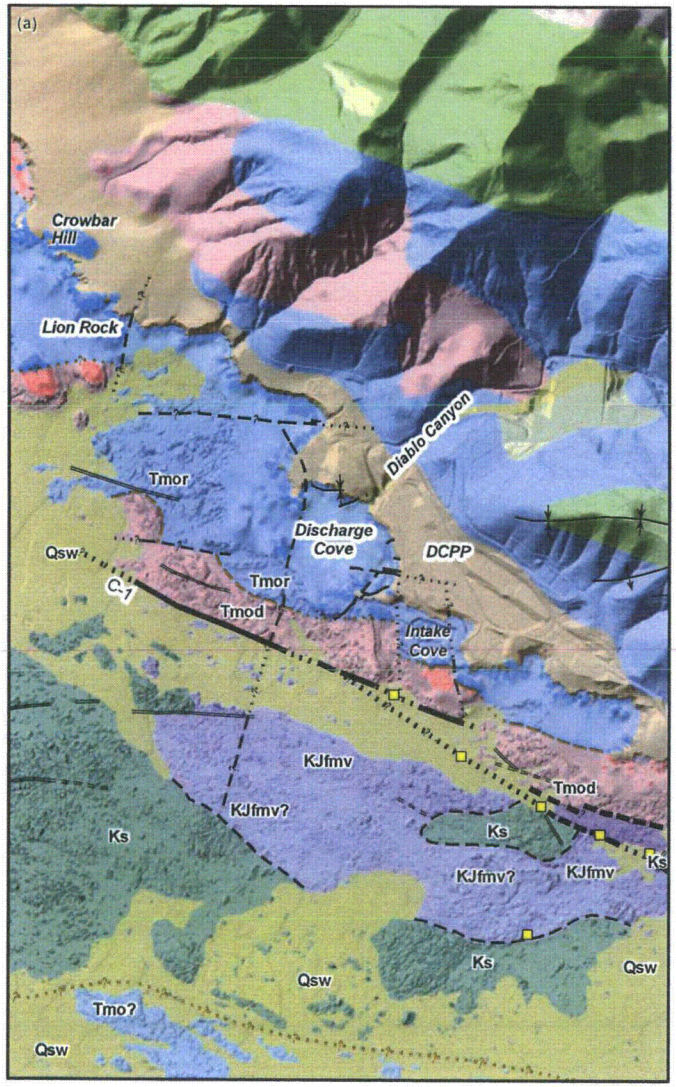

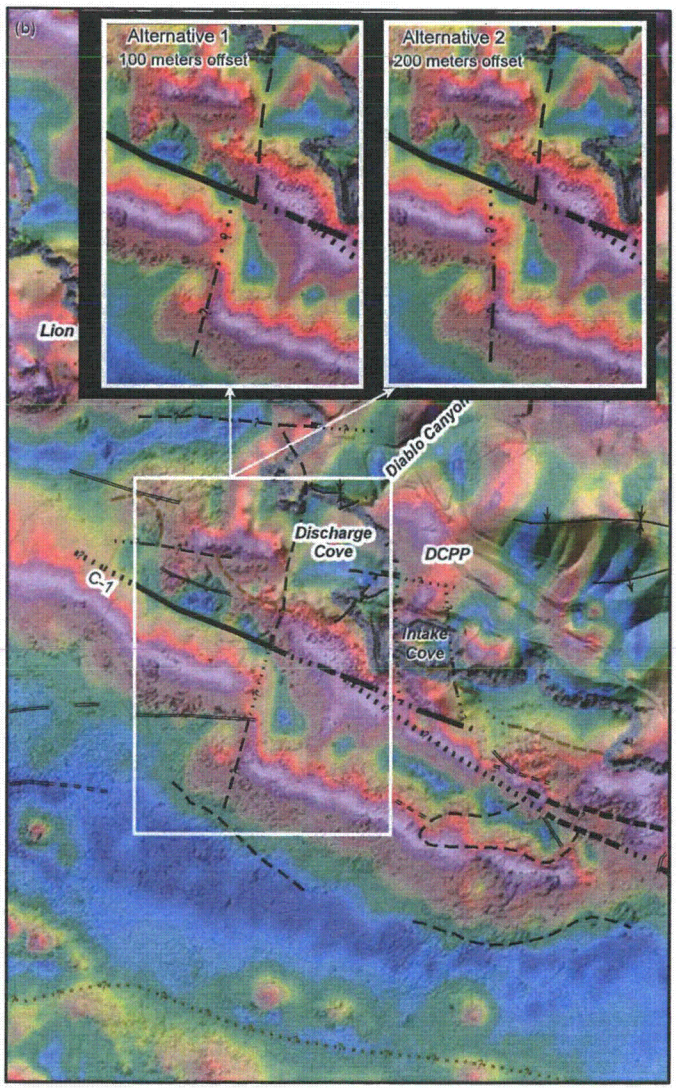

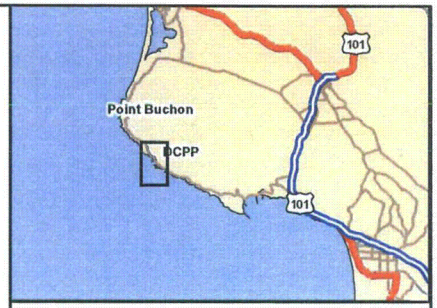

LEGEND

45
21
-1
-21
-39
-55
-67
-78

2010 Helicopter Magnetic Survey Enhancement

Tilt angle of RTP is shown in degrees

See Appendix D for discussion of magnetic data

Notes:
The onshore right-lateral north-south fault north of Discharge Cove aligns with a north-south offset of two northwest-trending magnetic highs. The magnetic anomalies are interpreted to be offset by the same north-south fault. The Shoreline fault does not appear to displace the north-south fault laterally within the limits of resolution (estimated to be about 100 meters per "Alternative 1" but clearly less than 200 meters per "Alternative 2").

See Plate 1 for geology legend.

Map scale: 1:20,000
Map projection: NAD 1983, UTM Zone 10 North

0 1,000 2,000 Feet

0 500 1,000 Meters

Comparison of (a) the geology with (b) the magnetic-field anomalies in the DCPP area

SHORELINE FAULT ZONE STUDY

Pacific Gas and Electric Company | Figure **4-22**

File path: S:\13800\13838\13838.002\Figures\20101112_Report\Appendix_B\Figure_B-5-1.mxd; Date: [12/20/2010]; User: S. Bozkurt

File path: S:\13800\13838\13838.002\Figures\20101112_Report\Appendix_B\Figure_B-5-10.ai; Date: [12/21/2010]; User: Serkan Bozkurt, AMEC Geomatrix, Inc.

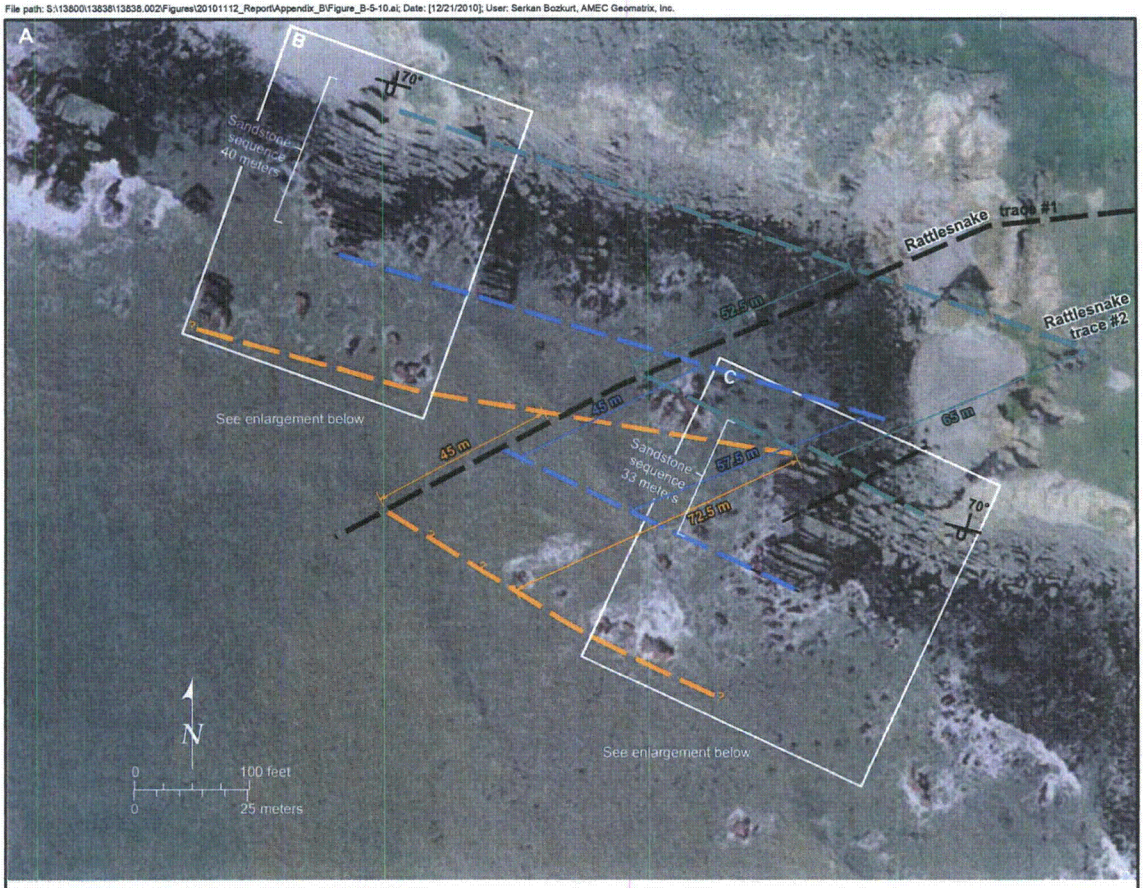

Base image is low tide aerial photograph, aquired 01/28/2010

Interpreted Correlation

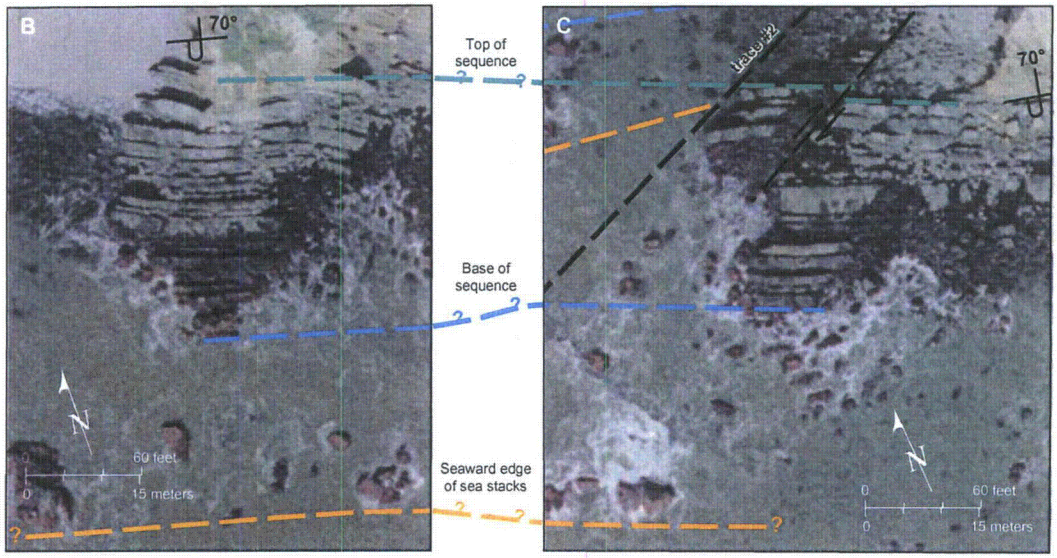

See Figure 4-14 for location

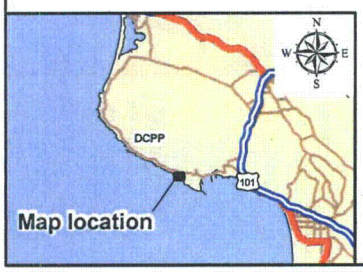

Explanation

- Top of sequence
- Base of sequence
- Seaward edge of sea stacks
- Faults, approximately located
- 70° Strike and dip of overturned bed

Apparent offset of Cretaceous sandstone beds across the Rattlesnake fault, San Luis Bay fault zone

SHORELINE FAULT ZONE STUDY

Pacific Gas and Electric Company | Figure **4-23**

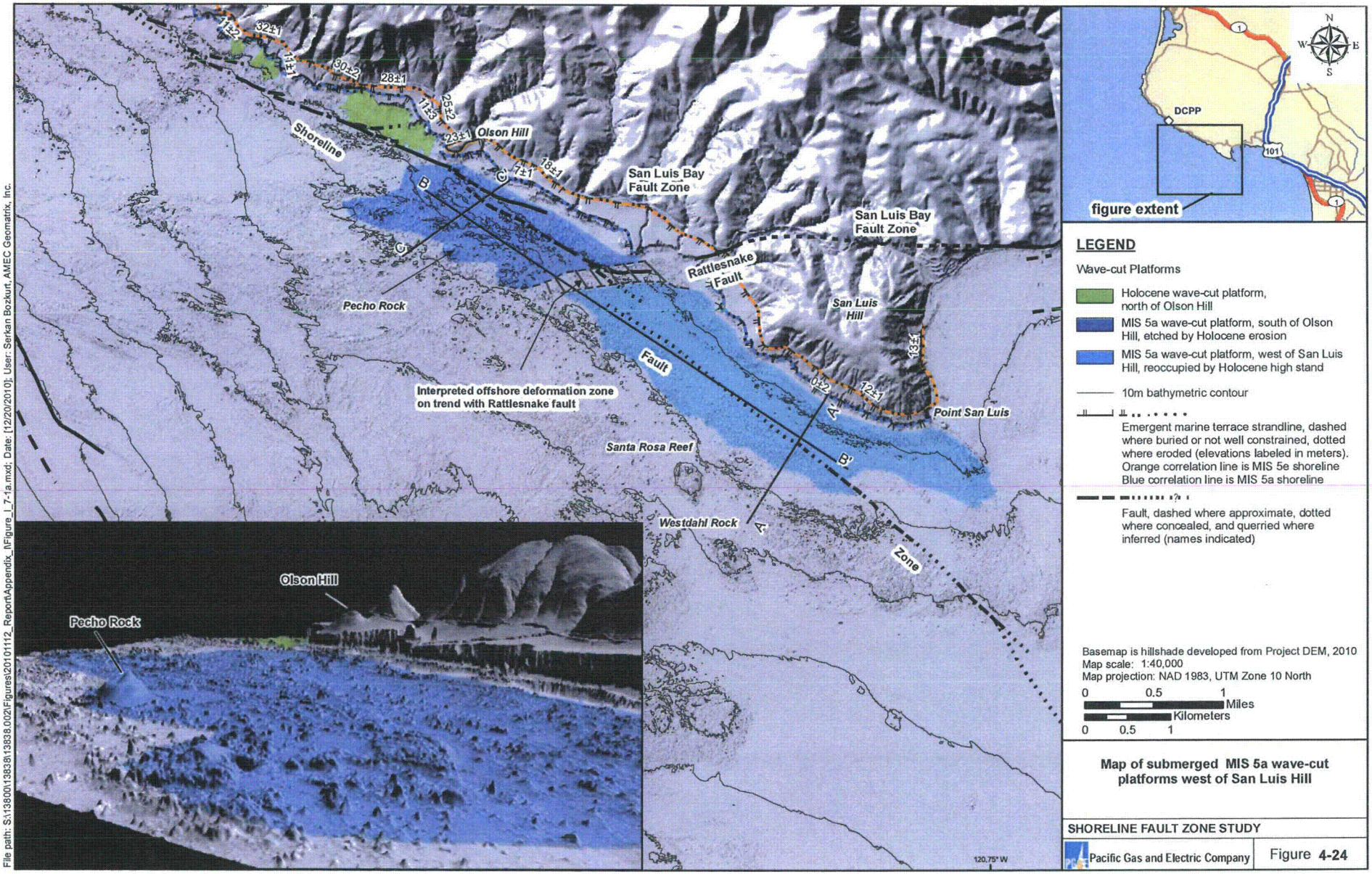

Map of submerged MIS 5a wave-cut platforms west of San Luis Hill

SHORELINE FAULT ZONE STUDY

Pacific Gas and Electric Company | Figure **4-24**

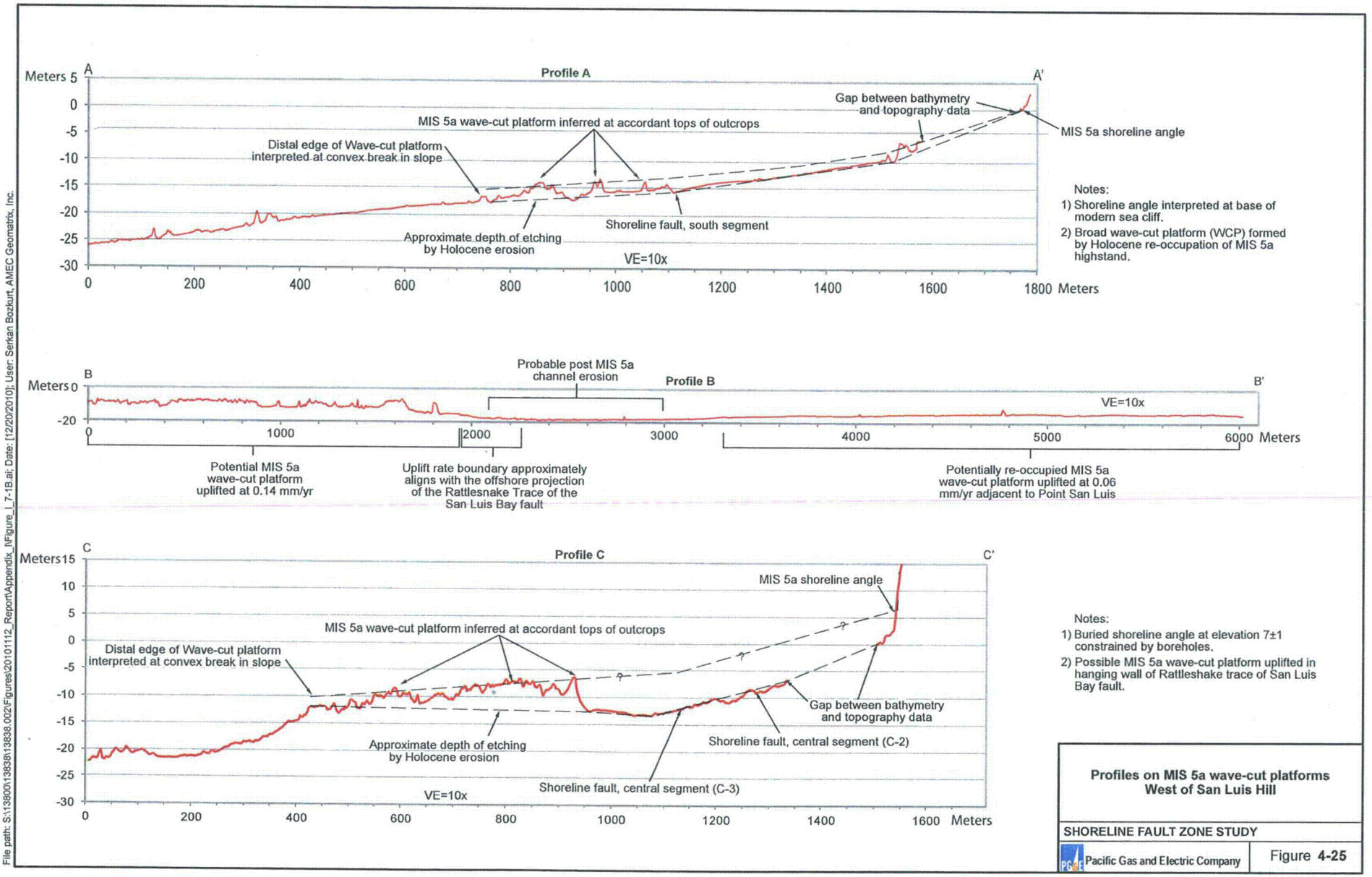
Profile A
A
A'
Meters 5
0
-5
-10
-15
-20
-25
-30
0
200
400
600
800
1000
1200
1400
1600
1800 Meters
Gap between bathymetry and topography data
MIS 5a shoreline angle
MIS 5a wave-cut platform inferred at accordant tops of outcrops
Distal edge of Wave-cut platform interpreted at convex break in slope
Approximate depth of etching by Holocene erosion
Shoreline fault, south segment
VE=10x
Notes:
1) Shoreline angle interpreted at base of modern sea cliff.
2) Broad wave-cut platform (WCP) formed by Holocene re-occupation of MIS 5a highstand.
Profile B
B
B'
Meters 0
-20
0
1000
2000
3000
4000
5000
6000 Meters
Probable post MIS 5a channel erosion
VE=10x
Potential MIS 5a wave-cut platform uplifted at 0.14 mm/yr
Uplift rate boundary approximately aligns with the offshore projection of the Rattlesnake Trace of the San Luis Bay fault
Potentially re-occupied MIS 5a wave-cut platform uplifted at 0.06 mm/yr adjacent to Point San Luis
Profile C
C
C'
Meters 15
10
5
0
-5
-10
-15
-20
-25
-30
0
200
400
600
800
1000
1200
1400
1600 Meters
MIS 5a shoreline angle
MIS 5a wave-cut platform inferred at accordant tops of outcrops
Distal edge of Wave-cut platform interpreted at convex break in slope
Gap between bathymetry and topography data
Approximate depth of etching by Holocene erosion
Shoreline fault, central segment (C-2)
Shoreline fault, central segment (C-3)
VE=10x
Notes:
1) Buried shoreline angle at elevation 7±1 constrained by boreholes.
2) Possible MIS 5a wave-cut platform uplifted in hanging wall of Rattleshake trace of San Luis Bay fault.
Profiles on MIS 5a wave-cut platforms West of San Luis Hill
SHORELINE FAULT ZONE STUDY
Pacific Gas and Electric Company
Figure 4-25
File path: S:\13800\13838\13838.002\Figures\20101112_Report\Appendix_I\Figure_I_7-1B.ai: Date: [12/20/2010]; User: Serkan Bozkurt, AMEC Geomatrix, Inc.

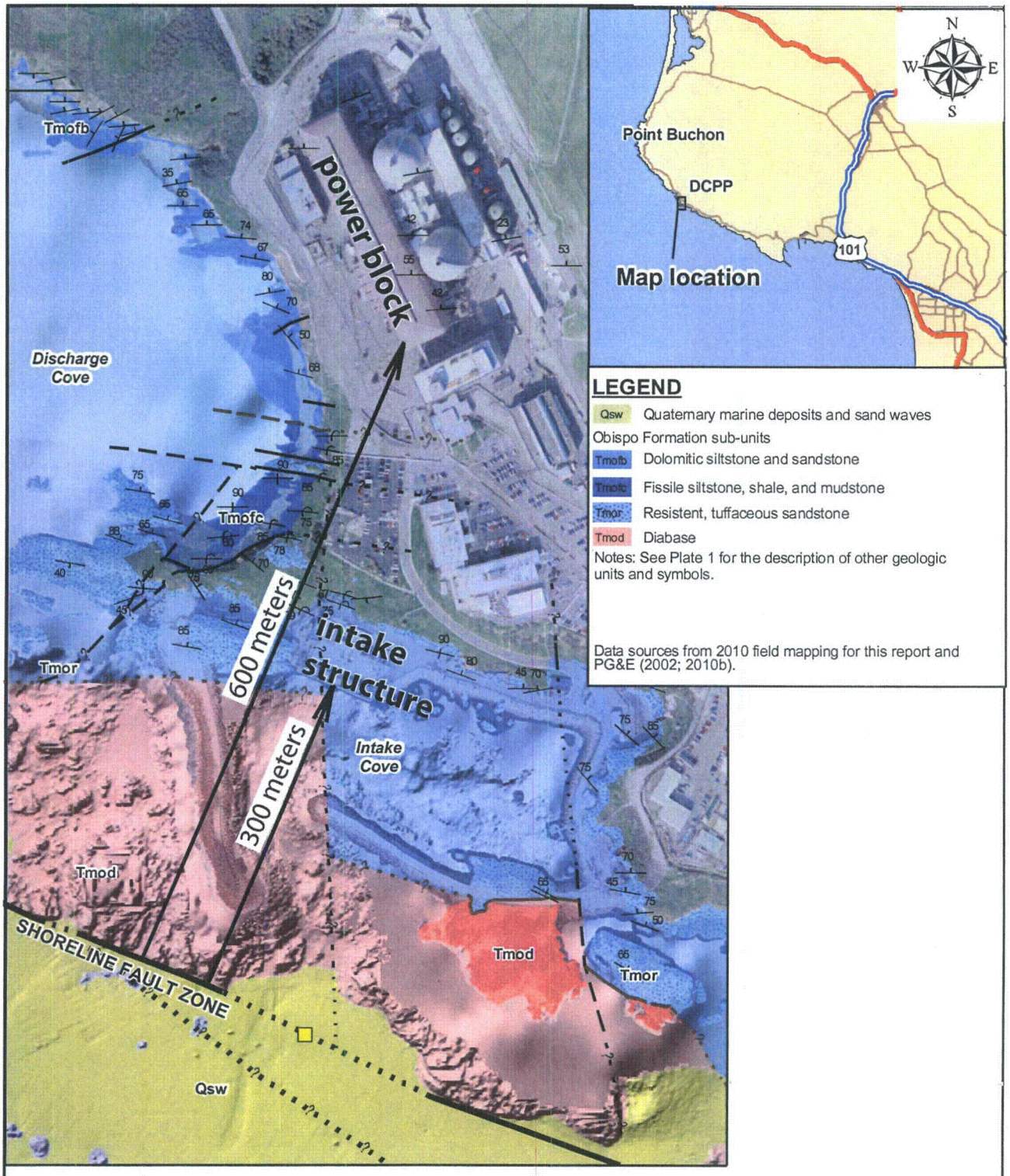

Distance to DCPP power block and Intake structure from Shoreline fault zone

SHORELINE FAULT STUDY

Pacific Gas and Electric Company | Figure **4-26**

5.0 SEISMIC SOURCE CHARACTERIZATION

This section presents the seismic source characterization used to model ground motions at the DCPP. The logic tree for the Shoreline fault zone source is presented in Section 5.1 and is based on findings presented in Sections 3.0 and 4.0. Figure 5-1 shows a map of the Shoreline fault zone source and adjacent San Luis Bay fault sources and portions of the nearby Hosgri and Los Osos fault sources. In addition to the new Shoreline fault zone source, logic trees for the Hosgri, Los Osos, and San Luis Bay fault sources are used that are based on the current understanding of those faults and the regional tectonic setting (Section 3.0). The logic trees for these other fault sources are presented in Section 5.2. Coordinates for the ends and bends in the fault sources (e.g., the labeled dots on Figure 5-1) are presented in Table 5-1, which appears at the end of this section.

The logic trees capture the range of values that characterize each fault source. Each tree consists of various nodes that define the fault source, including rupture length, rupture width, slip sense, and slip rate. Each node consists of one or more branches with values to capture the epistemic uncertainty of that node. The weight given to each branch is based on the strength of the evidence to support the branch value. The weights are between zero and one and sum to one for each node.

5.1 Shoreline Fault Zone Source Logic Tree

The logic tree to characterize the uncertainty in source parameters for the Shoreline fault zone source (Figures 5-2 to 5-6) is based on the data collected and evaluated to date. The logic tree considers two alternative rupture scenarios for the Shoreline fault zone, one in which the fault zone ruptures as an independent source, and the other in which the Shoreline fault zone is kinematically linked to other faults in the Southwestern Boundary fault zone, and may rupture with the San Luis Bay fault. Because the results of dynamic rupture modeling show that rupture on the Hosgri fault zone is inhibited from rupturing onto the Shoreline fault zone (Appendix J), this scenario is not considered in the logic tree.

The logic tree for the Shoreline fault zone source consists of 30 nodes that define the rupture dimensions, segmentation, sense of slip, and slip rate of the seismic source (Figures 5-2 to 5-6). Nodes 1–4 define the surface trace of the Shoreline fault zone source, which is shown in map view on Figure 5-1. Nodes 5–10 define the fault source dip and width, and node 11 defines the slip sense of the fault. Node 12 defines the kinematic relationship of the Shoreline fault zone with the intersecting San Luis Bay fault zone by asking whether the two faults are "linked" (Figure 5-3). The "no" branch represents a Shoreline fault zone that is separate and distinct from the San Luis Bay fault zone, wherein the two faults move independently. The "no" branch in node 12 is followed by nodes 13 to 16 to define the rupture dimensions and fault slip rate for the Shoreline fault zone source (Figure 5-4); the independent San Luis Bay fault source is characterized in a separate logic tree (Section 5.2.3). The "yes" branch represents a structural model in which the Shoreline fault zone and East segment of the San Luis Bay fault zone are linked in the sense that they may rupture together in the same earthquake. The linked model also allows for alternative rupture scenarios in which the two faults may either partially rupture together or rupture separately. The linked Shoreline and San Luis Bay faults may partially rupture together in the same earthquake or separately. The "yes" branch in node 12 is followed by nodes 17 to 30, which define the fault geometry and dimensions of the San Luis Bay fault

source, and the rupture dimensions and fault slip rate for the Shoreline and San Luis Bay fault sources (Figures 5-5 and 5-6).

The weights determined for each branch at a node are shown as a number in brackets, such as [1.0] for one branch or [0.3] and [0.7] for two branches, etc. The sum of the weights at each node is always 1.0.

Node 1

Node 1 defines the southern end of the Shoreline fault zone source (Figure 5-2). This point, labeled S1 on Figure 5-1, is located about 3.5 km south-southeast of Point San Luis and is based on the findings presented in Section 4.3. A weight of 1.0 is assigned to this location, as the approximately 0.5 km uncertainty in its exact location has negligible effect on the overall source dimensions.

Node 2

Node 2 defines the boundary between the South and Central segments of the Shoreline fault zone (Figure 5-2). This point, labeled S2 on Figure 5-1, is located about 1.2 km west of the Rattlesnake (San Luis Bay) fault intersection with the coastline (Section 4.3) near the northern termination of a distinct magnetic anomaly associated with the South segment of the fault zone (Figure 4-22). A weight of 1.0 is assigned to this location, as the <0.25 km uncertainty in its exact location has negligible effect on the overall source dimensions. The approximately 7 km distance between points S1 and S2 defines the length of the South segment of the Shoreline fault zone source.

Node 3

Node 3 defines the northern end of the Central segment of the Shoreline fault (Figure 5-2). This point, labeled S3 on Figure 5-1, is located about 0.5 km south-southwest of Lion Rock, and about 1.5 km due west of Discharge Cove. Point S3 is based on the boundary between the Northern and Central seismicity sublineaments (Section 4.2), the approximate northern end of the distinct magnetic anomaly high associated with the Central segment of the Shoreline fault zone (Figure 4-22), and the approximate geologic boundary where the N40W fault may intersect the Shoreline fault zone (Section 4.3). The location of point S3 is selected such that the shortest distance from DCPP to the Shoreline fault zone source is the same as the shortest distance from the DCPP to the Shoreline fault zone as mapped on the MBES bathymetric data (Plate 1). A weight of 1.0 is assigned to this location, as the <0.5 km uncertainty in its along-strike location has negligible effect on the overall source dimensions. The approximately 8 km distance between points S2 and S3 defines the length of the Central segment of the Shoreline fault zone source.

Node 4

Node 4 defines the northern end of the Shoreline fault zone and the length of the North segment of the Shoreline fault zone source (Figure 5-2). There are four branches to this node that reflect the epistemic uncertainty in its location (Figure 5-1). Specifically, there is uncertainty as to whether earthquakes within the Northern seismicity sublineament occur on a distinct North segment of the Shoreline fault zone or whether some or all of the seismicity in the Northern seismicity sublineament may be occurring on a steeply east-dipping Hosgri fault zone (see Section 4.2). In the former case, additional uncertainty exists regarding the location of the North

segment of the Shoreline fault zone: whether the segment is spatially coincident with the Northern seismicity sublineament, either on a blind fault or along a small, en echelon fault observed in Tertiary strata, or whether the North segment is coincident with the preexisting N40W fault. As discussed below, the highest weights are assigned to the branches in which the North segment of the Shoreline fault zone source coincides entirely or in part with the Northern seismicity sublineament. In all cases, the lengths described below are surface lengths. The subsurface depth extent of the Shoreline fault zone source is limited by the Hosgri fault zone in cases where the Hosgri fault source dips to the east.

The first branch of node 4 coincides with point S6 on Figure 5-1, which represents the northern endpoint of the N40W fault. This permissible alternative assumes that seismicity at the southern end of the Northern seismicity sublineament is associated with a moderately well-defined fault in Tertiary strata (see Section 4.3). In this case, seismicity along the north part of the Northern seismicity sublineament is assumed to be related to the Hosgri fault zone. This first branch of node 4 has a weight of 0.2. The approximately 8 km distance between points S3 and S6 defines the maximum length of the North segment of the Shoreline fault zone source (Figures 5-1 and 5-2). The maximum length of the Shoreline fault zone source on this branch is 23 km (Figure 5-2, Node 4').

The second branch of node 4 coincides with point S4, which is located near the intersection of the Northern Shoreline seismicity sublineament with the Hosgri fault source. Supporting this interpretation are the best-fit trend of the Northern seismicity sublineament (see Section 4.2) and the near-surface fault within inferred Tertiary strata, tentatively imaged on the shallow seismic reflection lines, that approximately aligns with the Northern seismicity sublineament (Section 4.3). This second branch has a weight of 0.4. The length of this segment (approximately 8 km) and the total length of the Shoreline fault zone source are the same as on branch one (Figures 5-1 and 5-2).

The third branch of node 4 coincides with point S5 on Figure 5-1, which is half way between points S4 and S3. This branch considers the earthquakes north of point S5 to have occurred on faults within the steeply east-dipping Hosgri fault zone, instead of on a distinct Shoreline fault zone. The seismicity section oriented perpendicular to the Hosgri fault zone (Figure 4-8, Section 4.2) illustrates the possible association of deeper earthquakes with the Hosgri fault zone. It is reasonable to assume that most of the seismicity near the steeply east-dipping Hosgri fault zone is associated with the more active Hosgri fault zone rather than a less active secondary fault. However, this alternative is given slightly less weight [0.3] than the second branch based on the alternative that there is a fault in Tertiary bedrock, which is mapped farther to the north. The 4 km distance between points S3 and S5 defines the minimum length of the North segment of the Shoreline fault zone source (Figures 5-1 and 5-2). The total length of the Shoreline fault zone source on this branch is 19 km (Figure 5-2, Node 4').

The fourth branch of node 4 defines the northern end of the Shoreline fault zone source to be at point S3, coincident with the northern end of the Central segment of the Shoreline fault zone source. This alternative, which interprets no distinct North segment of the Shoreline fault zone, attributes all of the seismicity on the Northern seismicity sublineament to be related to a steeply east-dipping Hosgri fault zone. As described above and in Section 4.2, the seismicity seen in

cross section appears to better correlate to the trend of the Northern seismicity sublineament than to the Hosgri trend. The fourth branch of node 4 has a weight of 0.1; the low weight assigned to this branch is based on consideration of both seismicity and geologic data that suggest a fault may extend further to the north. The total length of the Shoreline fault zone source on this branch is 15 km, or the combined length of the South and Central fault segments (Figure 5-2, Node 4').

Node 5

Node 5 defines the dip of the Shoreline fault zone source (Figure 5-2). This node has a single branch value of 90°, which has a weight of 1.0. This value is supported by the vertical alignment of seismicity (within the 0.5 km epicentral location uncertainty) for the entire length of the Shoreline seismicity lineament (see Section 4.2).

Node 6

Node 6 includes two branches for alternative lines of evidence used to evaluate the maximum seismogenic depth of the Shoreline fault zone source (Figure 5-3). The top of seismogenic crust is assumed to be at zero depth in all instances. Because the fault is vertical, the maximum seismogenic depth is equivalent to the maximum source rupture width. The first branch suggests that estimates of maximum seismogenic depth (i.e., seismogenic thickness) based on regional data (Section 4.2) being used to characterize other nearby faults (i.e., the Hosgri, Los Osos, and San Luis Bay seismic sources [Section 5.2]) should be used to constrain the seismogenic depth of the Shoreline fault zone source. This branch has a weight of 0.7 based on the more robust data set used to inform the values in node 7. The second branch assumes that the seismicity along the Shoreline fault zone (Section 4.2) provides a better representation of maximum depth of rupture, which may vary among the North, Central, and South segments of the Shoreline fault zone (Section 4.2). This branch, which is based on a limited seismicity data set and the assumption that the short period of time over which the seismicity lineament has manifested itself (21 years) accurately represents the full extent of the seismogenic area for all three fault segments, is thus judged less reliable and given a lower weight (0.3).

Node 7

Node 7 follows the first branch of node 6 and defines the distribution for estimated regional seismogenic thickness (Figure 5-3). As described in Section 3.2, the regional distribution of seismicity defines a preferred seismogenic thickness of the crust of about 12 km, with a range of probable values between 10 and 15 km. Branch values are assigned to this node of 10, 12, and 15 km, which are weighted 0.2, 0.6, and 0.2, respectively.

Node 8

Node 8 follows the second branch of node 6 and defines the maximum depth of the Northern Shoreline seismicity sublineament (Figure 5-3). Based on the evaluation of seismicity described in Section 4.2, the node has branch values of 12 and 15 km, which are weighted 0.8 and 0.2, respectively. The weights assigned to these two branches are consistent with the weights assigned to the regional seismogenic thickness values (i.e., the highest weight is assigned to the preferred 12 km maximum depth and a lower weight is given to the maximum hypocentral depths.

Node 9

Node 9 follows the second branch of node 6 and defines the maximum depth of the Central seismicity sublineament (Figure 5-3). Based on the evaluation of seismicity described in Section 4.2, the node has branch values of 8 and 10 km, which are weighted 0.4 and 0.6, respectively. These weights reflect a slight preference for the 10 km maximum depth because it is more consistent with the regional seismogenic thickness.

Node 10

Node 10 follows the second branch of node 6 and defines the maximum depth of the Southern seismicity sublineament (Figure 5-3). Based on the evaluation of seismicity described in Section 4.2, the node has branch values of 8 and 10 km, which are weighted equally at 0.5. The slightly shallower weighted mean depth for the Southern seismicity sublineament compared to the Central seismicity sublineament is consistent with the observation that hypocentral depths of earthquakes on the Southern seismicity sublineament are shallower than depths observed on the other two sublineaments (see Section 4.2).

Node 11

Node 11 defines the style of faulting (slip sense) of the Shoreline fault zone source (Figure 5-3). The fault dip and focal mechanisms in the current tectonic regime all suggest right-lateral strike-slip motion (Section 4.2), and this slip sense is given a weight of 1.0.

Node 12

Node 12 considers whether the Shoreline fault zone source and San Luis Bay fault source are kinematically linked or whether they are separate, independent faults (Figure 5-3). The "yes" branch represents a Shoreline fault zone and intersecting San Luis Bay fault zone to the east that are linked in the sense that the East segment of the San Luis Bay fault may rupture with the Shoreline fault (Central segment or North and Central segment) during a single earthquake. This structural model considers the Shoreline fault zone to be part of a longer system of strike-slip and oblique-slip faults within the Southwestern Boundary fault zone. The North and Central segments of the Shoreline fault, together with the intersecting San Luis Bay fault to the east, would form part of a left restraining bend in the fault system. The size of the step-over to other faults in the system such as the Oceano, Los Berros, or Wilmar Avenue faults, which is on the order of a few kilometers, suggests that ruptures on the combined Shoreline fault and San Luis Bay fault to the east would not continue onto other structures. This description of the Southwestern Boundary zone as a strike-slip fault system that accommodates regional transpression differs from the LTSP categorization of the Southwestern Boundary fault zone as a block boundary mostly accommodating reverse faulting and shortening (PG&E, 1988; Lettis et al., 1994). The "yes" (linked) branch is given a weight of 0.3, and the continuation of this branch of the logic tree is described by nodes 17–30 (Figures 5-5 and 5-6).

The "no" branch in node 12 represents a Shoreline fault zone that is separate and distinct from the San Luis Bay fault, wherein the two faults move independently and accommodate distinctly different directions of slip. This characterization is consistent with a regional kinematic model more similar to the LTSP, in which the San Luis Bay fault is part of the reverse or oblique Southwestern Boundary fault zone that forms the block boundary between the uplifted San Luis–Pismo block and the adjacent Santa Maria Valley block to the southwest (Section 3.1). The

Shoreline fault zone in this kinematic description is fundamentally separate from the Southwestern Boundary fault zone, and instead accommodates a minor amount of right-lateral strike-slip displacement within the San Luis–Pismo block. The "no" branch is given a weight of 0.7, and the continuation of this branch of the logic tree is described by nodes 13 to 16 (Figure 5-4). The higher weight for the "no" branch is based on two primary lines of reasoning: (1) the direct evidence from the San Luis Bay fault documented to date indicates reverse movement on a north-dipping fault (PG&E, 1988), whereas the "linked" model predicts a significant strike-slip component and, at least locally, a subvertical dip; and (2) several lines of evidence support the change in uplift rate documented across the San Luis Bay fault zone onshore to continue offshore to the west-northwest and across the Shoreline fault zone, rather than along it (see Sections 4.3 and 4.4; Appendix I).

Node 13

Node 13 defines the rupture mode for an independent Shoreline fault zone source (Figure 5-4). Specifically, two branches consider whether (1) the Shoreline fault zone source is segmented, with segmentation points that are strong barriers to rupture propagation, or (2) the fault source is unsegmented, with no physical barriers that are able to repeatedly arrest rupture. The branches in this node reflect the epistemic uncertainty in the rupture behavior of the Shoreline fault zone. Section 4.3 discusses the basis for the segmentation points between the South, Central, and North segments of the Shoreline fault zone (i.e., points S2 and S3 on Figure 5-1). The branch weights are 0.6 and 0.4 for the segmented and unsegmented rupture modes, respectively, reflecting the moderately strong basis for a segmented fault presented in Section 4.3.

Node 14

Node 14 defines the rupture lengths following the segmented rupture branch of node 13 (Figure 5-4). The four branches show the possible combinations of one-, two-, and three-segment ruptures involving the North (N), Central (C), and South (S) segments of the Shoreline fault zone source. The combinations [and corresponding weights] are one-segment ruptures N, C, and S [0.15]; two-segment N+C rupture and one-segment S rupture [0.6]; one-segment N rupture and two-segment C+S rupture [0.1]; and three-segment N+C+S rupture [0.15]. The distribution of weights reflects the relatively strong evidence for a segmentation point between the Central and South segments (at the intersection of the Shoreline fault zone with the Rattlesnake fault of the San Luis Bay fault zone; Section 4.3), and the relatively weak evidence for a segmentation point between the Central and North segments (Section 4.3). These rupture lengths are fixed to the defined fault source segments, implying that the segmentation points are unbreakable.

The branch values and weights of node 14 are modified for that part of the logic tree where the North segment of the Shoreline fault zone does not exist (specifically, the branch of node 4 that defines the northern end of the Shoreline fault zone source at the northern end of the Central segment; Figure 5-2). In this case, the upper two and lower two branches of node 14 combine so there are only two branches [with combined weights]: one-segment ruptures C and S [0.7] and two-segment ruptures C+S [0.3].

Node 15

Node 15 defines possible rupture lengths for the unsegmented rupture branch of node 13 (Figure 5-4). In this case, defined rupture lengths are assumed to "float" anywhere along the fault

length. The distinct fault segments and segmentation points defined in Section 4.3 are thus geometric constructs, but do not affect seismogenic fault rupture. Rupture lengths considered in the unsegmented rupture model are based on an assumed rupture aspect ratio, defined as the ratio of rupture length L to rupture width W, or L:W. The three branch values [and weights] are 1:1 [0.3], 1.5:1 [0.4], and 2:1 [0.3]. Empirical data from historical continental earthquakes (e.g., Wells and Coppersmith, 1994; Leonard, 2010) provide a basis for weighing the three branch values.

Figure 5-7 is modified from Leonard (2010) and shows a log-log plot of rupture length versus width for a subset of instrumental strike-slip earthquakes (data compiled mainly from Wells and Coppersmith, 1994). The shaded gray region of the plot reflects the approximate rupture length and width of the Shoreline fault zone, and the three solid, diagonal lines provide the fits to constant aspect ratios of 1:1, 1.5:1, and 2:1. The data show considerable scatter and broadly support the three constant aspect ratios as valid rupture dimensions in the shaded region. Aspect ratios of less than 1:1 are not considered as branch values, following the widely held view that small ruptures are generally circular and larger ruptures generally are associated with larger aspect ratios and more rectangular shapes (Leonard, 2010). The preferred relationship of Leonard (2010) to fit the broader data set (shown by the thin solid and bordering dashed lines) is a power-law relationship between W and L, whereby W is proportional to $L^{2/3}$ for the range 5 km $< L <$ 50 km.

For purposes of defining rupture dimensions on an unsegmented Shoreline fault zone source (which has a length not greater than 23 km), the three constant aspect ratios of 1:1, 1.5:1, and 2:1 and the rupture widths defined by nodes 5 to 10 sufficiently capture the range of probable values. Because the rupture length cannot exceed the fault source length, an important constraint on this node is that given a defined rupture width, the calculated rupture length is truncated to be no greater than the fault source length (i.e., maximum of 23 km). For example, fault length would be truncated to 23 km for rupture widths of 12 or 15 km and an aspect ratio of 2:1.

Node 16

Node 16 defines the slip rate of the Shoreline fault zone source (Figure 5-4). The uncertainty in fault slip rate and lines of reasoning supporting the range in slip rate values are presented in Section 4.4.3. Four lines of reasoning are used to provide constraints on the minimum, maximum, and preferred values for slip rate, including (1) comparison to the Hosgri-San Simeon fault zone, (2) seismicity rate, (3) observed vertical separation, and (4) observed lateral separation. These analyses provide estimates of slip rate ranging from 0.05 to 1 mm/yr, with a preferred range between 0.1 and 0.6 mm/yr. The five slip rate branches [and corresponding weights] are 1.0 [0.05]; 0.6 [0.15]; 0.3 [0.35]; 0.1 [0.35]; and 0.05 mm/yr [0.1]. Seventy percent of the weight is given to slip rates of 0.1 and 0.3 mm/yr, values most consistent with the available constraints (Section 4.4).

Node 17

Nodes 17–30 characterize the linked Shoreline and San Luis Bay seismic sources that follow the "yes" branch of the logic tree under node 12 (Figure 5-3). Node 17 defines the location and total length of the San Luis Bay fault east of its intersection with the Shoreline fault (the "East segment"; Figure 5-5). These points, labeled L2 to L6 on Figure 5-1, extend from the

intersection with the Shoreline fault on the west (point L2, which is equivalent to point S2), eastward to Mallagh Landing and the probable eastern end of the San Luis Bay fault (Section 3.1). A weight of 1.0 is assigned to this location, and the points define an approximately 8 km long East segment of the San Luis Bay fault source. Intermediate points labeled L3, L4, and L5, which are considered in defining ruptures scenarios, are described in the discussion of node 25.

Node 18

Node 18 defines the average dip of the East segment of the San Luis Bay fault source in the linked model (Figure 5-5). Because the linked model includes the characterization that the Central segment of the Shoreline fault and the East segment of the San Luis Bay fault smoothly intersect and may rupture together, the dip of the East segment at the branch line must be very steeply dipping to subvertical, with the possibility of a slightly more inclined fault plane east of the fault intersection. On this basis, the 70° north dip of the San Luis Bay fault source considered in the independent San Luis Bay fault source logic tree (Section 5.2) is not considered here, as it does not allow for the required intersection geometry with the Central segment of the Shoreline fault zone source. This node has branch values [and weights] of 80° north [0.3] and 85° north [0.7]. The steeper geometry is preferred, as this dip is structurally more compatible with this rupture mode.

Node 19

Node 19 considers two alternatives for the western end of the San Luis Bay fault source in the linked model (Figure 5-5). In the linked model, the Shoreline fault zone is a barrier to rupture and a kinematic boundary such that the San Luis Bay fault east of the Shoreline fault zone (the East segment) has no physical connection with structures west of the Shoreline fault zone. The first branch describes an 8 km long West segment of the San Luis Bay fault source west of the Shoreline fault zone between points L1 and L2. This branch has a higher weight of 0.6, reflecting the preferred location of the uplift rate boundary identified from analysis of submerged marine terraces (Appendix I) that follows a strong magnetic and geologic trend (Section 4.5). The second branch to node 19 assumes that the West segment of the San Luis Bay fault does not exist under the linked model. In this case, either the Central and North segments of the Shoreline fault zone form the uplift rate boundary, or the uplift rate boundary is a poorly defined diffuse zone somewhere between the Shoreline and Hosgri fault zones that does not constitute a seismic source. This branch has a weight of 0.4.

Node 20

Node 20 defines the average dip of the West segment of the San Luis Bay fault source in the linked model following the upper branch of node 19 (Figure 5-5). Alternative branch weights are 70°, 80°, and 85° north, with a symmetric [0.3], [0.4], [0.3] weighted distribution, respectively. The dip values are determined to be at least 70° north because gentler dips would intersect the Shoreline fault zone at depths above the typical approximately 6–7 km deep nucleation depth for magnitude 5 or greater earthquakes (e.g., Sibson, 1984). The bottom and edges of the West segment source are truncated by both the east-dipping Hosgri fault source and the vertical Shoreline fault zone source where they intersect within the seismogenic crust.

Node 21

Node 21 defines the sense of slip for the West segment of the San Luis Bay fault source in the linked model following the upper branch of node 19 (Figure 5-5). Alternative branches are oblique-reverse slip with a weight of 0.35 and reverse slip with a weight of 0.65. The higher weight assigned to reverse slip, despite the overall linked and strike-slip-dominated kinematic model, is consistent with the concept that the West segment is a separate structure from the linked Shoreline-East segment of the San Luis Bay fault source and it primarily accommodates the change in uplift rate in the offshore (Appendix I).

Node 22

Node 22 defines the sense of slip for the East segment of the San Luis Bay fault in the linked model (Figure 5-5). The slip sense must accommodate both the change in uplift rate across the East segment and the strike-slip motion being transferred to it from the Shoreline fault zone. Alternative branches are strike slip, oblique-reverse slip, and reverse slip with horizontal-to-vertical ratios (h:v) of 2:1, 1:1, and 1:2, respectively. The highest weight of 0.45 is given to the oblique-reverse slip sense, followed by the reverse slip sense [0.4]. The remaining low [0.15] weight for the strike-slip branch reflects the evaluation that the East segment of the San Luis Bay fault would likely accommodate more oblique-reverse motion given its orientation relative to the strike-slip Shoreline fault zone (Figure 5-1).

Node 23

Node 23 defines the maximum depth to the bottom of rupture for the West and East segments of the San Luis Bay fault (Figure 5-5). The branch values and weights are identical to node 7 and are 10, 12, and 15 km with weights of 0.2, 0.6, and 0.2, respectively. The bottom and lateral margins of these sources are truncated by the south-dipping Los Osos fault zone, vertical Shoreline fault zone, and vertical to-east-dipping Hosgri fault zone where they intersect within the seismogenic crust (Figure 5-1).

Node 24

Node 24 defines the rupture mode for a linked Shoreline–East Segment San Luis Bay fault source (Figure 5-6). Similar to node 13 for the independent Shoreline fault zone source, two branches for node 24 consider (1) whether Shoreline–San Luis Bay fault ruptures are defined by discrete segments, with segmentation points that are strong barriers to rupture propagation, or (2) whether fault ruptures occur on an unsegmented fault source, with no physical barriers to limit rupture. Both rupture model branches consider the West segment of the San Luis Bay fault (in cases when it exists) to be a separate fault source that does not rupture with the Shoreline fault zone or the East segment of the San Luis Bay fault. The branch weights are 0.6 and 0.4 for the segmented and unsegmented rupture modes, respectively, reflecting the moderately strong basis for a segmented fault presented in Sections 4.3 and 4.5.

Node 25

Node 25 defines the rupture lengths following the segmented rupture branch of node 24 (Figure 5-6). The six branches outline possible combinations of one-, two-, and three-segment ruptures involving the North (N), Central (C), and South (S) segments of the Shoreline fault zone and the East (E) segment of the San Luis Bay fault. The combinations [and corresponding weights] are

one-segment ruptures N, C, S, and E [0.15]; two-segment N+C rupture and one-segment S and E ruptures [0.1]; one-segment N and E ruptures and two-segment C+S rupture [0.05]; one-segment N and S ruptures and two-segment C+E rupture [0.3]; three-segment N+C+S rupture and one-segment E rupture [0.05]; and three-segment N+C+E rupture and one-segment S rupture [0.35]. Segmented ruptures where the S and E segments rupture together are not considered.

The distribution of weights reflects a strong preference for combined rupture of the Central segment of the Shoreline fault zone and the East segment of the San Luis Bay fault given the linked kinematic model branch of node 12. An additional source of epistemic uncertainty not defined in a separate node is whether rupture on the Central (or Central + North) segment of the Shoreline fault zone would rupture the entire 8 km long East segment of the San Luis Bay fault, or whether rupture nucleating on the Shoreline fault zone would rupture only part way into the San Luis Bay fault restraining bend (Figure 5-1). To address this, earthquakes involving the C+E or N+C+E rupture segments are considered to have an eastern rupture limit at either point L3, L5, or L6 with equal weight (see note 4 on Figure 5-6). As in node 14, the rupture lengths in node 25 are considered to be fixed to the defined fault source segments, implying that the segmentation points are unbreakable.

The branch values and weights of node 25 are modified for that part of the logic tree where the North segment of the Shoreline fault zone does not exist (specifically, the branch of node 4 that defines the northern end of the Shoreline fault zone to be at the northern end of the Central segment; Figure 5-2). In this case, the branches of node 25 combine so there are only three branches [with combined weights]: one-segment ruptures C, S, and E [0.25], and two-segment ruptures C+S, E [0.1] and C+E, S [0.65].

Node 26

Node 26 defines possible rupture lengths for the unsegmented rupture branch of node 24 (Figure 5-6). Similar to node 15, defined rupture lengths are assumed to "float" anywhere along the fault length, although node 26 has the additional restriction that the floating rupture cannot involve both the South segment of the Shoreline fault zone and the East segment of the San Luis Bay fault (Figure 5-1). The distinct fault segments and segmentation points defined in Section 4.3 are thus geometric constructs but do not affect seismogenic fault rupture. Rupture lengths considered in the unsegmented rupture model are based on an assumed rupture aspect ratio, defined as the ratio of rupture length L to rupture width W, or L:W. As in node 15, the three branch values [and weights] are 1:1 [0.3], 1.5:1 [0.4], and 2:1 [0.3]. Because the rupture length cannot exceed the fault source length, an important constraint on this node is that given a defined rupture width, the calculated rupture length is truncated to be no greater than the fault source length (i.e, maximum of 23 or 24 km), as would be the case for rupture widths of 12 or 15 km and an aspect ratio of 2:1.

Node 27

Node 27 defines the slip rate of the Central and North segments of the Shoreline fault zone source (Figure 5-6). The uncertainty in fault slip rate and lines of reasoning supporting the range in slip rate values are presented in Section 4.4.3. Because the uplift rate across the San Luis Bay fault cannot be directly tied to the Shoreline fault zone even in the linked model, the slip rate branch values and weights in the linked model are identical to those developed for the

independent Shoreline fault zone source model in node 16 (Figure 5-4). The five slip rate branches [and corresponding weights] are 1.0 mm/yr [0.05], 0.6 mm/yr [0.15], 0.3 mm/yr [0.35], 0.1 mm/yr [0.35], and 0.05 mm/yr [0.1]. Because displacement on the Central and North segments is transferred to both the South segment of the Shoreline fault and the East segment of the San Luis Bay fault, the South segment of the Shoreline fault is assessed in node 29 based on a calculation described in the discussion of node 29.

Node 28

Node 28 defines the slip rate of the East segment of the San Luis Bay fault source for the linked model (Figure 5-6). The two branch values list alternative uplift rates for the San Luis Bay fault zone based on the LTSP analysis of the approximately 80,000-year-old and approximately 120,000-year-old marine terraces and longitudinal profiles of the marine terrace shoreline angles across the San Luis Bay fault (PG&E, 1990; Hanson et al., 1994). The net fault slip rates are calculated based on the fault dip (node 18) and slip sense (node 22) (Figure 5-5). The branch values for vertical uplift rate [and weights] are 0.14 mm/yr [0.8] and 0.08 mm/yr [0.2]. The greater (and more highly weighted) 0.14 mm/yr uplift rate is the difference between the uplift rate north of Olson Hill (0.2 mm/yr) and the uplift rate south of the Rattlesnake fault (0.06 mm/yr). The higher rate agrees with revised elevations and correlations of emergent marine terraces described in Appendix I, which suggest that this boundary is localized across the San Luis Bay fault zone north of Point San Luis. The lesser 0.08 mm/yr uplift rate is the difference in uplift rate across the Rattlesnake fault only. This lower-weighted value would be a valid estimate of the uplift rate for the San Luis Bay seismic source if the remaining differential uplift rate across the Olson Hill deformation zone were attributed to folding caused by another process (e.g., folding across an active axial surface tied to a deep bend in the Los Osos fault).

Node 29

Node 29 defines the slip rate of the South segment of the Shoreline fault zone source for the linked model (Figure 5-6). The alternative slip rates for this node are calculated values based on the slip rate for the Central and North segments of the Shoreline fault zone (node 27) and the slip rate for the East segment of the San Luis Bay fault zone (node 28). The South segment slip rate is calculated to be the node 27 slip rate minus the node 28 slip rate, with a minimum slip rate of 0.05 mm/yr.

Node 30

Node 30 defines the slip rate of the West segment of the San Luis Bay fault source for the linked model (Figure 5-6). The two branch values and weights are identical to those in node 28. The difference in net slip rate for the West segment source is based on the different dip and sense of slip values and weights in nodes 20 and 21 (Figure 5-5). The branch values for vertical uplift rate [and weights] are 0.14 mm/yr [0.8] and 0.08 mm/yr [0.2]. Because they are treated as separate structures, the slip rate of the West segment of the San Luis Bay fault source is independent of the slip rate of the East segment source in the linked model.

5.2 Logic Trees for Other Fault Sources

This section briefly summarizes the logic trees for other fault sources used to calculate ground motions at DCPP described in the LTSP Final Report and Addendum (PG&E, 1988, 1991a). These other fault sources are the Hosgri, Los Osos, and San Luis Bay fault zones (the last as an

independent fault source compatible with the independent Shoreline fault zone source branch). The locations of these sources relative to the Shoreline fault zone source and DCPP are shown on Figures 5-1 and 5-8. Table 5-1 lists the coordinates for these fault sources. Figures 5-9 to 5-11 show the logic trees that characterize the source geometry, slip sense, and slip rate.

Modifications to the LTSP Final Report characterizations are based on current understanding of the regional seismotectonic setting (Section 3) and current assessments of specific fault source parameters. Modifications to the LTSP Final Report source characterization are being evaluated as part of the LTSP Update activities and are ongoing.

5.2.1 Hosgri Fault Zone Logic Tree

Figure 5-9 is the logic tree for the Hosgri fault zone source geometry, slip sense, and slip rate. Source parameters shown on Figure 5-9 are unchanged from the LTSP Final Report (PG&E, 1988) with the following exceptions:

Depth to Bottom of Rupture

The LTSP defined the maximum depth to the bottom of a fault rupture as 12 ± 3 km for all fault sources unless they were truncated by an intersecting fault (PG&E, 1988). A review of the regional earthquake catalog with well-located earthquakes since establishment of the PG&E–USGS network suggests a preferred value of 12 km, with alternative upper and lower values of 10 and 15 km (Section 3.2). Therefore, the branch values [and weights] for the depth to bottom of rupture for the Hosgri seismic source (node 2), as well as the Los Osos and San Luis Bay sources, are revised from the LTSP to be 10 km [0.2], 12 km [0.6], and 15 km [0.2].

Sense of Slip

The sense of slip for the Hosgri fault zone source is modeled as strike slip with a weight of 1.0 in this report (node 5). In the LTSP Final Report (PG&E, 1988), partial weight was given to oblique slip [0.3] and reverse slip [0.05] for the Hosgri fault zone. The oblique-slip and reverse-slip branches have been dropped because of information published subsequent to the LTSP that confirms strike-slip movement for the Hosgri fault zone, including geologic data (Hanson et al., 2004) and seismicity data (McLaren and Savage, 2001; Hardebeck, 2010) (Section 3).

Dip

Estimated values for the average dip of the Hosgri fault zone source (node 3) varied in the LTSP logic tree based on an assumed model for sense of slip. In the Hosgri fault source logic tree for this report, three values of dip are considered: 90°, 85° east, and 80° east. Evaluation of the Hardebeck (2010) earthquake catalog data (Section 4.2.4) plotted normal to the Hosgri fault zone (Figure 4-8) supports a vertical to steeply east-dipping zone, broadly constrained to lie within the range of these values. For this report, the branch values [and weights] are 90° [0.1], 85° east [0.4], and 80° east [0.5].

5.2.2 Los Osos Fault Logic Tree

Figure 5-10 is the logic tree for the Los Osos fault zone source geometry, slip sense, and slip rate. Source parameters shown on Figure 5-10 are unchanged from the LTSP Final Report (PG&E, 1988), with the following exceptions:

Sense of Slip

The LTSP Final Report (PG&E, 1988) heavily weighted reverse slip [0.9] over oblique slip [0.1] for the Los Osos fault zone. In this report, a higher weight is given to oblique slip [0.7] over reverse slip [0.3]. The currently preferred weighting is based on a reassessment of the regional seismotectonic setting that favors distributed dextral transpression in the south-central coastal California region (Lettis et al., 2009). In this tectonic model, strike-slip motion is transferred to the Hosgri fault zone and subparallel major strike-slip faults farther east (e.g., West Huasna and Rinconada faults) from the San Andreas fault across a broad left restraining bend or step-over (Section 3.1).

Dip

Estimated values for the average dip of the Los Osos fault zone vary between 30° and 75° southwest based on the assumed model for sense of slip in the LTSP Final Report (PG&E, 1988). The current logic tree defines the dip of the Los Osos fault zone source with branch values [and weights] of 75° [0.2], 60° [0.5] and 45° [0.3] southwest. The shallowest (30°) fault dip used in the LTSP Final Report (PG&E, 1988) is not supported by more recent studies that suggest the Los Osos fault is a more steeply dipping oblique-slip fault (Section 3.1).

Maximum Depth of Rupture

The LTSP Final Report (PG&E, 1988) considered the maximum depth of rupture for the Los Osos fault to be limited by the intersection depth of the Los Osos fault zone with the Hosgri fault zone. The intersection depth was dependent on the dip of both the Hosgri and Los Osos fault zones, and it was assumed that the Los Osos fault zone is truncated by the longer Hosgri fault zone. This geometric constraint warranted minor adjustments to the preferred values and weights for maximum depth of rupture assigned to the Hosgri fault zone. For simplicity in this report, however, the same maximum depth of faulting values and weights are adopted as were used for the Hosgri fault zone (Figure 5-9).

5.2.3 San Luis Bay Fault Logic Tree

From the onshore-offshore geologic mapping (Appendix B) and analysis of the Shoreline fault zone (Section 4), two rupture scenarios are considered for the San Luis Bay fault source. One rupture scenario treats the San Luis Bay fault zone as an independent source of earthquakes. The other rupture scenario considers the San Luis Bay fault zone to be kinematically linked to ruptures on the Shoreline fault zone, as discussed in Section 4.5. These alternatives are considered for the Shoreline fault logic tree on Figure 5-3, node 12. Figure 5-11 is the logic tree for the independent San Luis Bay fault source geometry, slip sense, and slip rate. When the Shoreline fault zone and East segment of the San Luis Bay fault zone are linked as part of a left-restraining bend in a longer system of right-lateral strike-slip and oblique-slip faults, Figure 5-11 is not needed; the appropriate characterization of the San Luis Bay fault source is provided on Figures 5-5 and 5-6. Source parameters shown on Figure 5-11 are unchanged from the LTSP Final Report (PG&E, 1988) with the following exceptions:

Total Fault Length

The San Luis Bay fault source had a maximum length of 19 km in the LTSP Final Report (PG&E, 1988). The maximum length was based on its western end terminating at the Hosgri fault source and the eastern end terminating near the Wilmar Avenue fault. This was not a preferred value in the LTSP logic tree, based on the lack of evidence supporting the westward extent at that time. In the independent San Luis Bay fault source model, the San Luis Bay fault source extends from point L1 at the Hosgri fault zone eastward to an assumed intersection with the San Miguelito fault zone near Mallagh Landing at point L6, for a total fault length of 16 km (node 1, Figure 5-11). In this scenario, the fault source crosses the Shoreline fault zone. The western part of the fault follows a distinct magnetic trend and possible south-side-down warp in the top of basement from the Shoreline fault zone to the Hosgri fault zone (Section 4.5 and Appendix B). This trend is consistent with the preferred interpretation of submerged marine terrace data, which suggests a permissible uplift rate boundary from the intersection of the Rattlesnake fault at the coast and continuing west toward the Hosgri fault zone (Sections 4.4 and 4.5 and Appendix I). The absence of a discrete lineament or mapped fault in the MBES bathymetry data suggests this structure is probably blind (Section 4.5) (Plate 1).

Maximum Depth of Rupture

Similar to the Los Osos fault zone source, the LTSP Final Report (PG&E, 1988) considered the maximum depth of rupture for the San Luis Bay fault source to be limited to the intersection depth of the San Luis Bay fault source with adjacent faults. The north-dipping San Luis Bay fault zone is considered a secondary fault to the southwest-dipping Los Osos fault zone source and the vertical to east-dipping Hosgri fault zone source, and thus is modeled as being truncated by these two fault sources. Given the distribution of dips for the Los Osos and Hosgri fault sources in the LTSP Final Report, there was a 0.4 probability that the San Luis Bay fault source was truncated at depths less than 7 km, and therefore not considered seismogenic. In this report, the steeper geometries for the Hosgri and Los Osos fault sources (Figures 5-9 and 5-10) result in greater potential depths for the San Luis Bay fault source. For simplicity, the same maximum depth of faulting values [and weights] are adopted as were used for the Hosgri and Los Osos fault sources (node 2, Figure 5-11).

Dip

The LTSP considered alternative dips for the San Luis Bay fault source of 70° north and 40° north with weights of 0.8 and 0.2, respectively (PG&E, 1988). Based on the current characterization of the San Luis Bay fault and its likely interaction with the Los Osos fault at depth beneath the Irish Hills, the slightly steeper branch values [and weights] of 50° north [0.2], 70° north [0.4], and 80° north [0.4] (node 3, Figure 5-11) are used.

Rupture Length

The LTSP considered alternative rupture lengths of 6, 8, and 12 km for the San Luis Bay fault source (PG&E, 1988). In this preliminary reassessment, two branch values are adopted: 8 km and 16 km for rupture length, weighted equally, consistent with rupture of separate West and East segments and rupture of the entire fault, respectively (node 4, Figure 5-11).

Sense of Slip

The LTSP Final Report (PG&E, 1988) gave a weight of 1.0 to a reverse sense of slip for the San Luis Bay fault source. In this report, equal weight is given to oblique and reverse mechanisms (node 5, Figure 5-11). The currently preferred weighting is based on a reassessment of the regional seismotectonic setting that favors distributed dextral transpression in the south-central coastal California region (Section 3).

Table 5-1. Coordinates for the Shoreline, San Luis Bay, Hosgri, and Los Osos Fault Sources

Fault Segment	Point (Long, Lat) (NAD 83)
Shoreline South	S1 (–120.742, 35.132) S2 (–120.799, 35.177)
Shoreline Central	S2 (–120.799, 35.177) S3 (–120.874, 35.213)
Shoreline North (N40W fault alternative)	S3 (–120.874, 35.213) S7 (–120.908, 35.242) S6 (–120.926, 35.264)
Shoreline North (S4 end point alternative)	S3 (–120.874, 35.213) S5 (–120.906, 35.235) S4 (–120.937, 35.256)
Shoreline North (S5 end point alternative	S3 (–120.874, 35.213) S5 (–120.906, 35.235)
Shoreline North (S3 end point alternative)	S3 (–120.874, 35.213)
San Luis Bay East	L2 (–120.799, 35.177) L3 (–120.769, 35.181) L4 (–120.751, 35.179) L5 (–120.739, 35.180) L6 (–120.714, 35.173)
San Luis Bay West	L1 (–120.889, 35.195) L2 (–120.799, 35.177)
Hosgri	H1 (–120.640, 34.670) H2 (–120.816, 35.044) H3 (–121.018, 35.386) H4 (–121.058, 35.440) H5 (–121.096, 35.496) H6 (–121.138, 35.553) H7 (–121.184, 35.618) H8 (–121.234, 35.618) H9 (–121.265, 35.694) H10 (–121.329, 35.739) H11 (–121.373, 35.772) H12 (–121.428, 35.822) H13 (–121.483, 35.865) H14 (–121.515, 35.913) H15 (–121.599, 35.977) H16 (–121.691, 36.041) H17 (–121.802, 36.122) H18 (–121.827, 36.122)
Los Osos	O1 (–120.459, 35.127) O2 (–120.523, 35.167) O3 (–120.672, 35.222) O4 (–120.709, 35.272) O5 (–120.791, 35.305) O6 (–120.900, 35.299) O7 (–120.995, 35.362)

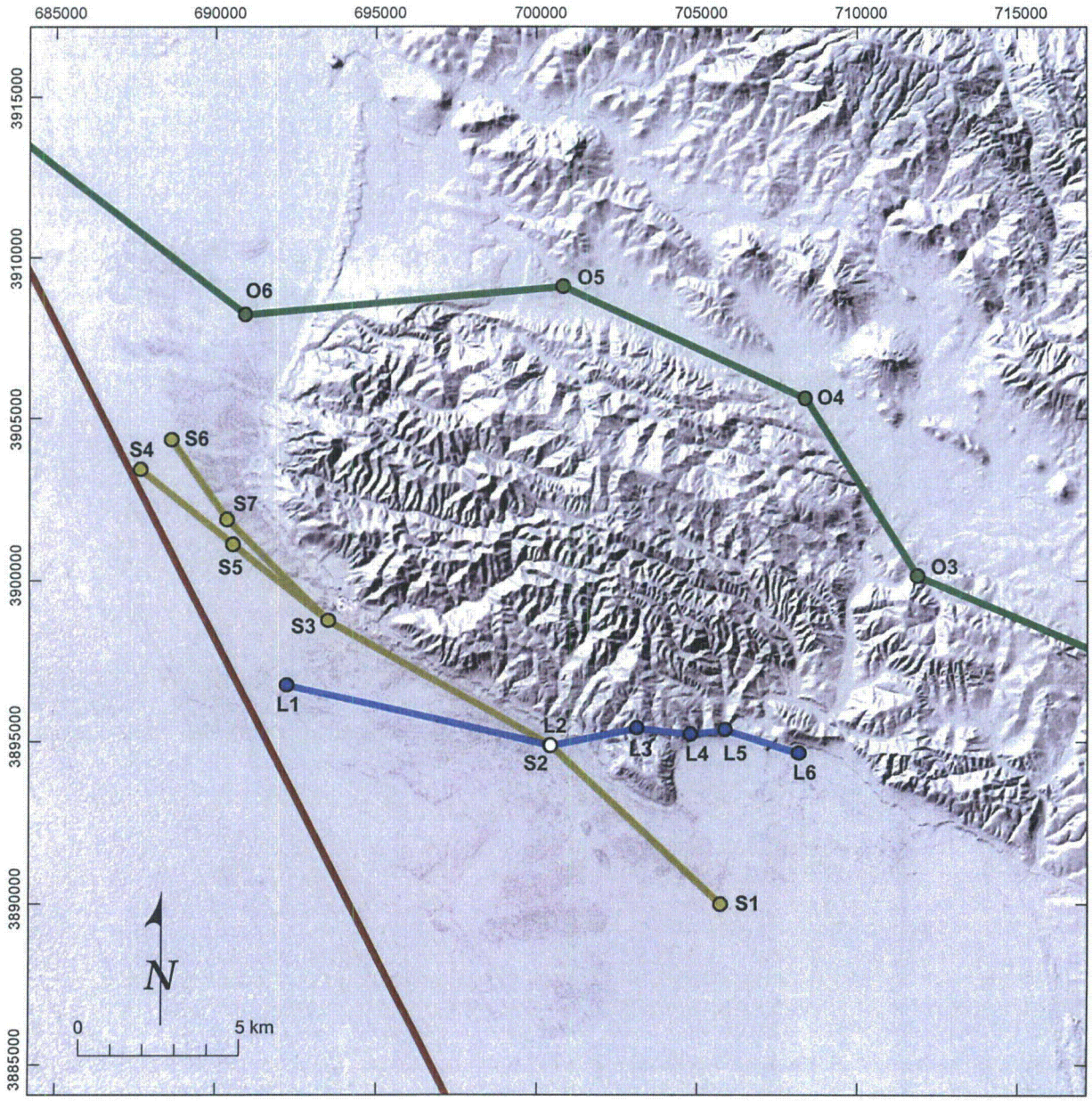

Note: Coordinates of fault sources are in Table 5-1

Legend

Seismic Sources

S1 S2 Shoreline

L1 L2 San Luis Bay

O1 O2 Los Osos

Hosgri

Seismic source model map traces of Shoreline, San Luis Bay, and Los Osos fault sources

SHORELINE FAULT ZONE STUDY

Pacific Gas and Electric Company | Figure **5-1**

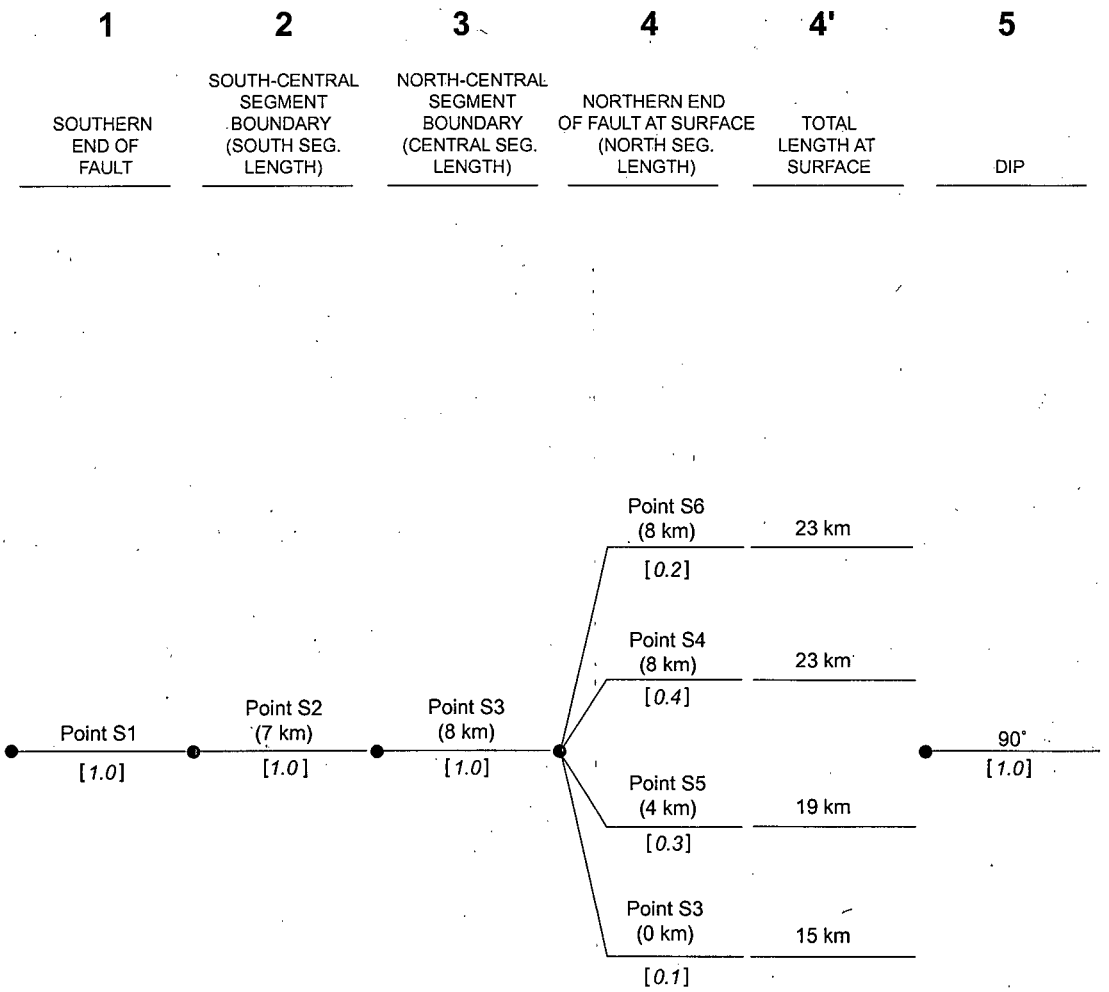

Note: Points S1 to S6 are located on Figure 5-1.

Shoreline fault logic tree nodes 1 to 5

SHORELINE FAULT ZONE STUDY

Pacific Gas and Electric Company | Figure **5-2**

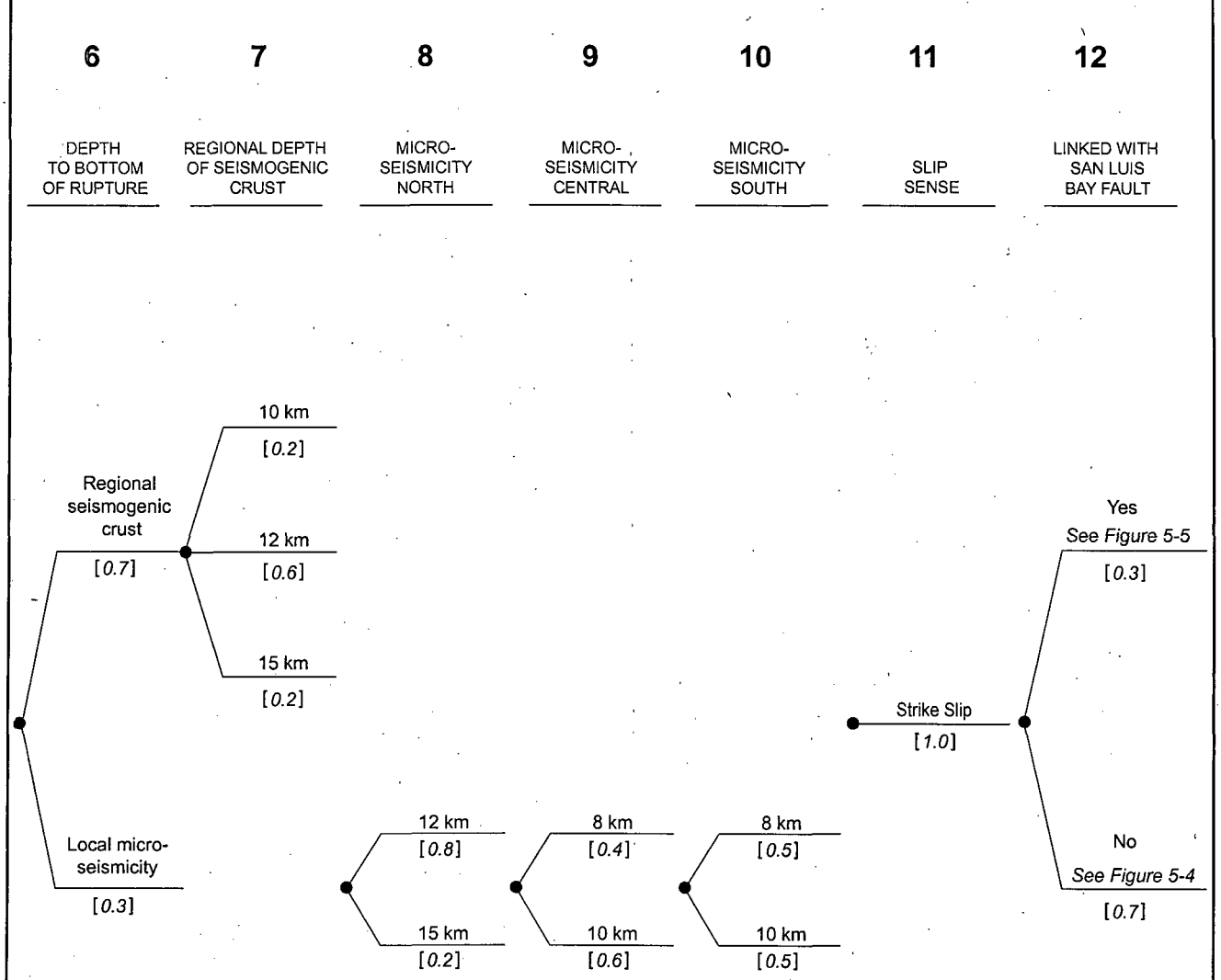

Notes:

(1) Top of seismogenic crust is assumed to be 0 km depth.

(2) The bottom and northern edge of the Shoreline fault source is truncated by the east-dipping Hosgri fault zone source where they intersect within the seismogenic crust.

Shoreline fault logic tree nodes 6 to 12

SHORELINE FAULT ZONE STUDY

Pacific Gas and Electric Company

Figure **5-3**

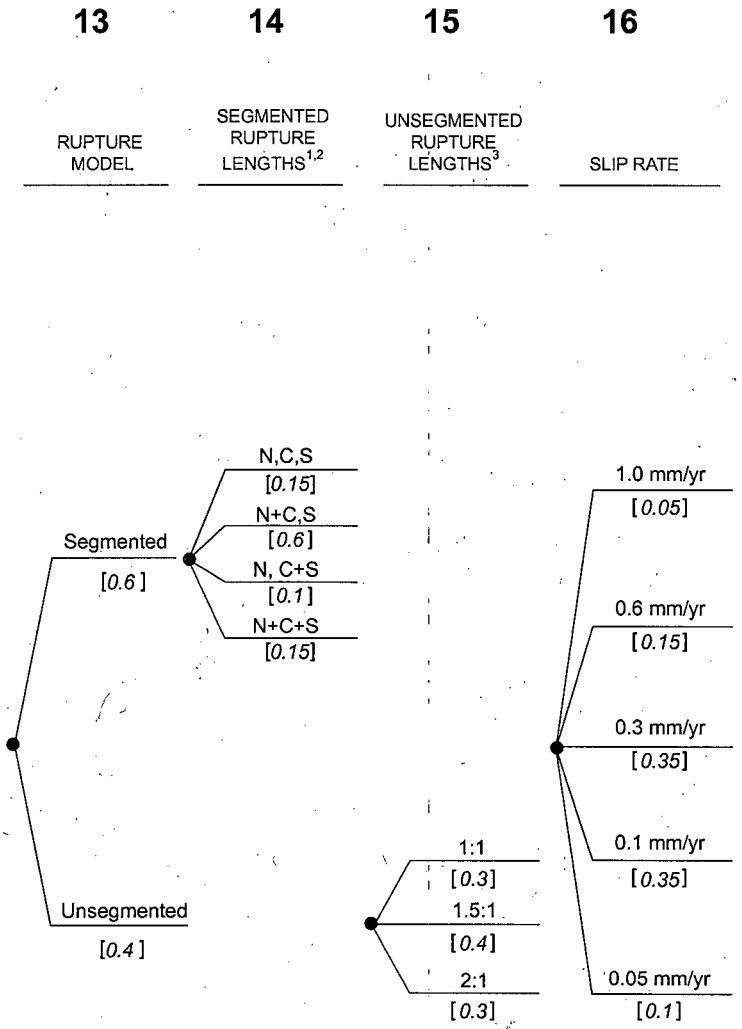

Notes:

(1) N=North Segment, C=Central Segment, S=South Segment.

(2) Under node 4 branch where northern end of fault is at Point S3, the North (N) segment does not exist, and the branches consolidate into C,S and C+S alternatives.

(3) Aspect Ratio expressed as Length:Width, with Width determined by nodes 5 to 11, and Length limited to be less than or equal to the total fault length as determined by nodes 1 to 4.

Shoreline fault logic tree not linked to San Luis Bay fault branch nodes 13 to 16

SHORELINE FAULT ZONE STUDY

Pacific Gas and Electric Company | Figure **5-4**

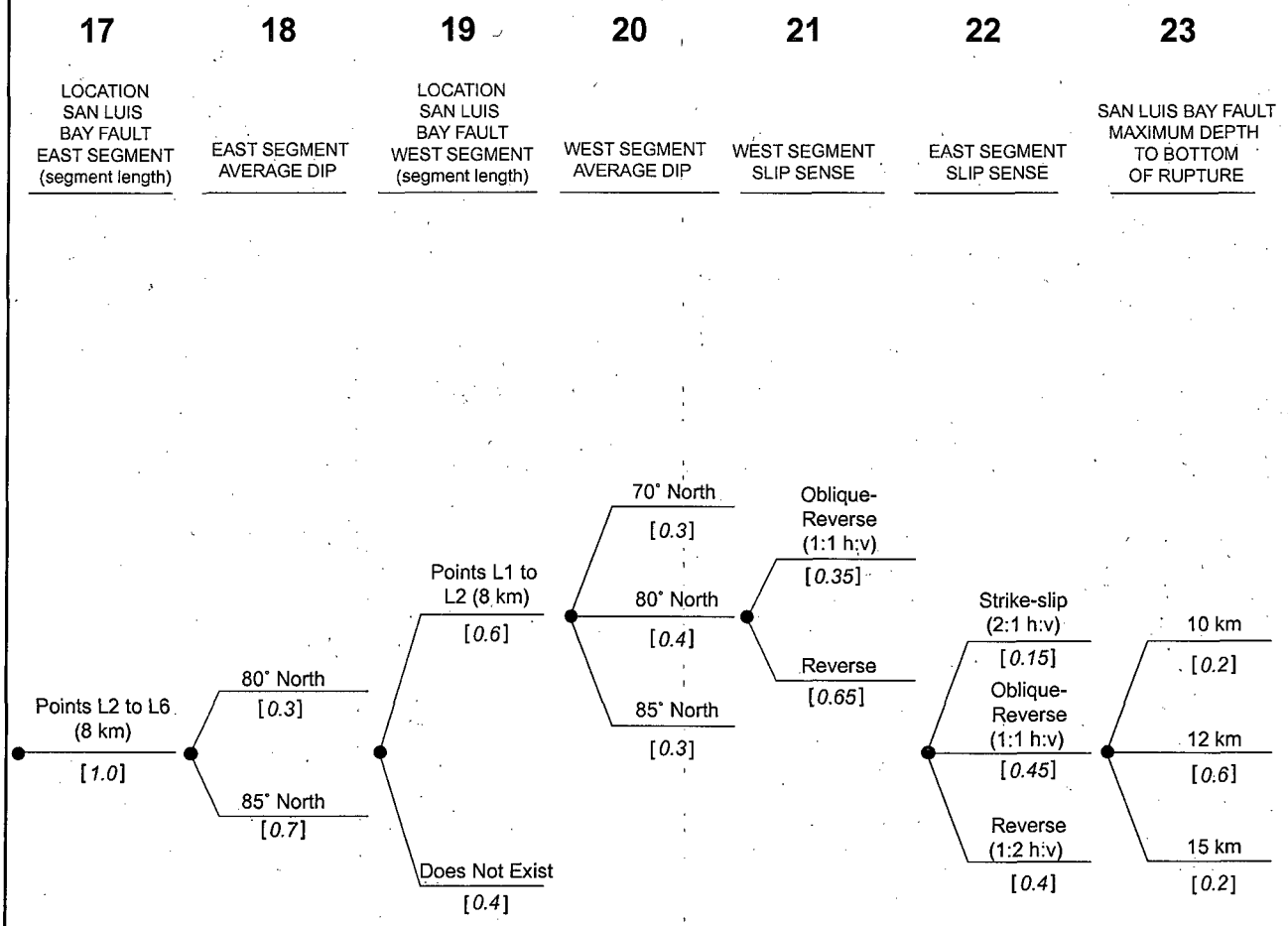

Notes:
(1) Points L1 to L6 are located on Figure 5.1.
(2) The bottom and edges of the San Luis Bay fault West segment source are truncated by the east-dipping Hosgri fault zone source and the vertical Shoreline fault source where they intersect within the seismogenic crust.
(3) The bottom of the San Luis Bay fault East segment source is truncated by the south-dipping Los Osos fault zone source where they intersect within the seismogenic crust.

Shoreline fault logic tree linked with San Luis Bay fault branch nodes 17 to 23

SHORELINE FAULT ZONE STUDY

Pacific Gas and Electric Company | Figure **5-5**

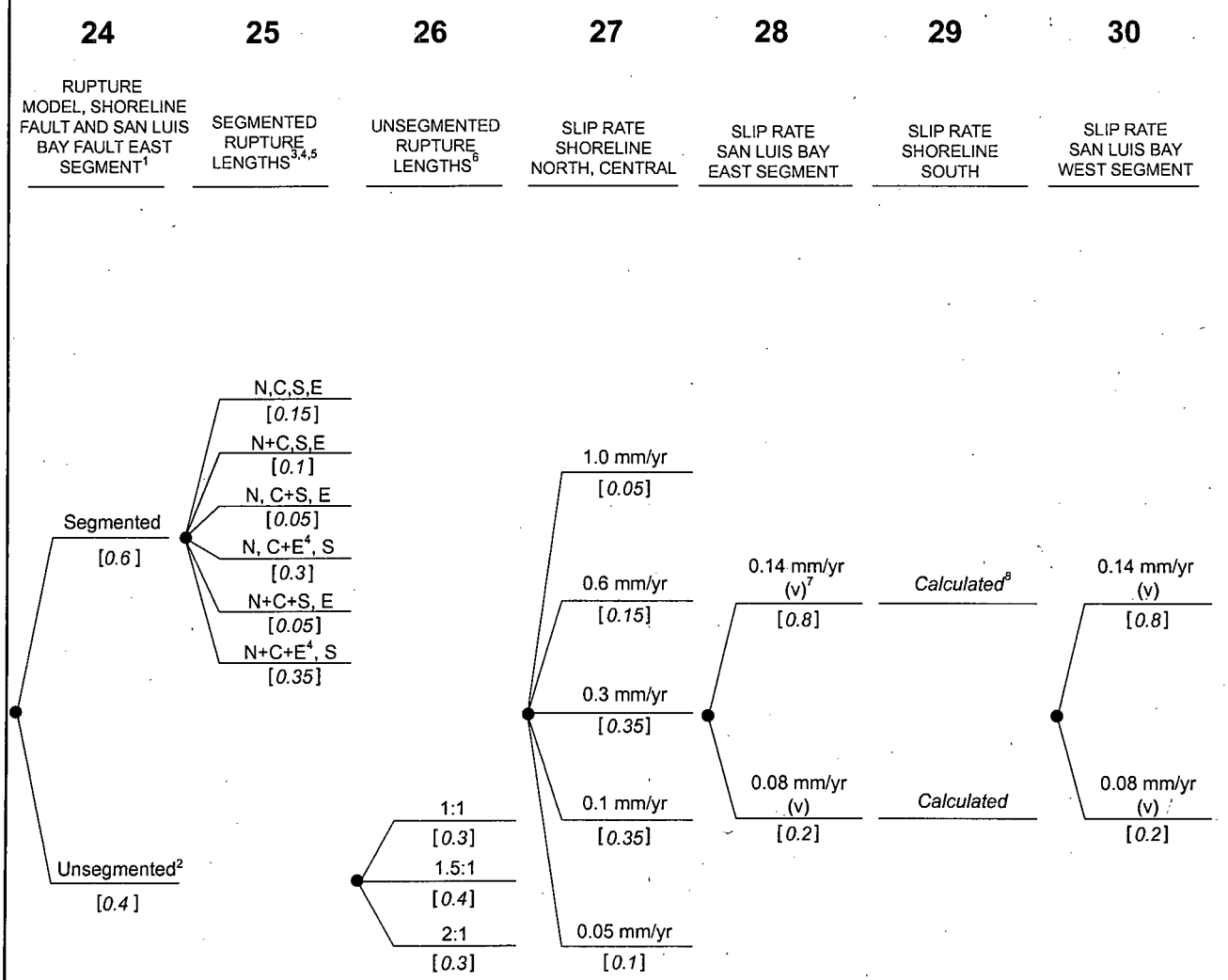

Notes:

(1) Both rupture model branches consider San Luis Bay fault West segment a separate fault that does not rupture with Shoreline or San Luis Bay fault East segment sources.

(2) Unsegmented ruptures do not linclude simultaneous rupture of Shoreline fault South segment and San Luis Bay fault.

(3) N=Northern Segment, C=Central Segment, S=South Segment, E=East Segment (San Luis Bay fault).

(4) For segmented ruptures where Central and East segments rupture together, the east end of the rupture may occur at Point L3, L5, or L6 and each is given 1/3 weight (Figure 5-1).

(5) Under node 4 branch where northern end of fault is at Point S3, the N segment does not exist, and the branches consolidate.

(6) Aspect Ratio expressed as Length:Width, with Length limited to be less than or equal to the total fault length.

(7) (v) = vertical component of slip rate. Fault slip rate calculated based on dip and slip sense nodes.

(8) Shoreline South slip rate calculated as North+Central slip rate minus San Luis Bay East slip rate, with a minimum rate of 0.05.

Shoreline fault logic tree linked with San Luis Bay fault branch nodes 24 to 30

SHORELINE FAULT ZONE STUDY

Pacific Gas and Electric Company | Figure **5-6**

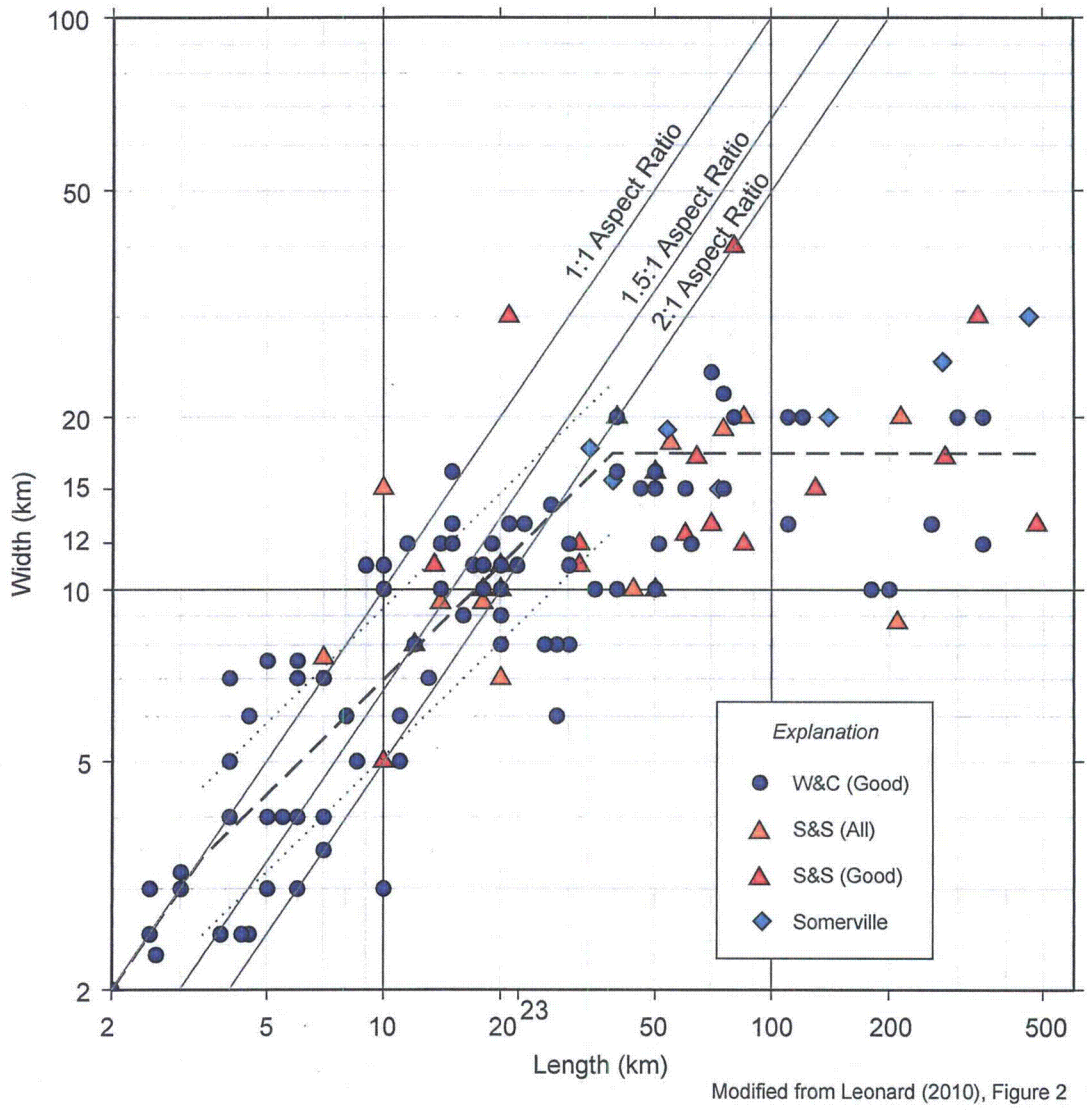

Modified from Leonard (2010), Figure 2

Notes from figure captions in Leonard (2010), Figures 1 and 2:
The length versus width data for strike-slip interplate earthquakes. As these faults become width-limited there is a narrow (5-50 km) range of the data that allows a large number of equally valid relations to fit the data. In the 50-km range a slope of 2:3 is assumed from the findings of the dip-slip data. The three gray dashed lines are from 0.5 km to 4 km with a slope of 1, from 4 km to 45 km length with a slope of 2:3, and a constant width of 17 km at lengths above 45 km. The gray dotted lines are the ±1σ uncertainties. The catalogs are W&C for Wells and Coppersmith (1994), S&S for Shaw and Scholz (2001) in Manighetti et al. (2007), and Somerville is Somerville et al. (1999).

Empirical rupture length versus width data for strike-slip earthquakes from Leonard (2010)

SHORELINE FAULT ZONE STUDY

Pacific Gas and Electric Company | Figure **5-7**

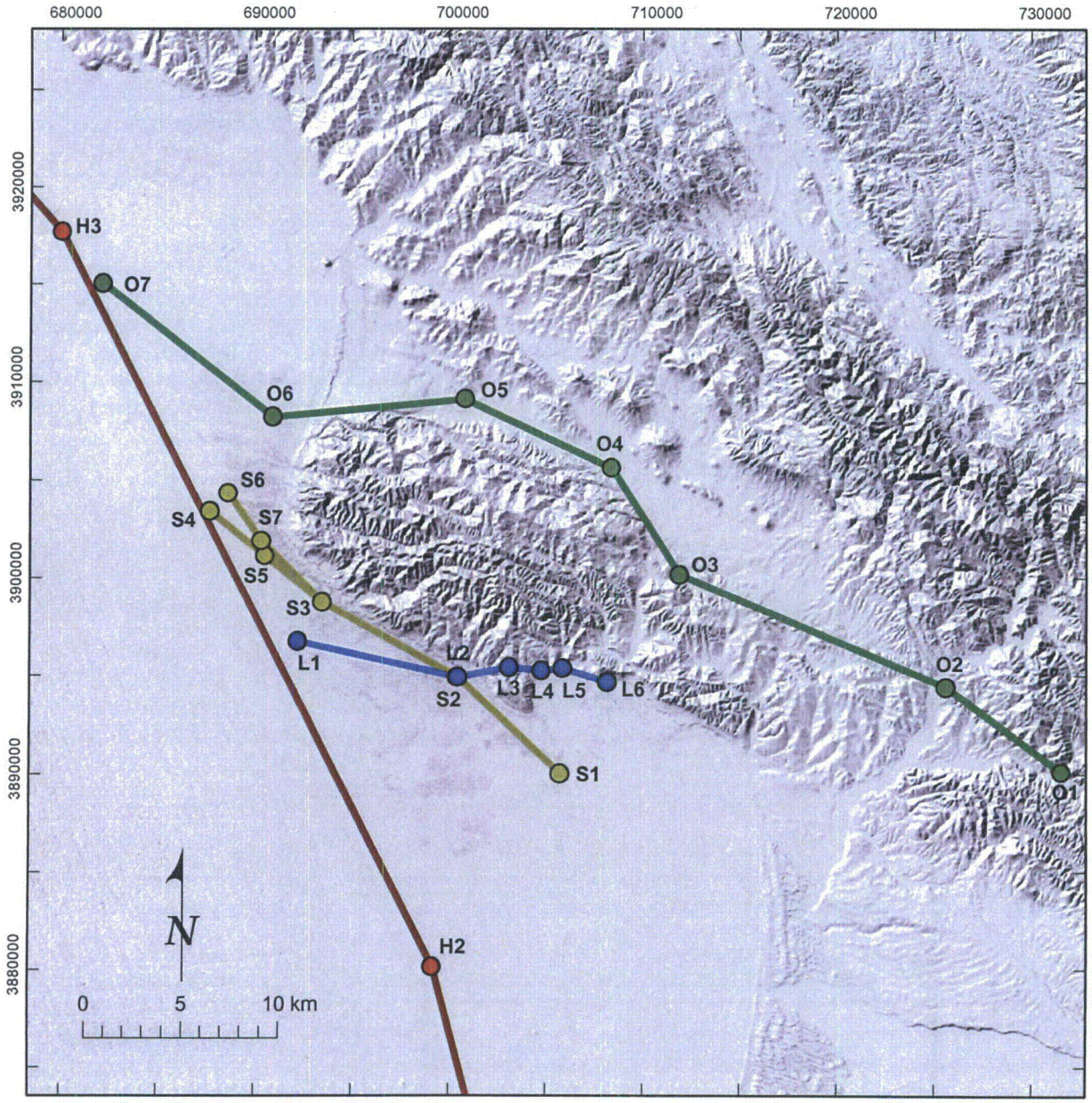

Note: Coordinates of fault sources are in Table 5-1

Legend

Seismic Sources

S1 S2 Shoreline

L1 L2 San Luis Bay

O1 O2 Los Osos

H2 H3 Hosgri

Seismic source model map traces of Hosgri, Los Osos, San Luis Bay, and Shoreline fault sources

SHORELINE FAULT ZONE STUDY

Pacific Gas and Electric Company

Figure **5-8**

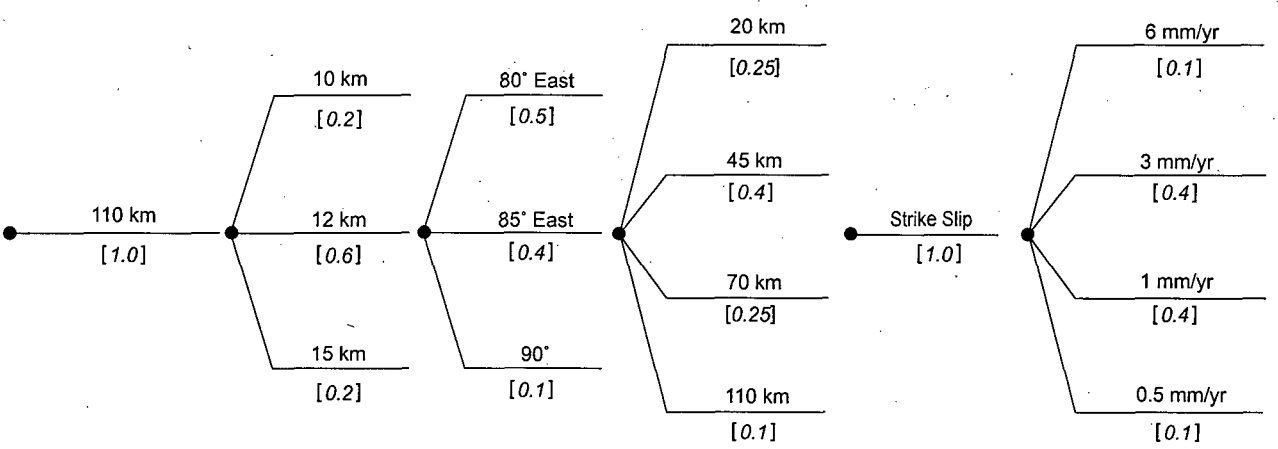

Hosgri fault zone logic tree modified from LTSP Final Report (PG&E, 1988)

SHORELINE FAULT ZONE STUDY

Pacific Gas and Electric Company | Figure **5-9**

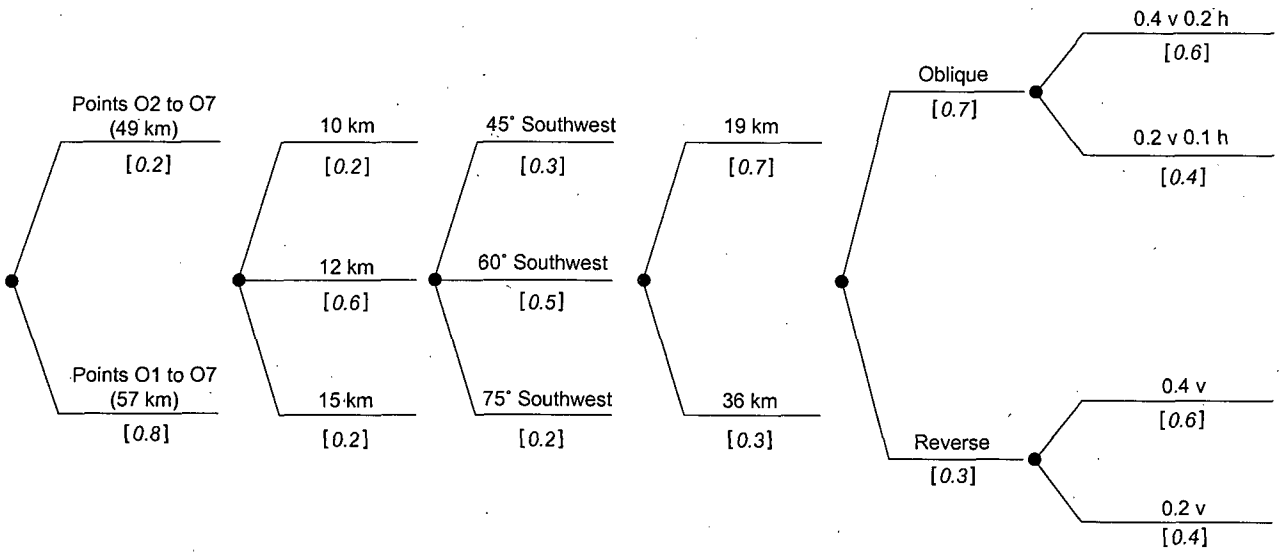

Notes:
(1) Points O1 to O7 are shown in Figure 5-8.
(2) The western margin of the Los Osos fault source is truncated by the east-dipping Hosgri fault zone source where they intersect within the seismogenic crust.
(3) h = horizontal component of slip rate
v = vertical component of slip rate

Los Osos fault zone logic tree modified from LTSP Final Report (PG&E, 1988)

SHORELINE FAULT ZONE STUDY

Pacific Gas and Electric Company | Figure **5-10**

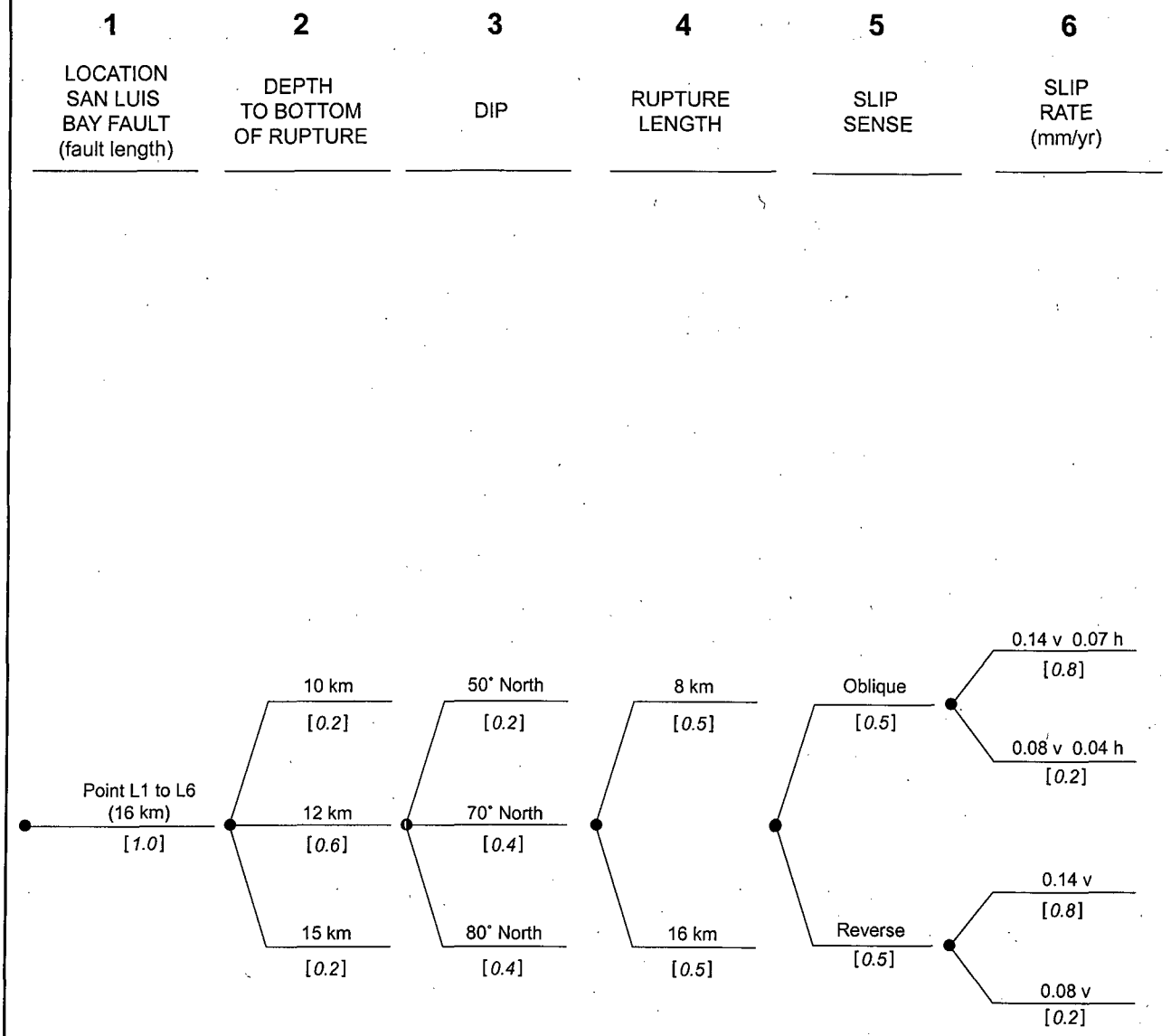

Notes:
(1) This logic tree is valid in conjunction with the Shoreline fault logic tree branch where Shoreline and San Luis Bay faults are independent structures (node 6, Figure 5-3).
(2) Points L1 to L6 are located on Figure 5.1.
(3) The bottom and western edge of the San Luis Bay fault source is truncated by the east-dipping Hosgri fault zone source and the south-dipping Los Osos fault source where they intersect within the seismogenic crust.
(4) v = vertical component of slip; h = horizontal component of slip.

San Luis Bay fault zone logic tree modified from LTSP Final Report (PG&E, 1988)

SHORELINE FAULT ZONE STUDY

Pacific Gas and Electric Company | Figure **5-11**